UNIVERSITY OF CALIFORNIA SAN DIEGO

Information Processing for Improved Performance of Optical Networks

A dissertation submitted in partial satisfaction of the

requirements for the degree Doctor of Philosophy

in

Electrical Engineering (Photonics)

by

Nikola Alic

Committee in charge:

Professor Yeshaiahu Fainman, Chair
Professor Philip E. Gill
Professor Laurence B. Milstein
Professor George C. Papen
Professor Paul H. Siegel
Professor Amin Vahdat

2006

The Dissertation of Nikola Alic is approved and it is acceptable in quality and form for publication on microfilm:

_____

_____

_____

_____

_____

_____
Chair

University of California San Diego

2006

DEDICATION

To my family, friends and colleagues, without whose support this thesis would not have been possible.

TABLE OF CONTENTS

Signature……..……..iii

Dedication…...……..iv

Table of Contents……..v

List of Figures and Tables ……...……ix

List of Abbreviations..……xv

Acknowledgements…….xvii

Vita…….....xviii

Abstract……...xix

Chapter 1 Introduction……..... 1

1.1. Dissertation Objective 1

1.2. Intensity modulated direct detection fiber optic systems 3

1.3. Optical Fiber-Channel Characteristics 5

1.3.1 Group velocity dispersion 6

1.3.2 Polarization mode dispersion 9

1.3.3 Four-wave mixing 10

1.4. Mitigation of impairments in optical links 14

1.5. Thesis organization 17

Chapter 2 Maximum Likelihood Sequence Estimation in Optical Links without Amplification…… 20

2.1. Introduction 20

2.2. Maximum Likelihood Sequence Estimation for Channels with Memory 22
2.3. MLSE in fiber optic links 28
2.3.1 Probability of Error and Performance 31
2.4. Performance of MLSE in Conjunction with Different Modulation Formats 39
2.5. Performance with A/D conversion 42
2.6. Experimental Validation 47
2.7. Conclusion 50
Chapter 3 Sequence Estimation with Constrained Run-Length Coding In Directly Modulated Multi-Mode Fiber Optical Links 53
3.1. Introduction 53
3.2. Multimode fiber response 54
3.3. Data dependent VCSEL response and data-pattern DC balancing by 8b/10b code 57
3.4. Experimental setup 62
3.5. Results and discussion 64
3.6. Chapter Summary 68
Chapter 4 Signal Statistics and Maximum Likelihood Sequence Estimation In Intensity Modulated Fiber Optic Links with Optical Amplification 71
4.1. Introduction 71

4.2. Maximum Likelihood (ML) Detection 73

4.3. MLSE in links containing a single optical pre-amplifier 84

4.4. Conclusion 91

Chapter 5 Transmission Experiments with Sequence Estimation 94

5.1. Introduction 94

5.2. Equalization of the NRZ format and receiver structure trade-offs.. 96

5.2.1 Experimental setup..... 97

5.2.2 Experimental Results and Discussion..... 98

5.3. Extended dispersion limited reach and spectral efficiency through narrow filtering and equalization..... 103

5.3.1 Experimental Setup 104

5.3.2 Results and Discussion 106

5.4. Chapter Summary..... 108

Chapter 6 Phase Coding for Suppression of Nonlinear Ghost Pulses in Long-Haul Fiber Optic Links……..... 111

6.1. Introduction 111

6.2. Physics of ghost pulses and intrachannel four-wave mixing 114

6.3. The pulse phase transfer in ghost pulse formation and simple data-independent encoding schemes..... 119

6.4. Data-dependent encoding 125

6.5. Chapter Summary..... 132

Chapter 7 Summary and Future Directions 135

7.1. Thesis Summary 135

7.2. Future Directions 141

Appendix A……..…....144

An upper bound to P_e 144

A lower bound to P_e 146

Appendix B.....148

References……..……..……..151

LIST OF FIGURES AND TABLES

Fig. 1.1 Intensity modulated direct detection (IMDD) fiber optic system schematic. (a) Direct modulation; (b) External modulation. 3

Fig. 1.2 Compensation in the optical domain vs. equalization in the electrical domain 15

Fig. 2.1 Evolution of the bit-by-bit signal space minimum distance $d_{1,0}$ for four different information-bearing pulse shapes: RZ (2 pulse widths), NRZ and RZ. 25

Fig. 2.2 System block diagram 29

Fig. 2.3 Performance of MLSE at four different propagation distances. Overlaid with the results are the error bounds calculated according to Eq. **(2.9)** 33

Fig. 2.4 Performance comparison of MLSE equalized links with different amount of accumulated dispersion from Fig. 2.3 35

Fig. 2.5 Signal space distance histograms for four different amounts of accumulated dispersion from Fig. 2.3. 36

Fig. 2.6 Evolution of MLSE signal space minimum distance d_{min} for four different modulation formats represented in Fig. 2.1 under bit-by-bit decision 41

Fig. 2.7 Performance of MLSE under A/D conversion for 2, 4 and 5 quantization bits. In solid line performance under infinite resolution is included for comparison. 43

Fig. 2.8 Effect of quantization on d_{min} at 160 km. Inside the dotted circle the infinite precision dmin is included for comparison. 44

Table 1. Power penalties incurred by a/d conversion depending on the accumulated span of ISI for three modulation formats 45

Fig. 2.9 Distribution of noiseless responses for NRZ (left) and Duobinary (right) for infinite resolution. This figure emphasizes bunching of responses for NRZ leading to a smaller requirement of quantization bits for the same span of ISI. Also see Fig. 2.5(c)-(d) 46

Fig. 2.10 Experimental schematic for the proof of concept experiment 48

Fig. 2.11 Eye diagram at the negative accumulated dispersion equivalent to 170 km in SMF 50

Fig. 3.1 Isolated Marks for three different launch conditions. (a) Random data. Substantial BLW in noticeable in the response; (b) Response for the same launch conditions after data have been encoded by a DC balancing 8b/10b code. A considerable mitigation of the BLW is achieved availing subsequent equalization 58

Fig. 3.2 Pictorial representation of direct modulation of a semiconductor laser 60

Fig. 3.3 Experimental setup for MLSE demonstration in multimode fiber links. The inset shows a photograph of the actual VCSEL mount. 62

Fig. 3.4 Back-to-back eye diagrams taken from a 0.5 m long 62.5 mm fiber (a) 2.5 Gb/s. (b) 10 Gb/s 63

Fig. 3.5 Eye diagrams after propagation through 400 m in 62.5 μm multimode fiber for two different launch conditions showed in the insets 65

Fig. 3.6 MLSE performance for two example launch conditions. The performance curve corresponding to a narrower-spread response is plotted in magenta, and the wider in red 67

Fig. 3.7 MLSE performance after propagation in 400 m of legacy 62.5 mm fiber under A/D conversion. (a) short differential group delay response; (b) long DGD response. 68

Fig. 4.1 Communication system block diagram 74

Fig. 4.2 Eigen-value distribution (in one quadrature) in log-log scale (when ordered in a descending order) for two filter shapes: Rectangular filter – the eigen-values correspond to Prolate Spheroidal Functions; and Lorentzian filter – the eigen-values correspond to harmonic functions. 80

Fig. 4.3 Histograms of samples (bars) drawn from a complex Gaussian noise source (in two orthogonal polarizations) undergoing band-limiting, square-law operation and integration. Also shown are fits of the chi square distribution (green line) and the pdf obtained through Karhunen-Loeve expansion (red line) for time-bandwidth products of (a) 5, and (b) 1 82

Fig. 4.4 (a) Comparison of the calculated PDF's (solid lines) with chi-square (dashed lines) for four channel responses at back-to-back for NRZ format at Eb/N0 = 10 dB for a rectangular filter for an '000', '111', '101' and '010' responses. (b) A zoomed in detail from the graph (a) that emphasizes how close the intersections

of the likelihood functions are on the x-axis for the two forms of likelihood functions. (c) PDF's from part (a) in logarithmic scale..... 84

Fig. 4.5 Performance of the SE based on the exact statistic (solid lines) and the chi-square metric (dashed lines) with sequence estimation at four different amounts of accumulated dispersion. (a) Ideal rectangular filter used. Performance of the two approaches is virtually the same; (b) Lorentzian filter..... 86

Fig. 4.6 Performance of sequence estimation for the exact and the chi-square distributions for BT = 1 at back to back and 150 km. (a) Rectangular filter; (b) Lorentzian shaped filter 89

Fig. 5.1 Experimental setup..... 98

Fig. 5.2 Non-ideal integrator (0.6 roll-off raised cosine shape) and "dirty" ~12ps sampler impulse response shapes..... 99

Fig. 5.3 Required OSNR for 10^{-3} BER for different receiver structures in sequence estimation (4-state VA with 3-bit A/D)..... 100

Fig. 5.4 Performance of different receiver structures in sequence estimation (4-state VA with 3-bit A/D) at 75km and 200km. 102

Fig. 5.5 Experimental setup block diagram for the 600 km NF-OOK reach..... 104

Fig. 5.6 (a) Comparison of narrowly filtered OOK (in red) and the conventional NRZ (in blue) spectra; (b) Eye-diagram at back-to-back..... 106

Fig. 5.7: (a) Viterbi equalizer performance for various receiver structure realizations; (b) Eye diagram at 600 km 107

Fig. 6.1 Ghost pulse formation. (a) 21-bit stream at the input. (b) Same bit stream after 1250 km of propagation with periodic dispersion compensation and amplification performed every 50 km 113

Fig. 6.2 Ghost pulse formation. (a) Echo pulses form in positions -3 and 3 as mirror images of genuine pulses in positions -1 and 1. (b) Higher order ghost pulse formation off first order ghost from part (a)..... 116

Fig. 6.3 Effect of dispersion map on Q factor evolution. Periodic map with fast Q drop in dashed line and aperiodic map much more resilient to intrachannel 4WM in solid line..... 117

Fig. 6.4 Eye diagram after 2000 km propagation in a periodic map shown in Fig. 6.3 119

Fig. 6.5 Phase transfer in ghost pulses formation. Formed ghost pulses bear the same phase difference as their parent pulses either 0 (101 case in solid line), or π (10-1 case in dashed line). 120

Fig. 6.6 (a) Destructive interference of ghost pulses from parent pulses having phase 0 and π. (b) Pitfall of phase encoding. Destructive interference of 2 outer pulses in the position where a genuine mark resides, but has an opposite phase from the outer pulses 121

Fig. 6.7 Data independent phase encodings: Alternate mark inversion (AMI); Duobinary encoding (DBC); One-bit inversion; 122

Fig. 6.8 Effect of three different data-independent (simple) phase encodings 123

Fig. 6.9 (a)Pulse triple interaction depending on the phase of one of the one side pulses. (b) zoom into the lower power values from part (a) concentrating on the energy leakage in position 4 and -4. 127

Table 2. Binary phase encoding patterns yielding the strongest ghost suppression..... 128

Fig. 6.10 Eye diagrams after 3000 km for average launch powers of 0 dBm. Means and deviations cited in arbitrary units. (a) Uncoded stream; (b) Stream coded by AMI, and (c) Data dependent phase encoding method. Simulated link consists of 30 spans of 100 km (approximately 95 km NZDSF fiber (D = -7.06 ps/nm-km) and 5 km DCF) with residual 20 ps/nm span and pre-compensation of –450 ps/nm. . 129

Table 3. Values of the Q factor and corresponding performance improvements for 3 different launch powers..... 131

Fig. 6.11 Q factor evolution for different encoding approaches in (a) periodic and (b) aperiodic dispersion maps shown in Fig. 6.3 132

LIST OF ABBREVIATIONS

4WM	For-wave mixing
A/D	Analog to digital (conversion)
AMI	Alternate mark inversion
ASE	Amplified spontaneous emission
ASK	Amplitude-shift keying (modulation)
AWGN	Additive white Gaussian noise
BCJR	Bahl-Cocke-Jelinek-Raviv (algorithm)
BER	Bit-error ratio
BL	Bandwidth – distance (product)
BLW	Base-line wander (of the directly modulated laser response)
BT	Time-bandwidth (product)
CD	Chromatic Dispersion
DB	Duobinary (modulation)
dB	decibel (unit)
dBm	decibel (relative to 1 mW power level)
DCF	Dispersion compensating fiber
DFE	Decision feedback equalizer
DGD	Differential Group delay
ECC	Error-correction code(s)
EDC	Electronic dispersion compensation
EDFA	Erbium-doped fiber amplifier
EFEC	Enhanced forward error correcting code (in the ITU standard)
FEC	Forward error correcting (codes)
FFE	Feed-forward equalizer
FWHM	Full-width at half maximum
Gb/s	Giga-bits per second
GVD	Group velocity dispersion
IMDD	Intensity modulation direct detection
ISI	Intersymbol interference
ITU	International Telecommunication Union
KL	Karhunen-Loève (expansion)
MDB	Modified duobinary (encoding)
MIMO	Multiple input, multiple output (communication system)
ML	Maximum likelihood
MLSD	Maximum likelihood sequence detection
MLSE	Maximum likelihood sequence estimation
MMF	Multi-mode fiber

NF-OOK	Narrowly filtered On-off keying (modulation format)
NLS	Nonlinear Schrödinger (Equation)
NRZ	Non-return to zero (modulation format)
OOK	On-off keying (modulation format)
OSNR	Optical signal-to-noise ratio
PDF	Probability density function
PMD	Polarization mode dispersion
PRBS	Pseudo-random bit sequence
PSS	Prolate spheroidal functions
RMS	Root-mean-square
RZ	Return to zero (modulation format)
SBI	Single-bit inversion (phase encoding)
SE	Sequence estimation
SMF, SSMF	(Standard) Single mode fiber
SNR	Signal-to-noise ratio
spb	samples-per-bit
SPM	Self-phase modulation
VA	Viterbi algorithm
VCSEL	Vertical cavity surface-emitting laser
VOA	Variable optical attenuator
WDM	Wavelength-division multiplex
XPM	Cross-phase modulation

ACKNOWLEDGEMENTS

The text in the Chapter 2 in part is a reprint of the material as it appears in the *Optical Communication Theory and Techniques*. Alic, Nikola; Papen, George C.; Milstein Laurence B.; Siegel, Paul H.; Fainman Yeshaiahu. "Performance Bounds of MLSE in Intensity Modulated Fiber Optic Links," (E. Forrestieri, Ed.), Springer, 2005. The dissertation author was the primary researcher and/or author and the co-authors listed in this publication directed and supervised the research which forms the basis for this Chapter.

The text in the Chapter 4, in part, is a reprint of the material as it appears in Optics Express, Alic, Nikola; Papen, George C.; Saperstein, Robert E.; Milstein Laurence B.; Fainman Yeshaiahu. "Signal Statistics and Maximum Likelihood Sequence Estimation in Intensity Modulated Fiber Optic Links Containing a Single Optical Pre-amplifier," Optics Express, Vol 13, 2005. The dissertation author was the primary researcher and/or author and the co-authors listed in this publication directed and supervised the research which forms the basis for this Chapter.

The text in the Chapter 6, in part, is a reprint of the material as it appears in IEEE Photonics Technology Letters, Alic, Nikola; Fainman Yeshaiahu. "Data-dependent

phase coding for suppression of ghost pulses in optical fibers," IEEE Photonics Technology Letters, vol.16, 2004. The dissertation author was the primary researcher and/or author and the co-authors listed in this publication directed and supervised the research which forms the basis for this Chapter.

VITA

1998	B.S. in Electrical Engineering, School of Engineering, Belgrade University, Serbia and Montenegro
1998 – 1999	Junior Scientist, Institute for Nuclear Sciences "Vinca", Belgrade, Serbia and Montenegro
1999 – 2006	Research Assistant, University of California San Diego
2001	M.S. University of California San Diego
2006	Ph.D. University of California San Diego

PUBLICATIONS

N. Alic, G.C. Papen, R.E. Saperstein, L.B. Milstein, and Y. Fainman, "Signal Statistics and Maximum Likelihood Sequence Estimation in Intensity Modulated Fiber Optic Links Containing a Single Optical Pre-amplifier," Opt. Express 13, 4568-4579 (2005),

N. Alic, G.C. Papen, L.B. Milstein, P.H. Siegel and Y. Fainman, "Performance Bounds Of Maximum Likelihood Sequence Estimation In Intensity Modulated Fiber Optic Links," *Optical Communication Theory and Techniques*, (Enrico Forestieri Ed.), Springer 2005, pp. 197 ? 203.

N. Alic and Y. Fainman, "Data-dependent phase coding for suppression of ghost pulses in optical fibers." IEEE Photonics Technology Letters, vol.16, no.4, pp.1212-14 (2004).

ABSTRACT OF THE DISSERTATION

Information Processing for Improved Performance of Optical Networks

by

Nikola Alic

Doctor of Philosophy in Electrical Engineering (Photonics)

University of California San Diego, 2006

Professor Yeshaiahu Fainman, Chair

Transmission in optical fiber offers long distance and high-speed, possibly tens of Terabits per second, optical communications. The utilization of the theoretically available bandwidth and/or the capacity is hindered by a number of impairments. Traditionally, these impairments are mitigated in the optical domain. The main subject of the dissertation is the investigation of performance and

applicability of advanced equalization and coding methods in high-speed optical communications, which relies on processing in the electronic domain. In particular, the investigated approaches rely either on processing of the received signal in order to recover information distorted in transmission, or on encoding and/or shaping of the transmitted signal in a specific way that mitigates the signal degradations imposed by the channel.

The specifics of the fiber-optic channel require that the well established approaches in other areas of communication theory, upon which the presented work leverages, be adjusted to the conditions of this communication channel (e.g. nonlinear effects in transmission, square-law detection and signal statistics). In the dissertation, firm theoretical foundation for the analysis of electronic equalization is established. Additionally, the proposed and theoretically analyzed techniques are validated experimentally, demonstrating feasibility of the proposed techniques and providing corroboration of the theoretical predictions.

Chapter 1

Introduction

1.1. Dissertation Objective

Fiber optic communications have experienced a remarkable growth during the last two decades. Wavelength division multiplexed (WDM) systems supporting tens of channels, each operating at speeds up to 10 Giga-bits per second (Gb/s) have become ubiquitous [1-2]. Fiber-optic links constitute the backbone of all of the information traffic, both on the national and the trans-oceanic levels.

There are several important impairments in the fiber-optic channel that limit transmission distance and/or the communication data-rate. An investigation of advanced techniques to overcome these issues that hinder reliable information transmission is the topic of this thesis. Special emphasis will be put on comparing how the mitigation is performed – optically (i.e. before the signal is detected), or electronically, after the signal is sensed. As will be demonstrated, the optimal

impairments mitigation is not a static problem, but a dynamic one, and requires an optimization approach in which the cost is a major concern.

Traditionally, impairment mitigation in fiber-optic links have been attempted in the optical domain, relaying on the knowledge of the physical origin of the sources of signal degradation. Although the field of optical communications has reached maturity on the physical layer level, little (if any) effort has been put into taking advantage of the vast area of knowledge from the communication theory that has ensured the steady performance improvement in other areas of communications, such as wireless and storage. For instance, error-correction codes (ECC) have been introduced to optical communications only recently [1-3] and their application still lags other areas of communication.

Investigation of equalization techniques and ECC applications to optical communications is the main subject of this thesis, especially in comparison to the optical domain compensation techniques. As it will be stressed throughout this work, owing to the fiber-optic channel peculiarities, approaches from other areas of communications cannot simply be translated to fiber-optic system, but need to be modified to correctly reflect the particular channel characteristics in these systems (i.e., noise statistics, detection strategies, etc.).

The bulk of the work in this dissertation discusses a number of pioneering attempts to apply advanced coding and equalization strategies in the field of optical communication. An important contribution of the work is the fact that, except for the

case of long-haul non-linear fiber optic impairments mitigation, all of the techniques have been experimentally demonstrated, providing verification against the practical circumstances, adding the validity to the theoretical models and predictions.

1.2. Intensity modulated direct detection fiber optic systems

All existing fiber optic systems are based on an the intensity modulated direct detection (IMDD) system shown in Fig. 1.1. A laser acts as source of coherent radiation, whereas the modulation process is performed either in terms of *(a)* direct modulation, where the laser current biased above the lasing threshold has a small signal modulation component, thus impressing the information content onto the intensity envelope of the emitted light; *(b)* externally modulated configuration, where

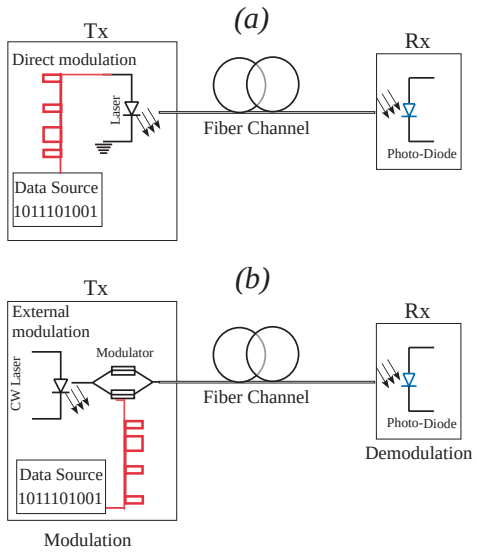

Fig. 1.1 Intensity modulated direct detection (IMDD) fiber optic system schematic. (a) Direct modulation; (b) External modulation.

the laser emits light at a constant power level, and the modulation process is achieved by an additional (external) modulator (through e.g. electro-optic, or electro-absorption effect [4-6]) to produce a intensity modulated stream. The signaling format used exclusively in the existing digital optical communications links is the non-coherent binary amplitude shift keying (ASK), or often referred to as On-off Keying (OOK). Within an appropriate bit-slot of duration T (the reciprocal of the bit-rate R), either a pulse is transmitted, representing a 1-symbol (sometimes called a "mark"), or no light is transmitted at all (sometimes denoted as a "space").

In the most common realization, the detection process is achieved by means of a photo-diode that produces electrical current proportional to the instantaneous power (magnitude squared) of the incident electric field, if the response time of the detector is assumed to be as fast as the envelope of the light intensity. Consequently, any information about phase of the optical fields is lost in the detection process. This, in turn, directly implies inferior overall performance of IMDD systems with respect to coherent detection strategies generally considered in communication theory [7-9]. An additional point of interest is the fact that a photo-diode is a square-law detector, such that the detection process in IMDD systems is inherently non-linear. This is a major difference with respect to linear coherent detectors in other areas of communication. Additionally, one might recognize similarity of the system at hand with the general concept of communication systems whereby the modulated laser output immediately represents an up-shifted version of the base-band signal,

whereas the square-law detector, in effect, provides non-coherent demodulation by down-shifting the received signal back to base-band due to its inability to follow the fast variations of the optical carrier.

1.3. Optical Fiber-Channel Characteristics

The main sources of signal degradation in fiber optic communication systems are due to the physical characteristics of the fiber-channel.

Signal attenuation occurs in any medium other than vacuum. The minimum loss in silica fibers occurs at a wavelength of approximately 1550 nm and equals only 0.2 dB/km. This fact was the determining factor to setting the operating window of the current long-haul fiber-optic telecommunications. Currently, this loss is compensated by Erbium Doped Fiber Amplifiers (EDFA) [10-12]. The real advantage of EDFAs is that they can provide up to 40 dB of gain in a fairly flat region around the minimum fiber loss wavelength, spanning approximately 30 nm (3.6 THz). This nurtured the widespread use of multi-wavelength systems, as a single EDFA could amplify many channels (frequency bands) simultaneously without the need for regeneration (i.e., conversion of signals into electrical domain, and then back to optical domain).

After this first obstacle (loss) was removed, and as the bit rates in the optical links have surpassed 1 Gb/s, several other sources of signal degradation that hindered reliable communication became apparent.

In this dissertation, communication links operating at speeds up to 40 Gb/s will be considered exclusively. There exist three dominant physical effects naturally occurring in any silica-based wave-guiding structure likely to affect the information-bearing pulses in IMDD systems at the considered communication speeds: *(i)* Group velocity dispersion (GVD) – often times (interchangeably) denoted – Chromatic dispersion (CD), *(ii)* Polarization mode dispersion (PMD) and *(iii)* Four-waved Mixing (4WM). The combined effects of these phenomena cause major obstacle to reliable information transfer through optical fibers.

1.3.1 **Group velocity dispersion**

Group velocity dispersion is a linear effect originating from the frequency dependence of the optical fiber index of refraction. The physics of GVD has been carefully studied [13-14, 6] and is very well understood.

The sources of frequency dependence of the group index of refraction, n_g, are two-fold: *(i) Material dispersion*, whereby silica's dielectric permittivity exhibits frequency dependence, implying straightforwardly the frequency dependence of the group index; and *(ii) Waveguide dispersion*, due to which a single mode fiber, being a wave-guiding structure, is also wavelength selective, adding to the net amount of the group index of refraction frequency dependence. The very notion of the group index of refraction being frequency dependent implies that different frequency components of the information-bearing pulses will travel at slightly different speeds. As a

consequence, pulses will continuously spread in propagation, and energy from a particular bit slot will leak into adjacent bit slots.

Mathematically, GVD effect on the slowly varying part of the optical-pulse-amplitude[1] *A(z,T)* can be described by the following equation [13-14]:

$$j\frac{\partial A(z,T)}{\partial z} = \frac{1}{2}\beta_2 \frac{\partial^2 A(z,T)}{\partial T^2}, \tag{1.1}$$

where β_2 is fiber group velocity dispersion parameter, z is the longitudinal propagation coordinate , T is time in the pulse reference frame [13-14] and $j = \sqrt{-1}$. Eq. (1.1), being a linear equation, can most efficiently solved in the Fourier domain, yielding:

$$\tilde{A}(z = L, \omega) = \tilde{A}(z = 0, \omega) \cdot e^{j\frac{\beta_2 \omega^2 L}{2}}, \tag{1.2}$$

where $\tilde{A}(z,\omega)$ is a Fourier Transform of *A(z, T)*, and ω is the angular frequency. Consequently, expressing Eq. (1.2) in the time domain yields:

$$A(z = L, T) = \mathbb{F}^{-1}\{A(z = L, \omega)\} = A(z = 0, T) * e^{-j\frac{2T^2}{\beta_2 L}}, \tag{1.3}$$

where F^{-1} stands for an Inverse Fourier Transform, and * for the convolution operators, respectively. We conclude that the effect of chromatic dispersion in a single mode fiber is equivalent to a convolution of the input information-bearing pulse with the quadratic phase-only function. In engineering terms, GVD is an all-pass filter with quadratic-phase characteristic with respect to frequency, also known

[1] Sometimes referred to as low-pass equivalent signal

as a chirp. The overall effect the quadratic phase term depends on the distance traveled, L, and fiber chromatic dispersion parameter, β_2. In standard single-mode fiber (SMF), at 1550 nm, $\beta_2 = -20 ps^2/km$. It is perhaps more useful to express the dimensions of the β_2 parameter as $ps/(km\ THz)$ which emphasizes that the rate of pulse spreading depends on its bandwidth content in addition to the distance traveled. This latter observation will be taken advantage of in Chapters 4 and 5 in order to extend the reach of the high-speed equalized links.

An important property of Eq. (1.1) is that it is isomorphic to the diffraction law in spatial optics [13,15]. However, in Eq. (1.1) time axis assumed a role of a spatial coordinate in the diffraction law. Thus, the information bearing pulses will experience diffraction-like spreading in time as they propagate. It is not difficult to foresee that, with propagation, energy pertinent to one bit of information will slowly start spreading into adjacent slots diminishing the ability to distinguish difference between marks and spaces in a communication system based on OOK. This symbol interposition in communication theory is denoted *Inter-symbol Interference* (*ISI*) [7-9, 5]. To summarize, once the fiber losses were made immaterial because of the ability to efficiently counter their effects through all-optical amplification, GVD-caused ISI becomes the dominant source of signal degradation in single-mode base optical links. Mitigation of the GVD-caused ISI through electronic signal processing will be the main subject of this dissertation.

1.3.2 **Polarization mode dispersion**

Although the name (single-mode fiber) seems to imply that this waveguide structure supports a single electromagnetic mode, in reality it does admit two equivalent modes in the two orthogonal polarizations. All of the effects discussed so far account for only one of the polarizations. In an ideally circularly-symmetric waveguide structure the propagation characteristics of these two polarization modes are exactly equivalent (e.g. mode profiles, group velocities, waveguide dispersion, etc.). However, it is impossible to achieve perfect circular symmetry of a fiber cross-section over long distances. First there are manufacturing effects in the drawing process. Secondly, fiber is often exposed to stress and mechanical vibrations and strain when laid in the ground (or undersea). As a consequence, in a slightly asymmetric waveguide that can either be a result of the manufacturing process, or a product of strain or vibrations, the characteristics of the two polarization modes are no longer degenerate, such that their group velocities differ. Additionally, owing to the existence of external perturbations in the propagation medium, the optical fields in either of the two polarization modes can couple from one polarization state to another in an uncontrollable fashion. The end result of these polarization mode dispersion (PMD) effects is generation of a (possibly large) number of slightly time-shifted replicas of an optical pulse, which have slightly different arrival times at the receiver [16]. The PMD, thus is an additional source of ISI in fiber optic channels, particularly of concern in 40 Gb/s and higher speed systems, owing to their reduced

signaling period (25 ps). To give an illustration of the magnitude of the effect, the common figure of merit for the PMD in standard fibers is the differential group delay (DGD) of 1 $ps/\sqrt{km}$ in the legacy single-mode fibers, and 0.1 $ps/\sqrt{km}$ in the new-generation SMF [16]. Compared to the effects of chromatic dispersion (CD), ISI introduced by PMD is at least one to two orders of magnitude smaller, in addition to the square-root dependence on the propagation distance (in contrast to linear dependence of GVD). Thus, PMD can become a primary source of degradation only if GVD-caused ISI is mitigated by all-optical dispersion compensation techniques.

1.3.3 **Four-wave mixing**

In addition to linear effects (loss, GVD and PMD), the optical fiber also possesses a nonlinear response to the optical fields. At the data rates of interest in this work, the dominant nonlinear effect is the four-wave mixing, (4WM) where any three quanta of the optical field (photons), with (not necessarily distinct) frequencies f_1, f_2, f_3 mediated by the propagation medium (i.e. nonlinear response of the silica optical fiber) can be mixed, producing a photon at a frequency f_4 [17, 13]:

$$f_4 = f_1 + f_2 - f_3 . \tag{1.4}$$

Obviously, 4WM can lead to energy transfer between both different WDM channels, as well as energy redistribution within a single channel bandwidth of interest. Note that both of the above possibilities are necessarily detrimental to the communication system performance as they introduce distortion to the transmitted information.

The evolution of the slowly varying amplitudes A_i of four pulses entering the interaction can be represented by a set of four coupled nonlinear equations:

$$\begin{aligned}
\frac{dA_1}{dz} &= i\gamma\left\{\left[|A_1|^2+2\sum_{k\neq 1}|A_k|^2\right]A_1+2\cdot A_2^* A_3 A_4 e^{j\kappa z}\right\}+\beta_{11}\frac{\partial A_1}{\partial T}+\beta_{11}\frac{\partial^2 A_1}{\partial T^2}-\frac{\alpha}{2}A_1\\
\frac{dA_2}{dz} &= i\gamma\left\{\left[|A_2|^2+2\sum_{k\neq 2}|A_k|^2\right]A_2+2\cdot A_1^* A_3 A_4 e^{j\kappa z}\right\}+\beta_{12}\frac{\partial A_2}{\partial T}+\beta_{22}\frac{\partial^2 A_2}{\partial T^2}-\frac{\alpha}{2}A_2\\
\frac{dA_3}{dz} &= i\gamma\left\{\left[|A_3|^2+2\sum_{k\neq 3}|A_k|^2\right]A_3+2\cdot A_1 A_2 A_4^* e^{j\kappa z}\right\}+\beta_{13}\frac{\partial A_3}{\partial T}+\beta_{23}\frac{\partial^2 A_3}{\partial T^2}-\frac{\alpha}{2}A_3\\
\frac{dA_4}{dz} &= i\gamma\left\{\left[|A_4|^2+2\sum_{k\neq 4}|A_k|^2\right]A_4+2\cdot A_1 A_2 A_3^* e^{jkz}\right\}+\beta_{14}\frac{\partial A_4}{\partial T}+\beta_{24}\frac{\partial^2 A_4}{\partial T^2}-\frac{\alpha}{2}A_4
\end{aligned} \tag{1.5}$$

Where non-linear terms in Eq. (1.5) are grouped inside the braces, and the linear effects (e.g. pulse walk-off, GVD and loss) are displayed in a lighter color suggesting we are concentrating on the non-linear effects only in this section. Out of the 3 non-linear terms inside the braces, the first one is usually denoted the self-phase modulation (SPM), the second one – cross-phase modulation, whereas the third term is usually referred to as the four-wave mixing[2]. In Eq. (1.5), κ is the wave-vector phase mismatch that governs the efficiency of the 4WM process. It has a contribution from material dispersion, waveguide dispersion and nonlinear effects, respectively ($\kappa = \Delta k_M + \Delta k_W + \Delta k_{NL}$) [13]:

$$\begin{aligned}
\Delta k_M &= \left[n_3\omega_3 + n_4\omega_4 - n_1\omega_1 - n_2\omega_2\right]/c\\
\Delta k_W &= \left[\Delta n_3\omega_3 + \Delta n_4\omega_4 - \Delta n_1\omega_1 - \Delta n_2\omega_2\right]/c\\
\Delta k_{NL} &= \gamma P
\end{aligned} \tag{1.6}$$

---

[2] Note that 4WM in this instance refers to mixing of pulse envelopes with different carrier frequencies f_i, rather than a more general 4WM that denotes any kind of interaction mediated by a material $\chi^{(3)}$ response.

In Eq. (1.6), c is the speed of light in vacuum, and n_i and Δn_i are the appropriate fiber material and waveguide group indices, respectively. When the four carrier frequencies are all distinct, it is rather difficult to achieve phase matching condition ($\kappa = 0$) assuming moderate power levels (which is invariably the case in fiber optic communication systems). The reason for this is that the common single mode fiber (SMF) has substantial material and waveguide dispersion, such that the pure 4WM effect, when A_i frequencies are all distinct, can never become appreciable. As a consequence, the last term inside the braces in all of the coupled equations (1.5) is typically negligible. Thus, of all the possible wavelength combinations in Eq. (1.5), only two degenerate cases are of practical importance in standard single mode fibers (SSMF): *(i)* Fully degenerate case ($f_1=f_2=f_3=f_4$) is usually denoted as self-phase modulation (SPM), and *(ii)* Partially degenerate case ($f_1=f_2\neq f_3=f_4$) is often referred to as cross-phase modulation (XPM or CPM) [18, 13].

The propagation equation in the fully degenerate 4WM case ($f_1=f_2=f_3=f_4$), in a single carrier frequency case (i.e. only one of the four equations (1.5)) and neglecting the effects of GVD, can be expressed as:

$$j\frac{\partial U}{\partial z} = \gamma P_0 e^{-\alpha z} |U|^2 U \tag{1.7}$$

where U is a normalized version of the slowly varying envelope, where A_i is scaled by the pulse peak power P_0 and the attenuation term ($A(z,\tau) = \sqrt{P_0}\exp(-\alpha z/2)U(z,\tau)$) Although nonlinear, partial differential equation (Eq. (1.7)) has a simple solution of:

$$U(z=L,T)=U(z=0,T)\cdot e^{j\phi_{NL}(z,T)} \tag{1.8}$$

Thus, when dispersive fiber characteristics are neglected, the effect of SPM is that of introducing a phase modulation ($\phi_{NL}(z,T)=\gamma P_0 |U(z=0,T)|^2 \frac{1-e^{-\alpha z}}{\alpha}$), caused by the pulse itself, and hence the name of the effect (self-phase modulation). Based on Eq. (1.8) it may appear that this phase modulation should not be of much concern, as it represents a phase distortion that becomes irrelevant in the square-law detection process of an amplitude modulated system. However Eq. (1.8) was derived without accounting for GVD. The interplay of SPM and GVD leads to phase-modulation-to-amplitude-modulation (PM to AM) transfer (and vice versa), which produces serious distortions and system performance degradations. Thus, including both linear and nonlinear effects above, we arrive at a nonlinear propagation equation that in a degenerate case (SPM) can be expressed as:

$$j\frac{\partial U}{\partial z}=\frac{1}{2}\beta_2\frac{\partial^2 U}{\partial T^2}-\gamma P_0 e^{-\alpha z}|U|^2 U \tag{1.9}$$

which is one form of the Nonlinear Schrödinger (NLS) Equation.

In the remaining partially degenerate case, the mutual effect of the two optical pulses at two distinct carrier frequencies (e.g. two WDM channels) can be expressed by a pair of coupled NLS-like equations:

$$\begin{aligned} j\frac{\partial U_1}{\partial z}&=\frac{1}{2}\beta_{21}\frac{\partial^2 U}{\partial T^2}-\gamma P_{01}e^{-\alpha z}|U_1|^2 U_1-2\gamma\sqrt{P_{01}P_{02}}e^{-\alpha z}|U_2|^2 U_1 \\ j\frac{\partial U_2}{\partial z}&=-jd\frac{\partial U_2}{\partial T}+\frac{1}{2}\beta_{22}\frac{\partial^2 U}{\partial T^2}-\gamma P_{02}e^{-\alpha z}|U_2|^2 U_2-2\gamma\sqrt{P_{01}P_{02}}e^{-\alpha z}|U_1|^2 U_2 \end{aligned} \tag{1.10}$$

where the $|U_i|^2 U_j$ $(i \neq j)$ terms represent the cross-phase modulation between the two fields, and the first partial derivative term in the second of the equations takes into account the possibility that, due to the difference of carrier frequencies the information-bearing pulses in the two channels U_1 and U_2, can propagate with different group velocities[3]. It is easy to envisage that in multi-channel WDM system supporting tens of wavelengths, XPM is going to become the dominant source of degradation. The mechanism of deterioration, similarly to the completely degenerate case is through the PM-AM conversion arising as a result of the interplay between GVD, XPM and SPM. An important property of Eq. (1.10) is the factor of 2 multiplying the XPM terms, leading to a twice as efficient process with respect to SPM. Consequently, in WDM systems, especially with many channels, XPM is the main source of performance degradation. As it was mentioned in the introductory section, only single-wavelength systems will be treated in this work, such that the effects of XPM and inter-channel 4WM will not be considered and are included in this section for completeness.

1.4. Mitigation of impairments in optical links

Major sources of signal degradation in fiber-optic links were introduced in the previous section. The combination of these effects hinder transmission at 10 Gb/s

---

[3] The time reference frame in Eq. (1.10) is set with respect to the pulse(s) at frequency ω_1 (i.e., the first equation)

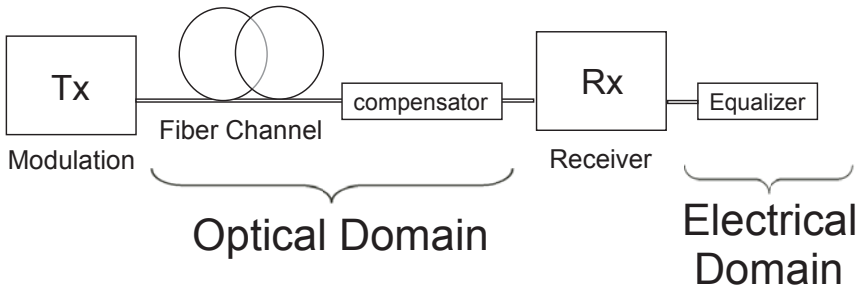

Fig. 1.2 Compensation in the optical domain vs. equalization in the electrical domain

beyond approximately 100 km [5,19]. Here we review existing approaches of the impairment mitigation. In theory, there exist two approaches to mitigation of channel impairments: *(i)* Compensation, and *(ii)* Equalization.

Compensators rely on the knowledge of the physical effects causing the distortion, and thus the performance degradation. The rational behind this approach is to attempt to reverse the physical effects leading to the distortion. Equalizers rely on the (electronic) signal processing (either analog or digital) performed in order to extract the information from the corrupted channel responses. In the field of fiber optic communications, the two approaches are illustrated in Fig. 1.2. Compensators, in this case, function in the optical domain, i.e. before the conversion from the optical to electrical domain, whereas equalizers operate in the electrical domain, that is, after the O/E conversion. An excellent survey of compensation techniques in use in deployed fiber optic links can be found in [19, 16]. Upon closer examination, it becomes apparent that all of the techniques applied in the existing links are

compensators, whether they are employed for GVD, PMD or 4WM mitigation [e.g. dispersion-compensating fiber (DCF) that has a positive sign of the GVD parameter β_2; PMD compensators that separate received light into two polarizations, adjust the delay between them and recombine the polarizations; parametric process phase conjugators in highly non-linear fibers (HNLF)]. Although application of compensation techniques yields exceptional results, the cost of these devices in large WDM systems containing many wavelengths becomes prohibitively high. In addition, the requirement that these devices be tunable and adaptive to ambient variations, especially in a network environment, adds another level of complexity, and consequently increases their cost. These were the main factors that motivated research of low-cost solutions for optical networks impairment mitigation, as well as this dissertation, in the early 2000s. Electronic signal processing (i.e. equalization) and error control coding were clearly primary areas of interest, especially as they have demonstrated exceptional results in other areas of communication in the last two decades. The equalization techniques for optical communications were suggested in the late 1980's, however a comprehensive and systematic investigation of the capabilities of electronic processing techniques has never been undertaken, and presented an interesting and unexplored research topic.

For the most part, the main area of research to be presented in this dissertation concerns processing at the receiving end, i.e. equalization, however two mitigation approaches rely on the application of error correction codes (ECC). Error

correction coding ensures reliable communication by appending redundant bits to the information at the transmitting end, thus making the information less prone to loss in transmission. Alternatively ECC provide means to detect and/or correct the pieces of information that were corrupted beyond recovery due to either channel aberrations, noise, or both. The two instances of error control coding applications discussed in the dissertation are both examples of modulation codes. Modulation codes [20] impose redundant information in such a way that will altogether shape the channel response in a specific, desirable, way, such as to mitigate the deleterious channel response, in addition to providing error correction functionality. Although examples of modulation codes exist that have found applicability in more than one area of communication, generally new classes of codes need to be designed for the particular channel or application. In fact, of the two ECC examples to be presented in this dissertation one of the encoding schemes is in wide use in electrical Ethernet applications, whereas the other code was custom designed for the fiber optic channel to mitigate a certain type of non-linear effect occurring in 40 Gb/s and higher speed long-haul fiber optic links.

1.5. Thesis organization

The dissertation is organized as follows: Equalization in short-haul fiber optic links containing no optical amplifiers is examined in Chapter 2. In addition to performance simulations in single mode fiber optic links, the investigation will be

focused on particular achievable performance bounds of equalization techniques, stressing the applicability and achievable performance of equalization for different modulation formats, as well as under analog-to-digital conversion. We focus on the difference between the traditional bit-by-bit detection, and sequence detection. Equalization in directly modulated multimode links is treated in Chapter 3. The center of attention of this Chapter is in the experimental demonstration of equalization and, to date, unmatched equalization results facilitated through the usage of modulation coding that enabled stationarity of the directly modulated laser.

The scope of Chapter 4 is equalization in all-optically amplified links. The transformation of signal and noise by a square-law detector plays a paramount role on the statistics in these links, such that the common Euclidean metric is no longer optimal in detection. In fact, the statistics in all-optically amplified links have long been treated as chi-square. As it will be shown in Chapter 4, the assumed chi-square statistics do not correspond to the true statistics in these links, and the exact statistical distributions will be derived, and used to achieve superior performance. In addition, a novel modulation format – the Narrowly Filtered On-Off Keying (NF-OOK) capable of substantially increasing the dispersion limited reach and spectral efficiency of the WDM systems will be introduced.

In Chapter 5, transmission experiments relying on equalization will be presented. In particular the equalization of two modulation formats will be presented: NRZ and NF-OOK. In addition to examining the receiver design trade-offs

in equalization, the superior performance of the NF-OOK format with respect to receiver sensitivity and dispersion limited reach is demonstrated.

A particular form of ISI mediated by the nonlinear effects in ultra-long-haul transmission will be covered in Chapter 6. An approach of phase coding for mitigation of these intra-channel 4WM effects is proposed and investigated. It will be shown that data-dependent phase manipulation can substantially outperform data-independent coding techniques that were initially suggested for this purpose. Finally, the summary and conclusions of the dissertation, along with directions of future work will be presented in Chapter 7.

Chapter 2

Maximum Likelihood Sequence Estimation in Optical Links without Amplification

2.1. Introduction

In this Chapter we introduce and rigorously assess the performance of a powerful equalization technique, maximum likelihood sequence estimation (MLSE) that has been extensively studied and applied in data-storage applications and mobile telephony in the last decade. Our study is motivated by the fact that MLSE minimizes the probability of sequence error for channels with intersymbol interference (ISI) [8], hence our results are a lower bound on the achievable performance for any electronic dispersion compensation (EDC) technique in intensity modulated direct detection fiber optic links where additive Gaussian noise dominates.

Electronic dispersion compensation was first suggested for coherent optical links in [21], whereas MLSE for coherent optical links has been introduced in [22].

The concept of using MLSE has been revived in [23], where a theoretically optimal receiver, incorporating a combination of a bank of matched filters and a Viterbi Algorithm (VA), was suggested for the mitigation of polarization mode dispersion (PMD). Recently, a mathematical treatise of signal dependent noise in optical links in conjunction with MLSE was presented [24]. In this Chapter, we examine the performance of MLSE approach in short-haul intensity modulated fiber optic links. In particular, we investigate fiber optic communication links assuming that the noise in the channel is dominated by the thermal noise in the detector. This model is valid for the case of short haul and metropolitan links [25] that either contain no optical amplifiers, or where the total noise is dominated by the noise component originating in the detector and the electronics in the post-detection circuitry [26]. The dominant noise in this case is the thermal noise from the electronic components that is modeled as the additive white Gaussian noise process (AWGN). This noise model allows that the performance of maximum likelihood sequence detection (MLSD) be evaluated in detail. In contrast to the previous work, we assume a simple receiver structure that consists of only an integrate-and-dump filter. The employment of this "mismatched" filter implies that the detection process will be sub-optimal. We quantify, the reduction in performance resulting from utilization of this practical, but suboptimal, filter in conjunction with sequence estimation (SE) in fiber optic links.

In the next Section the signal detection theory behind MLSE is introduced, whereas in Section 2.3. the theory is extended to the single-mode fiber optic links. In

Section 2.4, the performance of performance of MLSE with different modulation formats is investigated, whereas the performance of the approach under A/D conversion is discussed in Section 2.5 Experimental validation of the approach is described in Section 2.6. Finally, the Chapter closes by the conclusion in Section 2.7.

2.2. Maximum Likelihood Sequence Estimation for Channels with Memory

The broadening of waveforms due to GVD leads to a smaller distinction between marks and spaces. The incurred deterioration depends on the power spectral density of the waveform, and the distance traveled [13]. In the case of non-coherent on-off keying (OOK), the detected quantity is the presence or the absence of the optical power in a bit period. The corresponding signal space contains, consequently, only two points (a 0-symbol and a 1-symbol) and is non-negative. A sequence of N bits, on the other hand, can be represented as a single point in an N-dimensional space. This signal space is defined as a generalized *N*-dimensional vector space with an orthonormal basis function set $\{\zeta_i(t)\}$, chosen such that any of the possible transmitted (noiseless) signal sequence of N bits can be represented as a linear combination of the basis set functions. As will be clarified in Section 2.3. , the signal space for bit-by-bit decision is a one-dimensional subspace of the space corresponding to MLSE, leading to the superior performance of the latter.

If the detection in an optical link is performed on a bit-by-bit basis, the probability of error can be expressed as [26]:

$$P_e = Q\left(\frac{i_1 - i_0}{2\sigma_0}\right), \tag{2.1}$$

where $Q(x) = (2\pi)^{-0.5}\int_x^\infty \exp(-u^2/2)\,du$, i_1 and i_0 are the average photo-currents corresponding to marks and spaces respectively, and σ_0 is the standard deviation of an additive Gaussian noise source. Given that the noise variance is constant, the performance is completely determined by the distance $d_{1,0}^{ini}$ ($d_{1,0}^{ini} = i_1 - i_0$) between the two symbols in the one-dimensional signal space. Note that the bit error probability can simply be expressed through the pair-wise error probability for the two constituent symbols $P_e\{1 \to 0\}$ under a rationale that an error in detection is going to be made provided that a noise sample is larger then the half of the separation between the two symbols in the signal space. The argument of the Q function can be rewritten as:

$$\rho = \frac{d_{1,0}^{ini}/2}{\sigma_0}. \tag{2.2}$$

In the presence of ISI, the distance $d_{1,0}^{ini}$ in the numerator of Eq. (2) is reduced as the optical energy is transferred from marks to spaces[4]. To first order, when a fraction of

[4] Note that the transfer of the optical energy, after (photo-) detection is equivalent to the diminution of difference electrical currents corresponding to marks and spaces.

the mark energy δ leaks out of an isolated mark, the resulting distance between the two symbols, $d_{1,0}^{ini}$, is reduced to:

$$d_{1,0} = d_{1,0}^{ini} \cdot (1 - 2\delta) \quad . \tag{2.3}$$

In order to fully quantify the performance degradation, it is necessary to take into account all possible bit combinations and average the resulting pair-wise probabilities of error. All of the pair-wise error probabilities have the Q-function dependence from Eq. (2.1). However, for the high signal to noise ratios (SNRs) typically used in optical communications, owing to the sharp descent of the Q function, the total performance is dominated by the worst case scenario of Eq. (2.3), i.e., the separation between an isolated mark and an isolated space. The isolated mark (space) is defined as a mark (space) preceded and followed by at least as many spaces (marks), as the span of ISI. We define the span of ISI as the number of bit-slots on one side of an isolated mark whose energy content is larger than 1% of that in the proper mark time-slot after propagation. As an example, assume that an isolated mark has broadened such that its tails extend to two extra bits on each side. We define the "span of ISI" in this case is 2 bits. Because spreading affects both past and future pulses in the single-mode fiber channel, one isolated mark would occupy 5 signaling intervals (its proper bit-slot plus 2 bit slots on each side). Thus, of all the possible patterns, the distance between an isolated mark and an isolated space is the smallest. We define this distance as $d_{1,0}$. Fig. 2.1 displays the evolution of $d_{1,0}$ at 10Gb/s as a

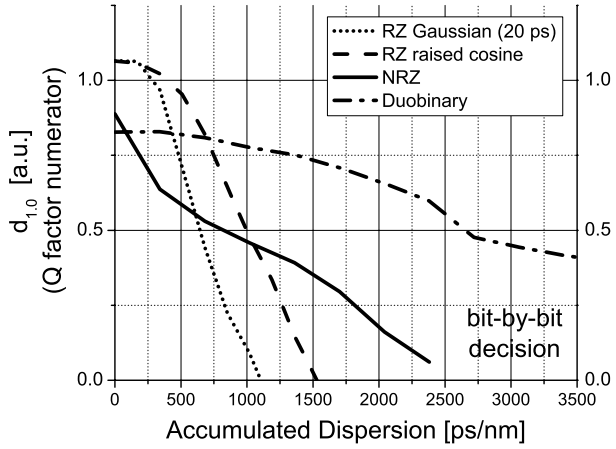

Fig. 2.1 Evolution of the bit-by-bit signal space minimum distance $d_{1,0}$ for four different information-bearing pulse shapes: RZ (2 pulse widths), NRZ and RZ

function of the accumulated dispersion for three different modulation formats: Return-to-zero (RZ) – simulation was performed for two different pulse shapes (see Fig. 2.1); non-return-to- zero (NRZ); Duobinary (DB) [27]. The results were generated assuming equal average launch powers for all four modulation formats. This constraint causes $d_{1,0}$ for NRZ and DB modulation to be initially slightly smaller than for RZ pulses. In the back-to- back case, for NRZ, this degradation is attributed to the finite rise-time and partial energy leakage into bit-slots where spaces reside. In the case of DB, the reduction in $d_{1,0}$ is caused by the side-lobes that appear in 0-bit slots as a consequence of filtering, and deteriorates the performance in the initial stages of propagation [27-29].

As the amount of the accumulated dispersion increases, the performance for all four formats deteriorates [30]. The rate of deterioration is a function of the spectral

power density (SPD) width, with DB modulation [27] providing the largest dispersion-limited reach of the four formats because of an approximate factor of two reduction in the width of the transmitted PSD with respect to NRZ (and a factor of 4 with respect to RZ) [31].

We first examine the effect of ISI in a noiseless scenario. Broadening of the waveforms beyond their pre-assigned bit-slots can be interpreted as the introduction of correlation between the adjacent information bits, which are assumed to be initially uncorrelated and independent. Conversely, the response in any given bit slot is defined by the information content transmitted in the preceding bit-slots, as well as the signaling intervals immediately following the monitored bit-slot. Therefore, the number of possible channel responses depends on the temporal span of the waveforms and is directly related to the link distance. Quantitatively, if the input pulse shape is symmetric, and the ISI spans m bits, there will be 2^{2m+1} possible responses. If the original pulse is not symmetric, which may be the case in practice, there will be 2^{m+n+1} possible responses assuming that ISI spans past m and n subsequent bits. Alternatively, the span of ISI can be defined as $\max\{m,n\}$. For the remaining part of the, we shall assume that the input pulses are sufficiently symmetric such that that m = n in the previous relationship.

The ISI due to GVD is a deterministic phenomenon. Therefore, the responses at any given distance of propagation are static if the communication channel is time invariant. Consequently, in the absence of noise, and over time scales short with

respect to the time scale of stochastic variations of the channel, it is always possible to retrieve the information from an ISI-corrupted signal, provided the channel does not produce ambiguous responses for different inputs. To retrieve the information, it is no longer sufficient to make the decision on a bit-by-bit basis, but to take into account as many bits as dictated by the channel memory. In our case, this is approximately twice the span of the ISI. Therefore, in the simplest realization, after the receiver is properly trained, the information in an ISI channel can be retrieved by correlating the received signal against each of the known responses.

The introduction of noise implies that it will generally not be possible to map the received signal into the set of "known" responses without a finite probability of a symbol error. In general, minimization of the error probability leads to the maximum likelihood (ML) test [8,32]. If the signals are corrupted by both ISI and noise, the ML test can be extended to include the effects of the channel memory (or the deterministic correlations). It has been proven [33] that for ISI channels with AWGN and no compensation, or the incomplete compensation of the channel ISI characteristics, the optimal receiver that minimizes the sequence error probability is the Maximum Likelihood Sequence Estimation (MLSE) receiver. The bit-error minimization leads to the maximum *a posteriori* (MAP) receiver and the BCJR algorithm [34]. However, in practice, the BCJR algorithm was abandoned for application to ISI channels without error correction coding due to its substantial complexity and memory requirements, which do not yield significant performance

improvement compared to the sequence error minimization. Therefore, MLSE is equivalent to the detection of 2^{2m+1} signals in noise. If the transmitted sequence consists of N bits, the suggested receiver would have to calculate and compare 2^N likelihoods in the case of a binary input alphabet. However, it has been realized by Viterbi, Omura and Forney [35-36] that in cases when the communication system responses include correlations (e.g., through ISI, and/or error correction coding), the search for the most likely transmitted information sequence can efficiently be solved in terms of a dynamic programming problem taking advantage of the Viterbi algorithm (VA). The VA reduces the computational complexity of the search for the global minimum of the possible likelihood functions from an exponential to a linear problem with respect to the sequence length. The VA, on the other hand, introduces an exponential complexity, $O(2^{2m+1})$, with respect to the channel memory, which is typically much smaller than the sequence length. The latter property identifies the limit on the hardware implementation of VA in practice. Having briefly reviewed the theoretical background, we next investigate the application of the MLSE approach to the case of intensity modulated fiber optic links.

2.3. MLSE in fiber optic links

In contrast to RF communication systems that perform linear detection of amplitude and phase, optical communication systems employ non-coherent square-law (i.e. nonlinear) detection whose output is proportional to the magnitude squared

of the optical field. Due to nonlinear square-law detection, the MLSE approach cannot be directly transferred from RF applications, but needs to be modified to make it applicable in optical communication systems.

As stated in the previous section, MLSD in the IMDD optical links dominated by detector thermal noise is equivalent to detection of 2^{2m+1} signals in Gaussian noise. The optimal receiver in this case is a bank of 2^{2m+1} matched filters in the electrical domain [8]. The output of this filter-bank is an input for the VA. In contrast to the optimal structure above, we analyze a vastly simpler, suboptimal, scheme that relies on a single integrate-and-dump filter.

The continuous detected signal $\rho(t)=y(t)+n(t)$ includes the noiseless signal $y(t)$, and additive noise component $n(t)$ having a power spectral density $N_0/2$. This signal, $\rho(t)$, is then integrated and sampled periodically every T seconds (T being the bit period), resulting in a sequence of samples $\{\underline{r}(kT)\}$ ($k = 1, \ldots, M$ for a sequence of M bits) of the integrated signal and noise. The system model is illustrated in Fig. 2.2. The noise variance, resulting from the linear filtering operation of the integrate-and-dump circuit is $\sigma_0^2 = N_0 T/2$. In addition, noise samples from different bit-slots are

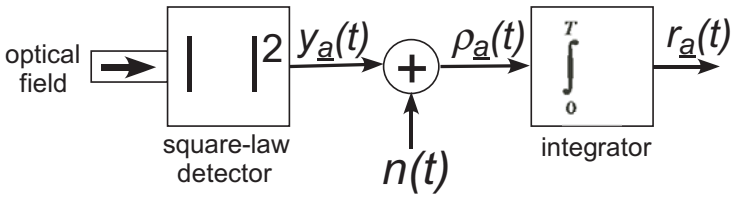

Fig. 2.2 System block diagram

independent and hence the joint conditional probability density function (PDF) can be represented as the product of the marginal PDFs corresponding to each one of the *M* bit slots. The conditional probability that a sequence of samples $\underline{r}$ was received, given that a sequence of noiseless responses $\underline{s}_{\underline{a}}$ (corresponding to the sequence of information bits $\underline{a}$) was transmitted, can be expressed as:

$$f_{R|S_{\underline{a}}}(\underline{r} \mid \underline{s}_{\underline{a}}) = \prod_{k=1}^{M} \exp\left[-\frac{\left(\underline{r}(k) - \underline{s}_{\underline{a}}(k)\right)^2}{N_0 T} \right]. \tag{2.4}$$

It is customary to introduce the log-likelihood function, defined as:

$$\phi_{R|S_{\underline{a}}}(\underline{r} \mid \underline{s}_{\underline{a}}) = \log\left[f_{R|S_{\underline{a}}}(\underline{r} \mid \underline{s}_{\underline{a}}) \right] = -\frac{1}{N_0 T} \sum_{k=1}^{M} \left(\underline{r}(k) - \underline{s}_{\underline{a}}(k)\right)^2 . \tag{2.5}$$

The sum of squares of the difference of vectors in Eq. (2.5) can be compactly represented as an *l-2* (Euclidean) norm of the difference of vectors $\underline{r}$ and $\underline{s}_{\underline{a}}$, yielding:

$$\phi_{R|S_{\underline{a}}}(\underline{r} \mid \underline{s}_{\underline{a}}) = \log\left[f_{R|S_{\underline{a}}}(\underline{r} \mid \underline{s}_{\underline{a}}) \right] = -\frac{1}{N_0 T} \left\| \underline{r} - \underline{s}_{\underline{a}} \right\|_2^2 , \tag{2.6}$$

where $\left\| \underline{x} \right\|_2^2 = \sum_{i=1}^{M} x_i^2$. The log-likelihood function in (2.5) or its equivalent form in Eq. (2.6), defines the metric that is used by the VA. The complete process can be interpreted as a search for a sequence of noiseless responses that is closest, in the Euclidean sense, to the received signal vector. Note that the form of the log-likelihood function [Eqs. (2.5)-(2.6)] is determined by the PDF of the noise statistics.

In order to use the VA, which is essential to reduce the computational complexity of the problem, the function whose extremum is to be determined must

be an additive quantity. By applying the natural logarithm to Eq. (2.4), the product of marginal PDFs is converted to a sum, and the problem is reduced to the form appropriate for dynamic programming (i.e., the VA). We stress that the joint probability of a sequence of bits can be expressed in terms of the product if and only if the noise samples are independent. Consequently VA is an optimal algorithm for sequence detection solely under the condition that the joint PDF can be factored on the bit-by-bit basis.

2.3.1 **Probability of Error and Performance**

From a theoretical perspective, the VA is an appealing procedure as it lends itself to an elegant error analysis. With the Euclidean distance interpretation of Eq.(2.5), the event that the VA has chosen an incorrect sequence, i.e., other than the one that had actually been transmitted, means that the Euclidean distance from the received vector to the incorrect, (i.e., erroneous) sequence is smaller than that to the correct one. Thus, the probability that an incorrect sequence is chosen by the VA is related to the (Euclidean) distance between the two sequences $d(s_1, s_2)$ [8]:

$$d^2(\underline{s}_1, \underline{s}_2) \triangleq \left\| \underline{s}_{\underline{a}_1} - \underline{s}_{\underline{a}_2} \right\|_2^2 \tag{2.7}$$

where $\underline{s}_{\underline{a}_1}$ and $\underline{s}_{\underline{a}_2}$ are two sequences of noiseless responses corresponding to the two information sequences $\underline{a}_1$ and $\underline{a}_2$. Specifically, in the case of AWGN with a noise variance $N_0 T/2$, we can now express the pair-wise error probability between sequences $\underline{s}_{\underline{a}_1}$ and $\underline{s}_{\underline{a}_2}$ as [8]:

$$P\{\underline{s}_1 \to \underline{s}_2\} = P\{\phi_{\underline{a}_1+\underline{e}} > \phi_{\underline{a}_1}\} = Q\left(\frac{d(\underline{s}_1, \underline{s}_2)}{\sqrt{2N_0T}}\right) \equiv Q\left(\frac{d(\underline{e})}{\sqrt{2N_0T}}\right). \quad (2.8)$$

The binary vector $\underline{e}$ satisfies the modulo 2 addition relationship $\underline{a}_2 = \underline{a}_1 \oplus \underline{e}$ that mathematically describes the error event of mistaking a binary information sequence $\underline{a}_1$ for $\underline{a}_2$. The end result of the analysis provided in the Appendix A are upper and lower performance bounds [37-38]:

$$\psi''(d_{\min}) \cdot Q\left(\frac{d_{\min}}{\sqrt{2N_0T}}\right) \le P_e \le \psi'(d_{\min}) \cdot Q\left(\frac{d_{\min}}{\sqrt{2N_0T}}\right), \quad (2.9)$$

where d_{min} is the distance between the most closely spaced sequences in the signal space; ψ' and ψ'' are weighting factors incorporating probabilities of all minimum distance error events, as well as the number of errors caused by these events. The contributions of the multiplicities ψ' and ψ'' to the bounds in Eq. (2.9) are significant only at low SNR's, while at the interval of interest in optical communications, i.e., moderate to high SNR, the bounds converge tightly, with the performance of the sequence estimation being uniquely defined by the most closely spaced sequences in the signal space, i.e., those separated by the distance d_{min}. Note that once the system parameters are fixed (input pulse shape, link distance, filter characteristics at the receiver), d_{min} is determined as well, such that this parameter can efficiently be used to predict system performance. Note also that, since the MLSE approach minimizes the probability of error, d_{min} can be used to assess (or upper bound) the penalty due to

using other suboptimal processing techniques such as Decision Feed-Back Equalization (DFE).

Fig. 2.3 displays the performance curves (BER vs. SNR) for a NRZ signaling format with four different amounts of accumulated dispersion. The (electrical) SNR is defined as the ratio between the average electrical power (average power of the M possible noiseless responses s_i) and the noise variance:

$$SNR = \frac{\frac{1}{M}\sum_{i=1}^{M} s_i^2}{\frac{N_0}{2}T}, \tag{2.10}$$

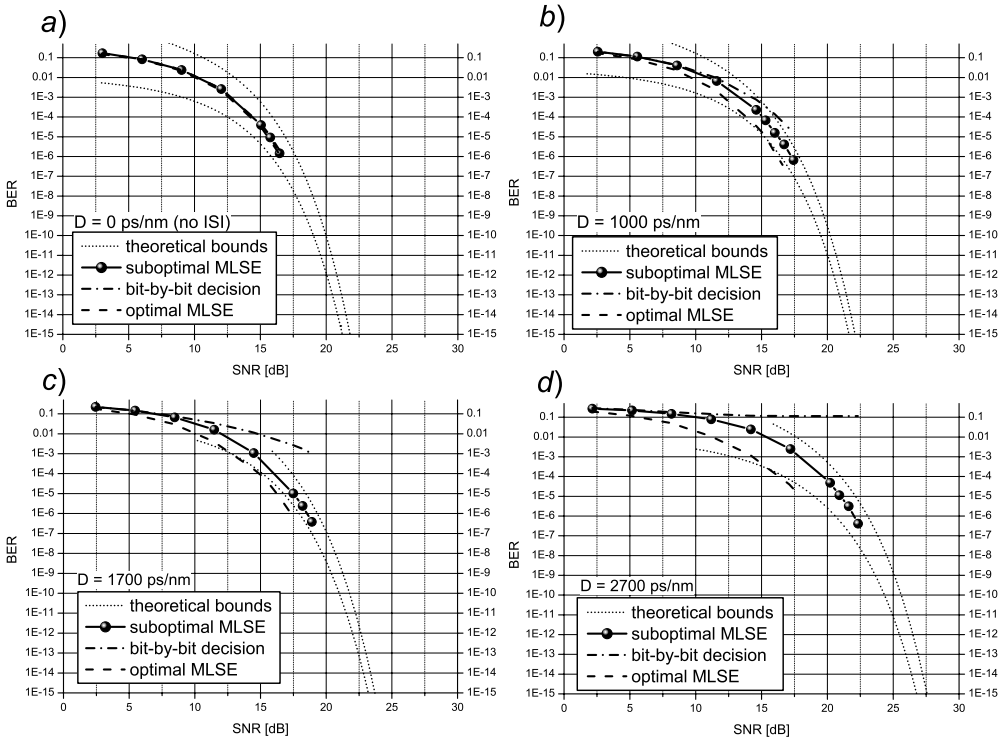

Fig. 2.3 Performance of MLSE at four different propagation distances. Overlaid with the results are the error bounds calculated according to Eq. (2.9)

hence the 3 dB difference to the common BER at back-to-back defined by Eq.(1). In addition, each of the graphs contains the analytical error bounds, as well as the performance of a bit-by-bit receiver. The dashed line in Fig. 2.3 corresponds to the case of the optimal MLSE approach described in [23]. The maximum propagation distance in Fig. 2.3d (160 km, i.e., DL=2700 ps/nm in SMF-28) corresponds to the propagation length at which the eye becomes completely closed ($d_{1,0} = 0$). In the case of RZ data, this occurs at approximately 70 km in an SMF fiber (equivalent to the accumulated dispersion of 1190 ps/nm), for a data rate of 10 Gb/s. The curves in Fig. 2.3 were generated for an idealized modulator with a short rise time that initially reduces the energy leakage to adjacent bit slots. This idealization was done intentionally to isolate the effect of ISI due to chromatic dispersion from that originating from the modulator imperfections. In the back-to-back case with no ISI, the performance of bit-by-bit decision is the same as that of the MLSE, and all three curves in Fig. 2.3(a) coincide. Two trends can be noticed in Fig. 2.3: (i), the larger the accumulated dispersion, the greater the difference between bit-by-bit and MLSE receiving strategies. The difference in performance is most pronounced in Fig. 2.3(d) where the eye is completely closed, such that bit-by-bit decision completely fails. On the other hand, at this distance, sequence estimation is still capable of recovering the information in this extreme case of ISI. The second important feature is that the power penalty of MLSE (from the back-to-back case) increases with distance. This fact

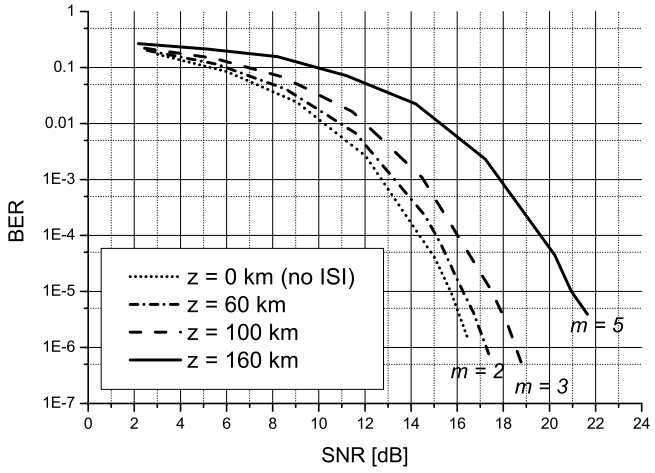

Fig. 2.4 Performance comparison of MLSE equalized links with different amount of accumulated dispersion from Fig. 2.3

is illustrated in Fig. 2.4 where the NRZ performance curves from Fig. 2.3 are superimposed. For an error rate of 10^{-6}, MLSE requires 6 dB more power relative to the dispersionless case (i.e. the input) to detect the data at the same BER. The error bounds in Fig. 2.3 were calculated using Eqs. (A5) and (A9). In each case, the corresponding d_{min} was found through an exhaustive search in the signal space, facilitated by the relatively small span of ISI (up to 5 bits). Note that according to Eq. (2.9), the power penalty is expressed in the amount of the reduction of d_{min}^2. The resulting histograms of signal space distances for the same four cases used in Fig. 2.3 are shown in Fig. 2.5. As illustrated in Fig. 2.5(a) – (d), the sequence separation distributions shift toward the smaller values with propagation distance, resulting in an increased power penalty with respect to the back-to-back case with no ISI. This result is in accord with intuition, since the information-bearing waveforms become

more broadened and uniform in shape as they propagate, making it more difficult to be distinguished and hindering the detection process. From the signal space point of view, the responses occupy a smaller volume of the signal space, and their number increases with propagation since the span of ISI is augmented. As a consequence, d_{min} is reduced, and the system performance is irreversibly degraded.

The importance of the error bounds in Fig. 2.3 is twofold. First, they provide a check of the simulation results. Second, owing to the convergence of the bounds [8,39-40], they facilitate the performance evaluation at low BER's. For a completely closed eye, i.e. $d_{1,0} = 0$, in order to attain the BER of 10^{-12}, an (electrical) SNR of 25 dB is

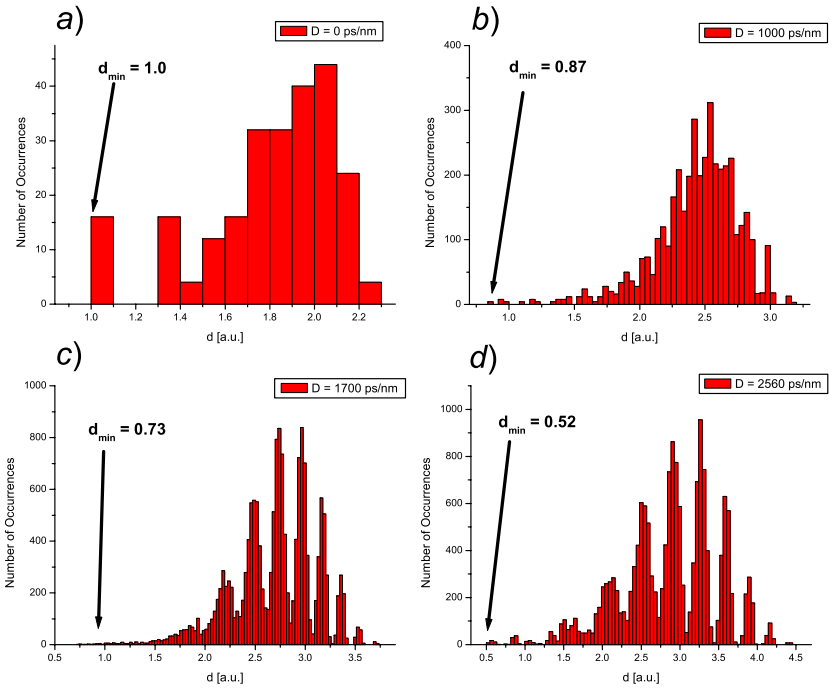

Fig. 2.5 Signal space distance histograms for four different amounts of accumulated dispersion from Fig. 2.3.

necessary. This power penalty of 6 dB is a consequence of the equal amount of reduction in d_{min}^2 with respect to the back-to-back case. Note, however, that the cited large power penalty corresponds to the extreme case of a complete eye closure. The optical communication system performance degradation due to the ISI is severe even at small amounts of the information-bearing optical pulses broadening, and in these cases, the power penalties of the MLSE approach, are considerably smaller, as illustrated in Fig. 2.4.

The results above were derived for a suboptimal integrate-and-dump receiver. While the optimal detector, consisting of a bank of matched filters, outperforms the much simpler receiving scheme under consideration, since it maximizes the signal to noise ratio, simulations indicate a surprisingly small power penalty for the suboptimal detector (see dashed lines in each of the four parts of Fig. 2.3). In the back-to-back case, with no ISI, (Fig. 2.3*(a)*) for the NRZ format, the integrator is the matched filter, and the optimal MLSE performance coincides with the suboptimal approach (as well as with bit-by-bit detection). Note that the previous statement assumes an idealized modulator with short rise-time that does not allow mark energy leakage to adjacent bit-slots before transmission. The results in this section were intentionally generated for an idealized modulator to make a clear (theoretical) comparison between bit-to-bit decision MLSE and the performance of the optimal receiver. In a realistic setting, the three performance curves in Fig. 2.3*(a)* do not coincide. The penalty for sub-optimality at back-to-back amounts to 0.5 dB, whereas

due to a finite modulator rise time, the difference in performance between bit-to-bit and MLSE is on the order of 1 dB (see Fig. 2.1). In all other simulation results presented in this Chapter (Sections 2.2. , 2.4. 2.5.), this idealization was not used. When ISI is present, d_{min} for the suboptimal scheme is somewhat smaller then that for the theoretically optimal receiver [8,23]. The resulting power penalty for the suboptimal integrate-and-dump receiver ranges from 1 to 2 dB for RZ waveforms. For NRZ waveforms, the power penalty has the same magnitude and can be as high as 3 dB for a completely closed eye when the ISI spans 5 bits. These results indicate that the performance loss using sub-optimal detection is unexpectedly small, given the reduction in the receiver complexity. The small power penalties can be intuitively explained by noting that the information carrying waveforms are broadened in the dispersive optical channel. Therefore, the matched filters corresponding to these broadened signals tend towards the uniform amplitude shape equivalent to the integrate-and-dump filter, reducing the overall power penalty. Our reasoning is supported by the calculation of the average SNR reduction caused by the utilization of a mismatched filter. The calculated reductions closely match the deviation from optimality. This small distance from optimality implies that there is little to be gained from oversampling the output of the integrate-and-dump filter in the thermal noise dominated system. The extreme case of oversampling is the matched filter, which is the largest possible achievable improvement. However, the matched filter performs

only on the order of a dB better than the receiving structure under consideration, which renders the gain from oversampling negligible.

We conclude this section with a discussion on the MLSE performance in the presence of polarization mode dispersion (PMD). In the case of time varying ISI, such as in the case of PMD, tracking and periodic updating of the lookup tables used by the VA is necessary. PMD tends to additionally spread the waveforms and consequently, according to the previously presented analysis, reduce d_{min}. However, the effect of PMD at speeds and lengths considered in this dissertation (10 Gb/s and lengths below 200 km) is much smaller than the effects of chromatic dispersion. Quantitatively, according to the responses generated by the VPI Transmission Maker PMD models [41], d_{min} is reduced by approximately 0.1-0.2 dB for a differential group delay of 30 ps when the accumulated dispersion is equal to 1900 ps/nm. For performance improvement due to MLSE in systems limited by PMD induced ISI, the reader is referred to Refs. [23-24].

2.4. Performance of MLSE in Conjunction with Different Modulation Formats

In this section, we investigate the dependence of the MLSE performance on the modulation format used. We consider three popular modulation formats in a 10 Gb/s scenario: RZ (2 shapes: (i) Gaussian with full width at half maximum (FWHM) of 20 ps and (ii) raised cosine shape (FWHM of 50 ps); non-return-to-zero (NRZ)

format; and the duobinary (DB) [27] format. The performance of these formats with bit-by-bit decision was examined in Section 2.2. (see Fig. 2.1). The raised cosine function, mentioned above, for a roll-off parameter α, on a unit time interval is defined as:

$$p(t)=\begin{cases} 1 & ,0\le|t|\le\dfrac{1-\alpha}{2} \\ \dfrac{1}{2}\left\{1+\cos\left[\dfrac{\pi}{\alpha}\left(|t|-\dfrac{1-\alpha}{2}\right)\right]\right\} & ,\dfrac{1-\alpha}{2}\le|t|\le\dfrac{1+\alpha}{2} \\ 0 & ,|t|\ge\dfrac{1+\alpha}{2} \end{cases} \tag{2.11}$$

The relative performance of MLSE for different modulation formats was determined by calculating d_{min} as a function of the accumulated dispersion for each format. Finding d_{min} is a difficult optimization problem. We applied well established techniques [3,42-43] for determining d_{min} for accumulated dispersion up to 3500 ps/nm. The results are shown in Fig. 2.6. Note that the ordinates in both plots are in the same interval of values, permitting direct comparison. The slight performance deterioration in the initial stages of propagation for DB and NRZ, mentioned in Section 2.2. , disappears when MLSE approach is used, and the performance of all four pulse shapes is virtually the same for those short propagation distances (see Fig. 2.6).

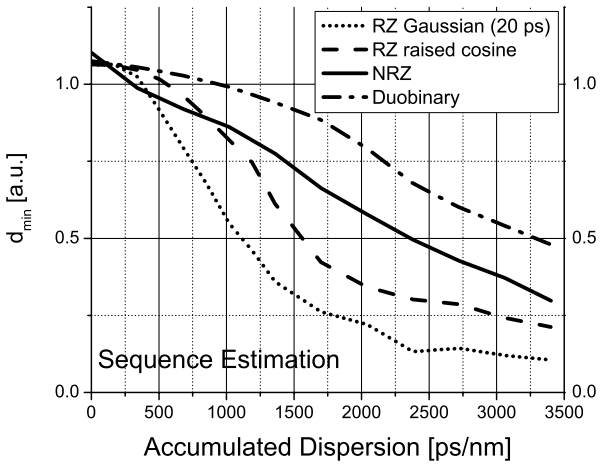

Fig. 2.6 Evolution of MLSE signal space minimum distance d_{min} for four different modulation formats represented in Fig. 2.1 under bit-by-bit decision

The application of MLSE to both duobinary and NRZ considerably reduces the difference in performance between the two formats, relative to bit-by-bit detection. The substantial performance improvement for NRZ comes at the cost of a considerably more complex VA, since the span of ISI for this format is larger than that for doubinary. Therefore, Fig. 2.6 defines a clear engineering trade-off between the complexity of the transmitter necessary for the modulation format, the complexity of the receiver structure, and the amount of launched power.

The results of this section can also be cast in terms of signal space concepts introduced earlier. As a general rule [8], the probability of error in an AWGN channel for moderate to large SNR is determined by a minimum distance d_{min} in the signal space. The main difference between Eq. (2.2)and Eq. (A6) in the Appendix A is that, due to ISI, the MLSE signal space becomes multidimensional. The signal space of the

bit-by-bit detection is one-dimensional, and is a projection of the MLSE space onto a single dimension. The minimum distance for the bit-by-bit detection is therefore necessarily constricted and eventually goes to zero when the eye completely closes (i.e., $d_{1,0} = 0$) (see Fig. 2.1), whereas d_{min} for the higher dimensional space can still be non-zero. Therefore, MLSE is able to extract the information from the ISI corrupted signal even when the eye is completely closed as illustrated in Fig. 2.1 and Fig. 2.6.

2.5. Performance with A/D conversion

The preceding discussion assumed continuous detected quantities. A practical system has to rely on the A/D conversion of the output of the receiving filter. To analyze the effect of quantization, the output of the detection filter was quantized to 2^n output values, where n is the number of quantization bits. The discretization was performed such that the quantization thresholds uniformly divided the range of available continuous responses to mimic the automatic gain control (AGC) usually preceding the A/D block. A typical behavior of the SE algorithm working on the discretized samples is displayed in Fig. 2.7. When the A/D resolution is insufficient (2 quantization bits in Fig. 2.7), an error floor is evident in the performance curves. However, as the number of the available quantization levels is increased, the performance gradually tends to that obtained in the continuous case shown in Fig. 2.3.

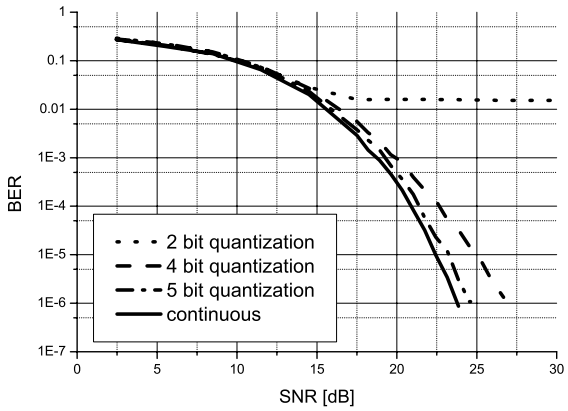

Fig. 2.7 Performance of MLSE under A/D conversion for 2, 4 and 5 quantization bits. In solid line performance under infinite resolution is included for comparison

A quantitative treatment of the performance degradation due to A/D conversion is a difficult task for the substantial amounts of ISI treated in this work. The analysis must include the calculation of the penalty due to the discretization effect of the underlying Gaussian process that can result in statistics that may be considerably different from Gaussian, especially for a low-resolution quantization [44]. Instead, we consider the effect of quantization on the minimum distance d_{min}. Fig. 2.8 shows the change of d_{min} as the number of the available quantization bits is increased. The minimum distance ascends from the value of zero, which corresponds to the existence of an error floor, towards the continuous case (dashed circle in Fig. 2.8) that is an upper bound on the performance. For low-resolution A/D conversion, the quantization noise dominates and the theoretical ML metric is no longer Euclidean [44-45]. The fact that the Euclidean metric is not appropriate is

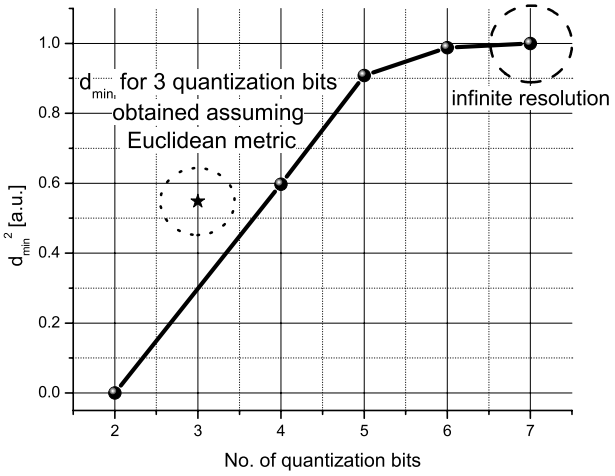

Fig. 2.8 Effect of quantization on d_{min} at 160 km. Inside the dotted circle the infinite precision dmin is included for comparison.

illustrated by the d_{min} value obtained for three bits of quantization shown in Fig. 2.8, which is substantially different from the one corresponding to the simulated performance in Fig. 2.7. However, at reasonable resolutions (q > 3 in Fig. 2.8), the Euclidean metric becomes close to the optimal 29, and calculated values in Fig. 2.8 match more closely to the simulated MLSE performance including the A/D conversion shown in Fig. 2.7.

The results of numerical simulations on the finite quantization effect are summarized in Table I, which contains power penalties in dB, for a given span of ISI, for three modulation formats under consideration. The general trend in performance with respect to the number of quantization bits is that more resolution is necessary for a larger extent of ISI. This trend stems from the fact that an increased span of ISI

Table 1. Power penalties incurred by a/d conversion depending on the accumulated span of ISI for three modulation formats

	ISI span	# of quantization bits				
Format		2	3	4	5	6
RZ	1	∞	1.4	0.4	0	-
	2	∞	5.5	1.5	0	-
NRZ	2	1.8	0.1	0	-	-
	3	∞	2.1	0.6	0.2	-
	5	∞	15	1.5	0.1	-
Duobinary	2	∞	2.1	0.9	0.1	-
	3	∞	11.9	1.5	0.4	-
	4	∞	∞	8.7	1.2	0.5

implies a larger number of channel noiseless responses (2^{2m+1} for the span ISI of m), therefore, finer resolution is required to enable the distinction between these responses. At the distance of eye-closure (span of ISI of 2 bits for RZ, and 5 bits for NRZ), RZ and NRZ modulation formats require four and five bits of A/D conversion, respectively, to operate at approximately 1 dB from the continuous case. However, owing to the different evolutions of the waveforms for the two signaling formats, the NRZ format is less stringent on the necessary number of quantization bits, regardless of the distance. The cause of this phenomenon can be determined by investigating how the noiseless responses are distributed. Fig. 2.9 shows a comparison of noiseless response distributions for the DB and the NRZ formats. While the DB (and RZ) responses tend to be distributed uniformly in the given interval of values, the NRZ responses tend to cluster into bands. The band-like structure reduces the penalty due to the A/D conversion as the discretized quantities behave similarly to their continuous counterparts. To elucidate how waveforms evolve with dispersion, we

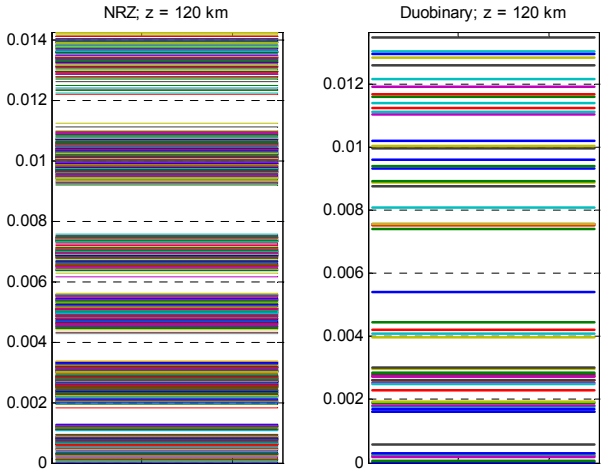

Fig. 2.9 Distribution of noiseless responses for NRZ (left) and Duobinary (right) for infinite resolution. This figure emphasizes bunching of responses for NRZ leading to a smaller requirement of quantization bits for the same span of ISI. Also see Fig. 2.5(c)-(d)

draw the analogy between dispersion in the time domain and diffraction in the space domain [5, 46]. The flat top associated with NRZ waveform under the influence of chromatic dispersion (which is equivalent to diffraction in the far field) evolves as the input waveform Fourier transform, i.e. the *sinc* function, which has the major part of its energy contained in the main lobe. In the case of DB and RZ, due to the shape of their temporal spectra [46], energy leaks uniformly across the span of ISI resulting in the uniform distribution of the noiseless responses in Fig. 2.9b. The compactness of the band-like structure depends on the quality of the modulator. With steeper edges of NRZ waveforms and a higher extinction ratio of the modulator, more compact bands will form and a lower power penalty due to quantization will result.

The behavior described above implies that MLSE, used in conjunction with NRZ in a realistic setting with A/D conversion, has potential advantages over the

other formats. When the A/D conversion penalties are taken into account (for low-resolution A/D conversion), the overall difference in performance between the NRZ and duobinary formats is smaller than that shown in Fig. 2.6. It drops below 2 dB for realistic modulators at an accumulated dispersion of 3500 ps/nm when MLSE is performed on both formats. The difference in performance is substantially smaller (0.9 dB) for an ideal modulator whose responses are shown in Fig. 2.9. However, since the span of ISI grows at a higher rate for NRZ, a more complex VA is necessary for this modulation format. The better overall performance of DB is due to the slower rate of increase of the span of ISI with propagation distance. We conclude the theoretical part of this Chapter by concluding that the span of ISI is the determining factor for the power penalty due to the A/D quantization.

2.6. Experimental Validation

To test various aspects of MLSE detection for fiber optic systems, a proof of concept experiment was performed. A practical realization of the MLSE involves several different elements that are beyond the scope of our analysis (e.g., sequence locking and synchronization algorithms, fast A/D conversion, etc.). Consequently, an experiment that demonstrates the ability of the MLSE approach to process the real data was conceived isolating the above mentioned aspects. The diagram of the experimental setup is shown in Fig. 2.10. The training and pseudo-random patterns

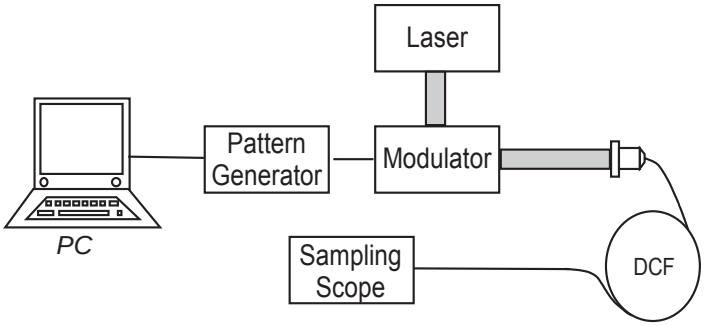

Fig. 2.10 Experimental schematic for the proof of concept experiment

were loaded into a pattern generator. The received signal was detected by an amplified detector, and the resulting waveforms were collected by a sampling oscilloscope triggered off the data sequence. To construct the lookup tables necessary for the operation of the VA, the waveforms were averaged to replicate the channel response in the absence of noise. Observe that the sole purpose of the sampling oscilloscope in the setup is that of an interface between the detector and the computer, which circumvents the need for fast electronics. Note also that the setup used, to a certain extent, duplicates the real system imperfections such as the timing jitter and power fluctuations. The received waveform for each of these patterns was collected and post-processed on a PC. The experiments were performed at OC-192 speed (10 Gb/s), at 1550 nm wavelength and with the accumulated dispersion of -1600 ps/nm, -2240ps/nm and -2700 ps/nm [corresponding to lengths of standard single-mode fiber (SMF-28) of 100 to 140 and 170 km]. Dispersion compensating fiber modules were used in the experiment instead of the standard single mode fiber in order to ensure sufficient SNR with DFB lasers at our disposal. The launched power

equaled 1.8 dBm in the first case and 3.8 dBm for the latter two cases. The received powers were -6.2 dBm, -10.4 dBm and -15.2 dBm, respectively. The noise characteristics of the channel were also collected. It was confirmed that, for the experimental conditions used (i.e., without optical amplifiers), the noise statistics were approximately Gaussian and signal-independent, thus justifying our hypothesis of the additive electrical noise dominant model, as well as the application of the Euclidian metric for the VA in Eq (2.6).

The sequence estimation was applied to two thousand pseudo-random 100-bit patterns in each case. The measured bit-to-bit BER in the first case was $6 \cdot 10^{-5}$, in the second $2 \cdot 10^{-2}$ and 0.14 in the last case. The decision threshold for the bit-by-bit decision was chosen as the mean value of the noiseless channel responses after the MLSE training was performed.

For MLSE, no errors were recorded in the first two cases, i.e. the measured BER was below 5×10^{-6}. In case of propagation on the equivalent length of 170 km, the BER employing MLSE was 3×10^{-5} with approximately four orders of magnitude improvement over the bit-to-bit BER. Fig. 2.11 shows the received eye diagram at -2700 ps/nm, for which MLSE BER was 10^{-5}, in contrast to the 10^{-1} raw bit-to-bit BER. Note that in all three cases, the experimental error rates were below 10^{-3}, which is considered the error correction threshold for fiber optic communication systems according to the ITU guidelines [47].

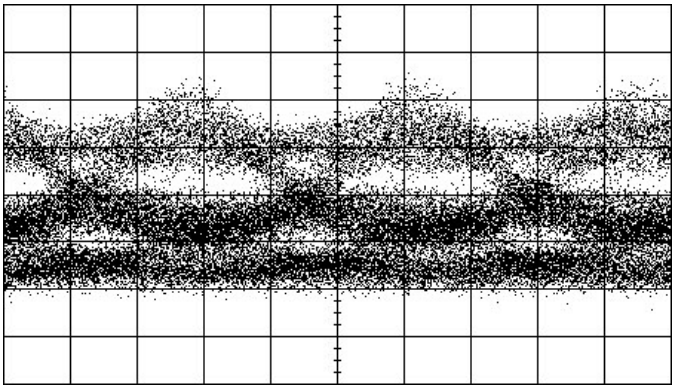

Fig. 2.11 Eye diagram at the negative accumulated dispersion equivalent to 170 km in SMF

2.7. Conclusion

In this Chapter, we have analyzed the performance of a suboptimal, but practical, MLSE receiver designed for short-haul intensity modulated fiber optic communication systems. The analysis was derived for the case of optical links where thermal noise originating from the detection process is the dominant noise source. In contrast to an optimal receiving strategy that relies on a large bank of matched filters, our study was based on a practical constraint of an integrate-and-dump circuit. We showed that the MLSE approach can retrieve the information from the ISI corrupted signal for substantial amounts of accumulated dispersion with an increase in complexity as well as launch-power. Simulations indicate that the power penalties associated with MLSE for NRZ data range from 0.2 dB (for distances around 20 km) to 6 dB at the distances 200 km when the eye is completely closed. It was found that

the suboptimal MLSE receiver performance is, on average, only 2 dB inferior in performance to an optimal matched filterbank, which is surprisingly small based on the significant complexity reduction in the receiving structure. The approach can substantially extend the dispersion limited reach for a variety of modulation formats.

The effect of the A/D conversion on the performance was also examined. It was found that without error-correction coding, for NRZ with a span of ISI of five bits, five quantization bits (32 levels) are required to provide performance within 1 dB of the continuous case. For RZ with a span of ISI of 2 bits, four bits of A/D conversion are necessary to keep the performance within the same margin above. The deciding factor on the number of quantization digits is the extent of ISI, as finer resolution is necessary to discern between an increased number of possible channel responses. Lastly, our proof-of-concept experimental verification supports the feasibility and the validity of the approach.

2.8. Acknowledgement

The text in the Chapter 2 in part is a reprint of the material as it appears in the *Optical Communication Theory and Techniques*. Alic, Nikola; Papen, George C.; Milstein Laurence B.; Siegel, Paul H.; Fainman Yeshaiahu. "Performance Bounds of MLSE in Intensity Modulated Fiber Optic Links," (E. Forrestieri, Ed.), Springer, 2005. The dissertation author was the primary researcher and/or author and the co-authors

listed in this publication directed and supervised the research which forms the basis for this Chapter.

Chapter 3

Sequence Estimation with Constrained Run-Length Coding In Directly Modulated Multi-Mode Fiber Optical Links

3.1. Introduction

In the previous Chapter, MLSE applied to short-haul single mode links was investigated. In this Chapter, we examine directly modulated multimode fiber based links. Multimode fiber links offer a low-cost solution for short-haul high speed data-communication, as well as optical interconnects [48]. In an attempt to further reduce the cost of these links, directly modulated lasers can be used at the transmitting end, instead of much more costly external modulation employed in single mode long-haul links. In particular, this Chapter will be focused on experimental demonstrations of MLSE equalized directly modulated multimode fiber links.

Before describing the experimental results, it is useful to briefly review the physical characteristics of the channel under consideration, pointing out specific differences from externally modulated single-mode-fiber based links, discussed in previous chapters.

3.2. Multimode fiber response

Unlike the single-mode fibers used in telecom, multimode fibers allow propagation of hundreds of electromagnetic modes. The specific characteristics of the modes, such as the transverse spatial pattern and group velocity, depend on the specific waveguide profile [5]. Unfortunately for communication purposes, the excited modes travel with substantially different group velocities, causing the splitting of a single launched optical pulse into multiple, slightly delayed, replicate pulses that develop within meters of propagation. Unless special care is taken most, or all of the allowed modes are excited when the light is coupled into a multimode fiber. A channel which produces a (possibly large) number of pulse replicas with different amplitudes and slightly different times of arrival at the receiver for each information bearing input pulse, in digital communications theory is defined as a *mulitpath channel* [7]. An important property of a multimode fiber response is the sensitivity of the mulitpath response (i.e. the distribution of the arrival times of the excited pulse replicas) to the launch conditions [49]. The modal spread can change by a number of bit signaling intervals depending on the exact conditions that light is

coupled into the fiber. Similarly, the span of ISI can be increased (or reduced) by several bits depending on the launch circumstances. At the bit-rates of interest (currently ~ 1 Gb/s – 2.5 Gb/s, whereas 10 Gb/s links are being developed), the modal-dispersion for a controlled launch limits the reach in multimode links to approximately 50 m [5]. Since the amount of dispersion is proportional to the distance traveled, the common figure of merit for multimode fibers is their bandwidth-distance product (BL). Legacy multimode fiber is characterized with low BL products typically on the order of 100 MHz-km, whereas newer multimode fiber achieves approximately 5 to 10-fold BL increase.

There are several existing approaches to mitigate the multimode impulse response (i.e. to reduce the time spread of the different mode arrival times at the receiver):

(i) Restricted launch and detection conditions: This approach takes advantage of employing precise launch conditions in an attempt of selective mode excitation. Alternatively, the detection can be performed in a similar manner, restricting spatial and/or temporal windows of the detector [50]. The idea behind this method is to prevent excitation of all supported modes, thus diminishing the temporal spread of the impulse response. This particular technique was demonstrated as early as 1998 [51], whereas recently spectacular results have been reported [52]. Note, however that this approach requires custom optical components, precise positioning systems, lasers, or

the combination thereof. This, together with the intricacy of coupling conditions that change from one fiber to another defeats the purpose of low-cost links that is a principle motivation for using multimode systems; Although the performance of communication systems in mulitpath channels in, for instance, wireless communications has been significantly improved by employing Multiple Input – Multiple Output (MIMO) techniques, such approaches have failed in multimode fibers. This was mostly due to the fact that it is virtually impossible to control coupling to (and detection of) a particular mode separately, making the MIMO approach nearly unfeasible. Secondly, energy can easily couple from one mode to another during propagation, such that the high degree of correlation exists between information contained in groups of modes after only tens of meters of propagation, making the channel unsuitable for classical MIMO approaches [54].

(ii) New generation multimode fiber. Carefully engineering (i.e., designing waveguide geometry and doping profile that control the exact index of refraction dependence along the fiber radius), novel multimode fibers having substantially larger bandwidth-length products (1-10 GHz-km) have emerged [53]. The larger BL product of this newly engineered multimode fibers allows longer dispersion limited reach [53];

(iii) Equalization. This ISI rich channel, as well as the relatively moderate data rates compared to telecom applications, made the multimode fiber channel an excellent candidate for equalization techniques. Numerous experimental demonstrations of equalization in multimode based links have been presented in the recent years. However, all of the demonstrations relied on analog FFE and DFE equalizers. These structures, however, tend to underperform in heavily noise-loaded conditions, often encountered in multimode fiber applications. In this section, we shall examine the application of MLSE, which, as noted previously, achieves optimal performance in these links that are dominated by Gaussian noise. An additional advantage of the equalization techniques is that they can be used in conjunction with any of the previous methods for group delay dispersion reduction mentioned above.

3.3. Data dependent VCSEL response and data-pattern DC balancing by 8b/10b code

Directly modulated lasers are normally used in data-communication MMF applications due to their low cost. A vertical cavity surface-emitting laser (VCSEL) is a specific type of a semiconductor laser, in which the lasing process is established in a cavity whose direction is orthogonal to the electrical current pumping the structure. The cavity is technologically realized by depositing multi-layered Bragg mirrors as a part of the growing process of the semi conductor laser. The combination of directly

modulated VCSELs and multimode fibers have been proposed to substantially reduce the cost of these links due to an increased reliability and high yields of VCSELs.

Recently, a deleterious effect in links incorporating VCSEL/multimode fiber combination was discovered. As discussed on a phenomenological level in [55], the VCSEL emitted spatial modes depend on the data pattern driving it. This slight change in the VCSEL-emitted spatial mode configuration represents an alteration in the launch condition for the multimode fiber. As discussed in Sec. 3.2. , slight changes

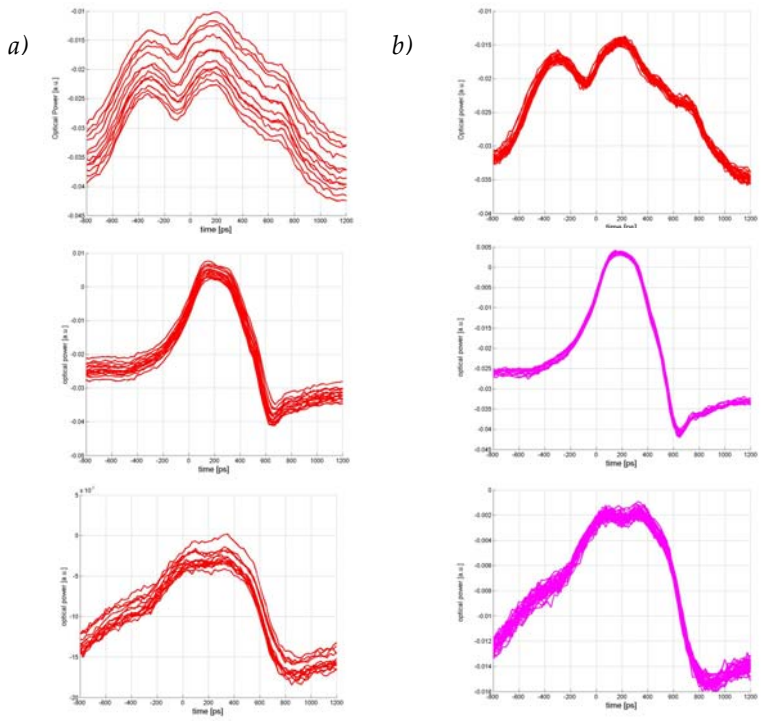

Fig. 3.1 Isolated Marks for three different launch conditions. (a) Random data. Substantial BLW in noticeable in the response; (b) Response for the same launch conditions after data have been encoded by a DC balancing 8b/10b code. A considerable mitigation of the BLW is achieved availing subsequent equalization

in the launch condition, can lead to substantial perturbation in the excited fiber modes. As an illustration, Fig. 3.1*a* shows experimentally obtained traces of isolated marks (surrounded by immediate five 0-bits on each side), enclosed by different random patterns (beyond the five – delimiting zeros). For obvious reasons, this effect was coined Base-line wander (BLW). As a consequence of this data-dependent VCSEL response, the overall communication channel response is non-stationary [55, 56]. Therefore, before any equalization technique can be applied, the effect of base-line wander has to be mitigated. The described pattern-dependent response entails VCSEL memory with respect to the data driving it. MLSE, as stressed in the previous Chapter, seems like a perfect solution to the problem, whereas, an additional memory of the channel as a whole encompasses the modal dispersion induced ISI, and the VCSEL memory. In fact this particular approach was proposed by Al-Sowayan and Lear in their original work on BLW [55]. However, we experimentally found, the memory of some VCSELs can span more than 20 bits, making the necessary underlying VA structure too complex for practical purposes. Thus, other means of mitigation are required.

To put BLW in an engineering perspective, one needs to bear in mind basics of the laser emitted power (P), driving current (I) characteristic shown in Fig. 3.2. In a

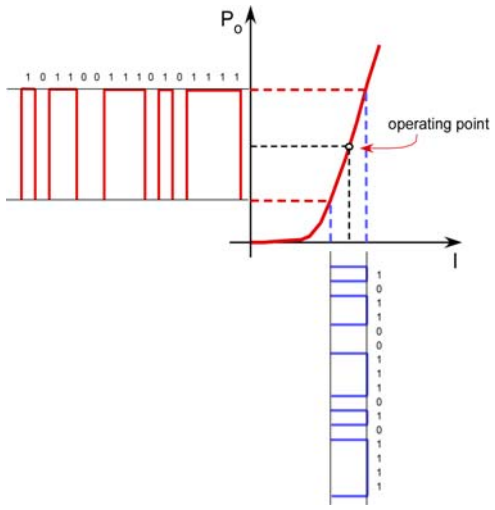

Fig. 3.2 Pictorial representation of direct modulation of a semiconductor laser

a directly modulated configuration, the emitted light can be modulated by applying signal modulation component directly to biasing current, thus affecting the emitted power and resulting in an intensity modulated laser output. However, if the data-pattern driving the VCSEL contains long consecutive strings of 1's and/or 0's, this local DC-imbalance of the data is equivalent to an additional DC-valued current that can cause a slight displacement of the operating point (See Fig. 3.2). As mentioned previously, this can lead to substantial differences in the response of the MMF/VCSEL system, since the effective additional DC term can change the launch condition. In order to mitigate the non-stationary VCSEL response, the data driving it need to be made DC-balanced. This can be achieved by imposing redundant bits, which depend on the transmitted information that will impose the DC balance on the information being supplied to a VCSEL as a driving current. In other words, by pre-

coding the information data-stream, it should be possible to achieve restriction of the operating point excursion, and consequently mitigate the VCSEL base-line wander and, as a result, reduce the pattern dependent effects.

For our experiment DC balancing was achieved using a well know 8b/10b code [57]. The 8b/10b code is a block-code, i.e. the encoding process is accomplished in terms of a table where every 8-bit block of the input data is encoded into a 10-bit block, according to the encoding table [57]. The 25% coding overhead is considerable. In order to retain the data throughput, the signaling speed needs to be increased by the same amount. However, at the speeds under consideration (2 Gb/s), this coding overhead does not represent serious trouble. In fact, 8b/10b code has been adopted as a part of XAUI standard for Gigabit Ethernet links [57] whereby the transmission is performed at a 2.5 Gb/s speed for the information stream of 2 Gb/s. Originally, the 8b/10b code was designed to facilitate synchronization in high-speed links by ensuring sufficient number of bit-transitions necessary for the clock-recovery. In our application, we took advantage of the fact that in addition to the mentioned 8b/10b property, in its original realization, this code also keeps track of the disparity between 1's and 0's, ensuring the same number of marks and spaces in any two consecutive encoded data blocks (20 bits). In effect, the application of the 8b/10 will achieve local DC balance for any 20 consecutive data bits, making it useful for our application. Fig. 3.1*b* shows the same isolated marks resulting from the three example launch conditions from Fig. 3.1*a*, with 8b/10b encoded data. As predicted, the imposed DC

balance significantly reduces the BLW to a level, where the channel responses are sufficiently repeatable to enable the application of equalization.

3.4. Experimental setup

The experimental setup is shown in Fig. 3.3. The laser was a 5 Gb/s Ulm electronics VCSEL (ULM850- 050TN-UT46FO) with a measured rise time of 70 ps for a 6 mA bias current and a differential resistance of 60Ω. The light was coupled into the fiber using a molded glass aspheric lens. Registration to the center of the fiber was accomplished by using a precision stage and a single mode fiber patch cord. The patch cord was subsequently replaced by the multimode fiber under test. The data-sequences were generated in a computer and downloaded into a 12.5 Gb/s HP 70843B pattern generator. The signal was detected using a 25 μm diameter New Focus 1580 detector. The resulting signal was then measured using an HP 83480A mainframe with an HP 83483A plug-in with an electrical bandwidth of 20 Ghz and 8 bits of resolution, triggered off the data sequence from the pattern generator.

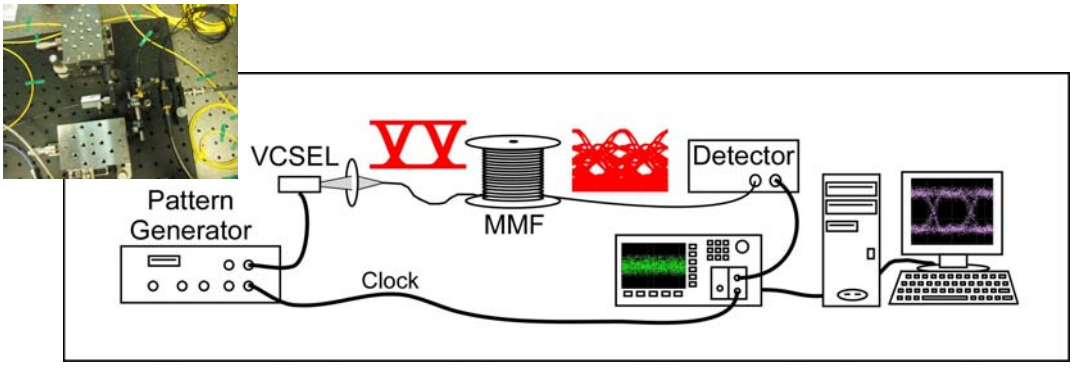

Fig. 3.3 Experimental setup for MLSE demonstration in multimode fiber links. The inset shows a photograph of the actual VCSEL mount.

The experimental procedure is as follows. First, training sequences of 100 bits were transmitted to gather possible channel responses. The received training signal, $r_i(t) = s_i(t) + n(t)$ was averaged to remove the effects of noise. The averaged sequences were subsequently integrated on a bit-by-bit basis, to produce the "noiseless" responses, stored in a computer, and used for sequence estimation processing. The training sequences also established the synchronization reference. After training, a test data-set was generated that consists of sequences of 80-bit blocks of random data. A block of data is next encoded using an 8b/10b code, resulting in a 100 bit sequence. This 100 bit sequence is transmitted through a fiber span. The detected waveforms were stored in the sampling scope producing 35-samples per bit with 8 bits of resolution per sample. These samples are then re-binned to replicate an n-bit flash A/D and are summed to replicate an integrate-and-dump filter. The resulting n-bit discrete sequence is the input to the Viterbi algorithm that determines the most likely transmitted sequence of information bits. The noise on the test data will produce errors. The test procedure ran until 100 errors have occurred in the processing, or

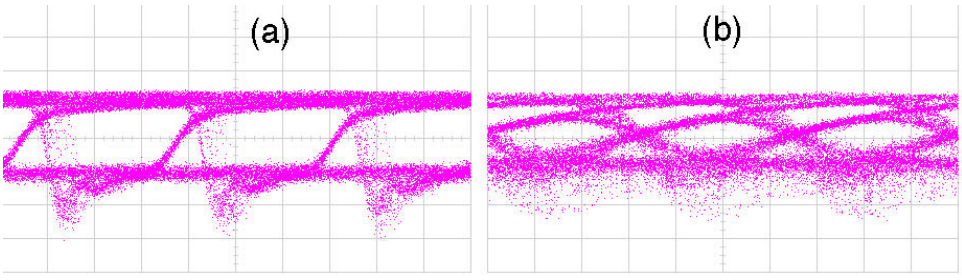

Fig. 3.4 Back-to-back eye diagrams taken from a 0.5 m long 62.5 mm fiber (a) 2.5 Gb/s. (b) 10 Gb/s

until 2000 sequences have been transmitted which corresponds to 2×10^5 bits. Therefore, the measurement procedure can measure error rates down to approximately 5×10^{-6}. The threshold for the traditional bit-by-bit error rate is generated as the average of the received responses. The clock phase for the bit-by-bit detection coincided with the sequence estimation clock.

3.5. Results and discussion

Two sets of measurements were conducted. In the first set of measurements, the back-to-back frequency response of the VCSEL driven at 10 Gb/s was measured and compensated (see Fig. 3.4*b*). The back-to-back eye at 10 Gb/s in Figure Fig. 3.4 shows significant degradation owing to the slow frequency response of the laser and the impedance mismatch of the VCSEL to the pattern generator caused by the series inductance. Fig. 3.4*a* shows the eye diagram when the VCSEL was modulated at 2.5 Gb/s speed. Post-processing the data at both data-rates with sequence estimation resulted in errorless performance over 2×10^5 detected bits.

Next, a set of experiments using multimode fiber was performed. As mentioned earlier, electronic equalization including both MMF and VCSELs is hindered by the data-dependent VCSEL response [55]. We estimate that the VCSEL response time exceeds 15 bits at 2.5 Gb/s, making sequence estimation prohibitively complex because of the large number of possible channel responses. Without any further compensation, the lowest measured bit-error rates using sequence estimation

were ~10^{-3}. To reduce the effect of the data-dependent VCSEL response, the 8b/10b line code, discussed earlier, was used. The measurements using 8b/10b coding were conducted at 2.5 Gb/s over 400 m of 62.5/125 μm fiber with a 3 dB overfilled bandwidth of 210 Mhz/km. Data collection and processing was tried for over 20 launch positions. In all cases, the processed BER was below 10^{-5}. At the distance under consideration, the span of ISI for various launch conditions varied between 7 and 9 bits total. The launch power was -3 dBm, whereas the detected power for different launch conditions varied between -6 dB and -8 dB. As an example, the resulting eye diagrams for two example launch conditions are displayed in Fig. 3.5 showing a completely closed eye with a measured bit-by-bit BER of 0.2. Using MLSE processing, no errors were measured on the set of 2×10^5 information bits for both launch conditions, making the overall BER below 5×10^{-6} even for these completely closed heavily multipath-corrupted eye patterns. We also note that even though the

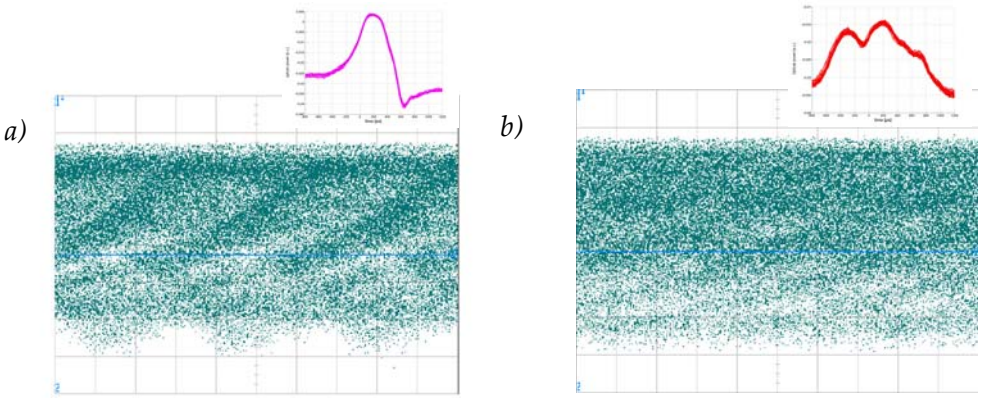

Fig. 3.5 Eye diagrams after propagation through 400 m in 62.5 μm multimode fiber for two different launch conditions showed in the insets

input data were encoded by the line-code, no error-control property of the 8b/10b code was used in the data retrieval. If needed, such error correction can easily be implemented in addition to the MLSE technique. However, our primary interest was in demonstrating the capability of equalization, whereas the error correction was out of the scope of the experiment.

Measurement of complete BER curves was hindered by the effect of the attenuator needed in the setup to control the SNR. It was found that the optical attenuator had considerable impact on the received pulse-shapes preventing reliable data collection for different SNR values. Therefore, in order to determine the attainable performance, simulations based on the responses collected from the experiment were performed. Results for the two launch conditions above are shown in Fig. 3.6. and are similar to the results in the single mode fiber. The shorter group delay spread response yields superior performance, which, for the best attainable launch (shown in magenta in Fig. 3.6) can approach the ideal case with no ISI. On the other hand, the large delay spread double pulse response (shown in red in Fig. 3.6) operates nearly 6 dB worse than a small delay-spread response at the same propagation distance. Thus, the optimal increase in modal dispersion limited reach in multimode fibers depends on both careful selection of the launch condition at the transmitting end, and the application of equalization at the receiving end of the link. Certainly, novel generation multimode fibers with improved modal dispersion properties will further improve this attainable reach.

The measured SNR in the experiment was 25 – 28 dB. At this signal level, the simulation results indicate an error rate below 10^{-5} (off the plot scale), which is consistent with no errors detected in the experiment within the processed $2 \cdot 10^5$ bits. As noted previously, the performance of MLSE is predicated on the precision of the quantized signal on which VA operates. To study the effect of quantization on the SE performance, the responses from the experiment above were quantized prior to sequence estimation in the same fashion as in the single mode case. Results are shown in Fig. 3.7. Again, it is clear that more dispersed pulses, i.e. stronger ISI, necessitates higher quantization precision. For a smaller DGD spread, 4-bit quantization yields MLSE performance close to infinite precision performance, whereas to achieve the similar performance in the large DGD case, 5-bit A/D is

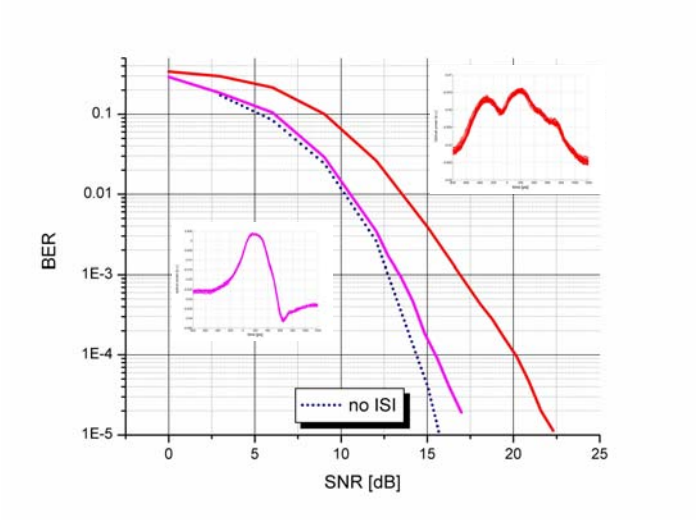

Fig. 3.6 MLSE performance for two example launch conditions. The performance curve corresponding to a narrower-spread response is plotted in magenta, and the wider in red

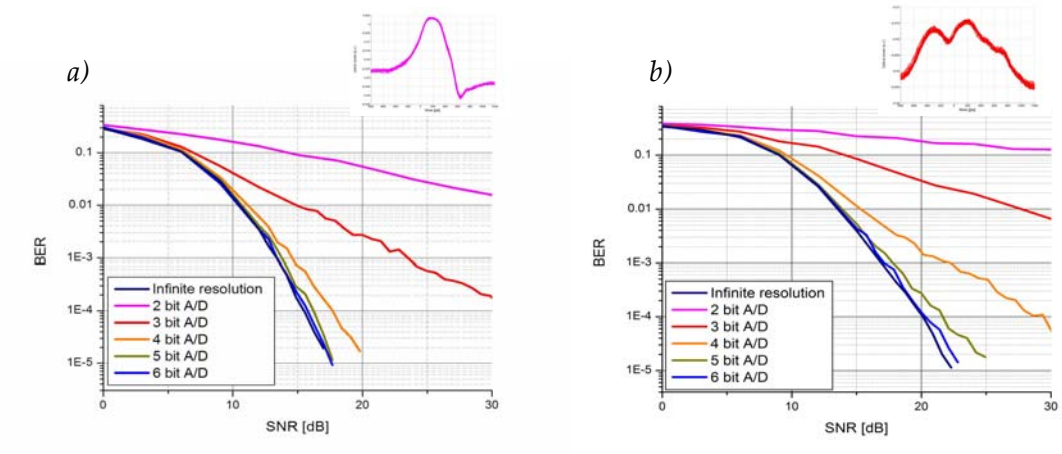

Fig. 3.7 MLSE performance after propagation in 400 m of legacy 62.5 mm fiber under A/D conversion. (a) short differential group delay response; (b) long DGD response.

necessary. From the results displayed in Fig. 3.7, it can be concluded that, similarly to the single mode fiber dispersion, even for the heavily ISI corrupted cases, performance of MLSE with 6-bit quantization coincides with infinite precision performance.

3.6. Chapter Summary

In this Chapter performance and applicability MLSE in directly modulated multimode fiber optic links was investigated. Similarly to the previous Chapter, performance in multimode fiber based links is dominated by the thermal noise in the detector. However, the major difference in behavior of directly driven VCSEL based multimode links is the laser (VCSEL) response. As demonstrated, VCSELs exhibit a nonstationary data-dependent response that is a consequence of the coupling of

spatial and temporal modes inside the laser cavity. This slight variation in spatial mode structure produces a change in the coupling condition into the multimode fiber, resulting in a different channel response. We have demonstrated that in the presence of the VCSEL base-line wander any type of signal processing is hindered due to the prohibitively long memory of the effect. Thus, to enable use of equalization in these links we resorted to the application of modulation codes in order to mitigate the base-line wander. Based on the conjecture that the main culprit for this nonstationary response of the laser is the DC imbalance of the data driving it, a well known 8b-10b code that is a part of the 1G-Ethernet standard was utilized to pre-code the data driving the VCSEL. In addition to preventing long patterns of ones and zeros from occurring, this code imposes DC-balance on any two consecutive bytes of the data. As demonstrated in the Chapter, the introduced DC balance mitigates the response of the laser to an extent that availed processing.

In the subsequent experiments, more than 20 different launch conditions were tried, and bit-error-rates below 10^{-5} were measured in all instances. Additional simulations were performed in order to estimate overall performance curves both with and without A/D quantization. Similarly to the single mode case, it was found that the performance depends on amount of the ISI that develops. Launches which initially have a smaller differential group delay perform close to a back-to-back BER when equalization is applied. On the other hand, power penalty for large differential group delays can be as much as 6 dB. Nevertheless, equalization was successful for

all the launch conditions tried. To the best of our knowledge this was the first successful demonstration of MLSE equalized multimode fiber-optic links based on directly modulated lasers. The ability to detect information in this heavily distorted multipath channel with an intrinsically non-stationary response comes at a cost of 25% overhead in using the DC-balancing 8b/10b code. This large amount of the coding overhead is acceptable for 2 Gb/s links, whereas if the base-line wander is present in the next generation 10 Gb/s VCSEL's, the development of novel substantially lower overhead DC-balancing codes will be necessary. We have demonstrated that the application of coding can in practice mitigate the deleterious effects of components in high-speed optical links, and could potentially reduce the required device tolerances, thus reducing the overall cost of manufacturing and/or extend the devices life-time.

Chapter 4

Signal Statistics and Maximum Likelihood Sequence Estimation In Intensity Modulated Fiber Optic Links with Optical Amplification

4.1. Introduction

As stated in the previous chapters Maximum Likelihood Sequence Estimator (MLSE) is the optimal equalizer that minimizes the probability of sequence error for channels with intersymbol interference (ISI) [8]. MLSE has been broadly utilized in other areas of communication over the past two decades. The use of MLSE in optical communications was first suggested for coherent systems in the early 1990's [21-22]. This research was not pursued because of the development of Erbium doped fiber amplifiers (EDFA) that enabled non-coherent communication schemes based on on-off keying (OOK) capable of spanning trans-oceanic distances [1] with all-optical

compensation. Interest in electronic equalization was revived in the early 2000's [23,58]. Recently, the first prototype of a Viterbi equalizer operating at transmission speeds up to 12.5 Gb/s was demonstrated [60-61].

The achievable performance bounds and error analysis of MLSE for electronic dispersion compensation (EDC) investigated in Chapters 2 and 3 was carried out for short-haul links containing no optical amplifiers, so that the noise could be modeled as additive white Gaussian (AWGN). In this Chapter, we extend the analysis of MLSE to optical links containing a single optical pre-amplifier. The approximate statistics in these links is often treated as non-central chi-square as reported by Humblet and Azizoglu [62]. However, while chi-square statistics are appealing because of the closed form expression for the statistical distribution and the error probability, it is relatively easy to show that they do not correspond to the true statistics of the detected signal for existing systems. In the first part of the Chapter, we present our results on the exact statistics of the electrical signal, derived by means of Karhunen-Loeve (KL) expansions, and provide insight into the results. In the second part of the Chapter, we apply these statistics to sequence estimation (SE) when the received signal is corrupted by the presence of intersymbol interference due to chromatic dispersion and/or narrow filtering. Finally, we introduce Narrowly Filtered OOK (NF-OOK) systems that have a potential of significantly increasing the dispersion limited reach and/or spectral efficiency of the existing fiber-optic systems when used in conjunction with EDC.

4.2. Maximum Likelihood (ML) Detection

A natural criterion of performance optimization in a communication system is that of minimizing the probability of error P_e [63]. Symbol-error minimization under the known signal statistics is equivalent to the Likelihood Ratio test [63,8]. Thus, for optimal detection, knowledge about signal statistics is of prime importance. The simplest (and the most widely studied) case is the detection of known signals in Gaussian noise. Application of the likelihood ratio test for this case simplifies to the minimization of the Euclidean distance between the detected signal and the noiseless responses in signal space [64-65,37]. When the noise is not Gaussian, the likelihood ratio test still provides the optimal solution but does not correspond to minimization of the Euclidean distance.

A KL-based approach to statistics derivation for optically preamplified systems has been reported previously [66-69]. However, KL expansion in [66] was applied in the frequency domain, whereas in [67-69] the authors apply the saddle-point approximation in order to calculate the bit-error-rate in a link without ISI, short of generating a PDF capable of describing channel statistics applicable for use in sequence estimation. More recently, KL expansion was used in [70-71] to calculate the statistics of the parametric gain in a link with a chain of optical amplifiers, as well as the effect of multipath interference (MPI) [72] in fiber optic links. At the time of preparation of this work, a group from Alcatel research has presented results on

sequence estimation at OFC 2005 [73]. Although initiated in the KL expansion, the PDF used in SE by the authors was signal-dependent Gaussian for the system under consideration.

The rest of the Chapter is organized as follows: first, we provide a derivation of signal statistics from a statistical optics point of view, irrespective of the modulation format and/or shape of the optical and electrical filters used. We then extend previously published results by comparing the error performance when detection is performed based on the exact statistics to those derived from approximate non-central chi square distribution. We focus on the fundamental reasons for the difference in the two approaches.

As a starting point consider detection in a single channel fiber-optic communication system with an optical pre-amplifier shown schematically in Fig. 4.1. The deterministic optical field with additive amplified spontaneous emission (ASE) noise is band-filtered by an optical band-pass filter with impulse response *h(t)*. The filtered optical signal and noise are converted to an electrical signal by a square-law

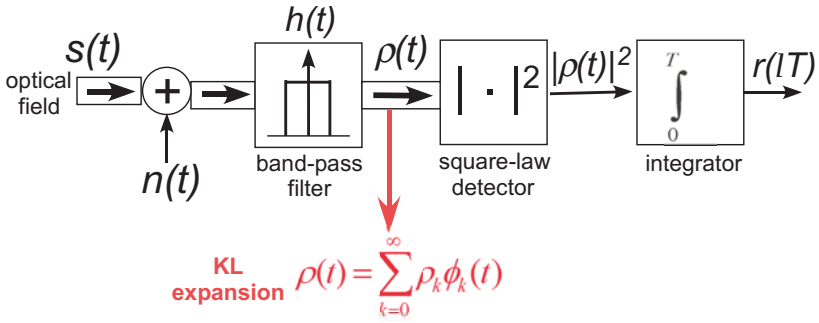

Fig. 4.1 Communication system block diagram

detector (photodiode). The detector is followed by an integrate-and-dump filter that performs an integration of the electrical signal over a signaling interval *T*, resulting in a single sample *r(lT)* produced every *T* seconds.

In this Chapter we treat propagation distances up to 200 km without all-optical dispersion compensation, such that the effects of polarization mode dispersion (PMD) can be neglected with respect to chromatic dispersion (see Chapter 1). For standard optical amplifiers, the statistics of the ASE are formally identical to a complex additive white Gaussian noise process with independent in-phase and quadrature components in both polarizations [74-75]. The total noise power per polarization is equal to $P_n = 2\nu_0^2 = n_{sp}(G-1)B_o hf$, where ν_0 is the noise variance per quadrature component, n_{sp} is spontaneous emission factor, *G* is the amplifier gain, B_0 is the optical filter bandwidth, *f* is the optical frequency, and *h* is Planck's constant. This noise power definition is related to that in other areas of communication theory, where the noise power spectral density per degree of freedom (including and quadratures and polarizations) is $N_0/2$.

The presence of the band-pass optical filter *h(t)* produces colored optical noise characterized by an autocorrelation function $\widetilde{R}_n(\tau)$ per quadrature component. In order to derive the statistics, it is necessary that the composite elements in the signal decomposition be independent. A standard approach of decorrelation of the noise is the Karhunen-Loéve (KL) expansion [63]. A random process *n(t)* in a time interval *T* can be represented as:

$$n(t) = \sum_{k=0}^{\infty} n_k \phi_k(t); \quad 0 \le t \le T \tag{4.1}$$

where $\phi_k(t)$ are orthonormal basis functions, and n_k are random coefficients obtained by projecting $n(t)$ onto the basis functions $\phi_k(t)$. In the KL expansion, the basis functions are the eigenfunctions of the solutions to an integral equation with the kernel $R_n(t - t')$ (see Appendix B for details). In this case, the random variables n_k, are uncorrelated [63]. Furthermore, since the initial noise process is a Gaussian process, the variables n_k are also Gaussian random variables. Because the variables n_k are uncorrelated and Gaussian, they are also independent.

In general, the resulting statistic can be related to the product of the optical filter bandwidth, and the time interval of observation (BT) [81]. If the bandwidth of the optical filter is sufficiently large, the correlation between noise samples becomes negligible, and the filtered noise process can be treated as approximately white, while the noise autocorrelation function can be approximated by a Dirac delta-function. In this case, any orthogonal set of functions satisfies the integral equation (B2) [76]. Particularly advantageous, when applicable, is the use of complex exponentials as a basis set, where the eigenvalues of the integral equation (B3) become samples of the noise power spectral density (or equivalently – the filter power spectral density). The results obtained by Azizoglu and Humblet were based on an expansion in terms of complex exponentials as the basis functions. In their original paper, the authors provide results for large time-bandwidth products, where the utilization of Fourier

harmonics assumption is acceptable (BT ~ 30). However, the time-bandwidth product in existing systems is between 3 and 5. Thus, a more rigorous approach is necessary.

To include the filtered deterministic signal waveform(s), the quanity $s(t)*h(t)$, before the square-law detector is projected onto the noise eigenfunction basis $\phi_k(t)$, resulting in a set of coefficients S_k, such that both signal and noise are expressed in terms of the basis functions $\phi_k(t)$:

$$\rho(t) = \left[s(t) + n(t)\right] * h(t) = \sum_{k=1}^{\infty} (S_k + n_k) \cdot \phi_k(t) = \sum_{k=1}^{\infty} \rho_k \cdot \phi_k(t) = \sum_{k=1}^{\infty} (\rho^{\parallel}{}_k + \rho^{\perp}{}_k) \cdot \phi_k(t) \qquad (4.2)$$

In the above equation, signal and noise coefficients are represented in both orthogonal polarizations (marked by subscripts $\parallel$ and $\perp$). The squaring operation (assumed to be instantaneous) transforms the statistics of the signal plus a complex Gaussian noise process of each term ρ_k in Eq. (4.2) into a non-central chi-squared distribution [63] with two degrees of freedom (one per each quadrature component) in each polarization. The joint probability density for two orthogonal polarizations of the k-th term in Eq. (4.2) is equivalent to the probability density of a sum of two independent random variables. The joint PDF is thus a convolution between the PDFs for each of the polarizations:

$$p_{R_k}(r \mid S_k) = \left\{ \frac{1}{2\sigma_k{}^2} \exp\left[-\frac{r + |S^{\parallel}{}_k|^2}{2\sigma_k{}^2} \right] \cdot I_0\left(\frac{\sqrt{|S^{\parallel}{}_k|^2 \, r}}{\sigma_k{}^2} \right) \right\} * \left\{ \frac{1}{2\sigma_k{}^2} \exp\left[-\frac{r + |S^{\perp}{}_k|^2}{2\sigma_k{}^2} \right] \cdot I_0\left(\frac{\sqrt{|S^{\perp}{}_k|^2 \, r}}{\sigma_k{}^2} \right) \right\} \qquad (4.3)$$

where * stands for the convolution operator, $\sigma_k{}^2$ is the k-th eigenvalue from the eigenvalue decomposition of Eq.(B3), I_0 is the modified Bessel function of order zero,

and $S^{\parallel}_{k}$ and $S^{\perp}_{k}$ are the coefficients corresponding to the projection of the deterministic signal in each polarization, in a bit slot, onto the k-th eigenfunction. The sum of the squares of the magnitudes of coefficients $S^{\parallel,\perp}_{k}$ equals the total energy of the deterministic waveform in the bit-slot. ($\sum_{k=0}^{\infty}|S_k^{\parallel}|^2+|S_k^{\perp}|^2=E$). Eq. (4.3) can equivalently be represented in terms of the characteristic function $\Phi_{R_k}(\omega)$ as:

$$\Phi_{R_k|S_k}(\omega)=\frac{\exp\left[-\frac{j\omega^2\,|S^{\parallel}_{k}|^2}{1+j\omega 2\sigma_k^{\,2}}\right]}{1+j\omega 2\sigma_k^{\,2}}\cdot\frac{\exp\left[-\frac{j\omega^2\,|S^{\perp}_{k}|^2}{1+j\omega 2\sigma_k^{\,2}}\right]}{1+j\omega 2\sigma_k^{\,2}} \tag{4.4}$$

The two polarization components from Eq. (4.3)-(4.4) have been left separated in a product to make the expression more readable. Each of the non-central variables S_k has a different underlying noise variance σ_k^2 that is a consequence of the decorrelation process through the KL expansion. Note that the characteristic functions of chi-square variables represent a rare case where the actual signs in the denominator(s), as well as in the complex exponential depend on the adopted signs in the Fourier kernel due to the fact that the PDF is defined for positive values only.

In the final part of the detection scheme, samples from the random process are integrated by means of an integrate-and-dump circuit. Taking advantage of the orthogonality of the basis functions, the integration process is equivalent to a summation of squares of the coefficients:

$$\int_0^T\left|\sum_{k=0}^{\infty}\left[\left(n_k^{\parallel}{}_R+S_k^{\parallel}{}_R\right)+j\cdot\left(n_k^{\parallel}{}_I+S_k^{\parallel}{}_I\right)+\left(n_k^{\perp}{}_R+S_k^{\perp}{}_R\right)+j\cdot\left(n_k^{\perp}{}_I+S_k^{\perp}{}_I\right)\right]\phi_k(t)\right|^2dt=\sum_{k=0}^{\infty}|\rho_k|^2 \tag{4.5}$$

where subscripts R and I stand for real and imaginary parts of the corresponding coefficients, and $j=\sqrt{-1}$. This step is equivalent to a summation of the independent (non-central) chi-square variables with four degrees of freedom (2 due to the complex nature of optical fields and 2 for the two polarizations of the field.). The resulting PDF is a convolution of an infinite number of terms of Eq. (4.3):

$$p_R(r)=\mathbb{F}^{-1}\left\{\prod_{k=0}^{\infty}\frac{\exp\left[-\frac{j\omega^2\,|\,S^{\parallel}{}_k\,|^2}{1+j\omega 2\sigma_k{}^2}\right]}{1+j\omega 2\sigma_k{}^2}\cdot\frac{\exp\left[-\frac{j\omega^2\,|\,S^{\perp}{}_k\,|^2}{1+j\omega 2\sigma_k{}^2}\right]}{1+j\omega 2\sigma_k{}^2}\right\}= \tag{4.6}$$

$$\underset{k=0}{\overset{\infty}{Conv}}\left\{\left[\frac{1}{2\sigma_k{}^2}\exp\left(-\frac{r+S^{\parallel}{}_k}{2\sigma_k{}^2}\right)\cdot I_0\left(\frac{\sqrt{S^{\parallel}{}_k r}}{\sigma_k{}^2}\right)\right]*\left[\frac{1}{2\sigma_k{}^2}\exp\left(-\frac{r+S^{\perp}{}_k}{2\sigma_k{}^2}\right)\cdot I_0\left(\frac{\sqrt{S^{\perp}{}_k r}}{\sigma_k{}^2}\right)\right]\right\}$$

where $\mathbb{F}^{-1}$ stands for the Fourier transform inverse. Note that it is correct to represent the net characteristic function as a product if and only if the variables ρ_k are independent. This is achieved only if the basis functions are chosen to be the eigenfunctions of the autocorrelation function of the colored Gaussian noise process. If the underlying process were not initially Gaussian, the use of KL expansion is not sufficient to provide independence, resulting in an incorrect expression for the PDF.

The electrical noise process originating from the detector and the supporting circuitry and/or an electrical filter can be readily included in Eq. (4.6). However, our prime interest is comparing the statistics when signal dependent noise is large, as in [62], so we omit those in our present investigation. Note that filtering in the electrical

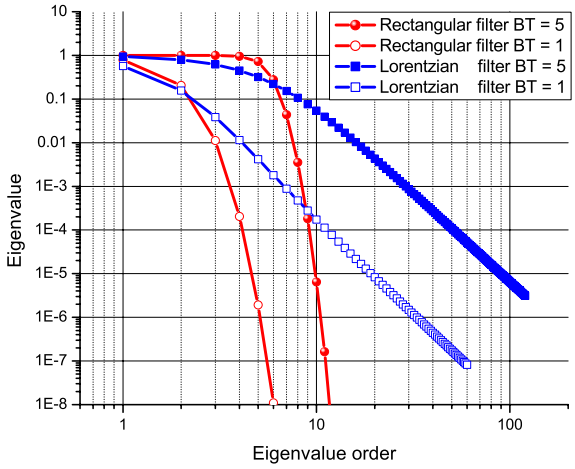

Fig. 4.2 Eigen-value distribution (in one quadrature) in log-log scale (when ordered in a descending order) for two filter shapes: Rectangular filter – the eigen-values correspond to Prolate Spheroidal Functions; and Lorentzian filter – the eigen-values correspond to harmonic functions.

domain will affect the performance even if the electrical noise is neglected in that excessive filtering will introduce additional ISI, and thus deteriorate the performance. The PDF (4.6) depends on both the eigenvalues of $\widetilde{R}_n(\tau)$ and signal coefficients $S^{\|}{}_k$ and $S^{\perp}{}_k$ (also uniquely defined by $\widetilde{R}_n(\tau)$). The eigenvalues determine the weight of a particular non-central chi-square distribution term in the overall expression (4.6). Fig. 4.2 shows the distribution of eigenvalues for two particular filter shapes: Ideal (rectangular) filter and a Lorentzian shaped filter. These two filter shapes were chosen because closed form solutions for the corresponding eigen-quantities are known and tabulated [77-79].

The usefulness of KL expansion approach lies in the fact that the infinite sum in Eq. (4.6) is dominated by a small number of terms [76]. An accurate representation

of the signal waveform requires that sufficient number of terms be kept in the expansion. This number depends on the compactness of the eigenfunctions. For example, the eigenfunctions of the ideal rectangular filter are prolate spheroid functions (PSS), known to be a complete set of functions with the smallest time-bandwidth product of all known functions [81]. It is owing to this property that PSS require the least number of terms in series expansions for a given accuracy [82]. On the other hand, the eigenfunctions for the Lorentzian-shaped filter are harmonic functions (sines for odd, and cosines for even orders). In order to have an accurate estimation of the signal energy, approximately six times more terms are necessary for the Lorentzian-shaped, with respect to a rectangular band-pass filter. Consequently, the two types of filter shapes represent two extreme filtering operations. Results for an arbitrary filter shape are generally between the two cases (unless an optical filter with a more gradual roll-off than that of a Lorentzian is used). In practice, it is sufficient to keep the terms down to 10^{-5} of the largest eigenvalue to compute the PDF. This last statement is particularly important in a case of a Lorentzian filter, as the time-bandwidth product for such a filter cannot be defined in terms of root-mean-square (RMS) quantities. Note that the information on the compactness of eigenfunctions is contained in the rate of decrease of eigenvalues for a particular filter [81,85], since, in effect, the eigenvalues provide information on the energy contained in each KL mode. For example, if ordered in descending order, the first few eigenvalues for the rectangular filter are approximately unity (see Fig. 4.2), whereas

after the sharp drop-off, the remaining eigenvalues are nearly zero. This sharp descent of eigenvalues was the foundation of the definition of Slepian's famous 2BT theorem (note that we define the full filter bandwidth as B, rather than 2B as used in Slepian's original work) [81]. If only the eigenvalues equal to one are included in Eq (4.6), the resulting PDF (for a rectangular filter) is a non-central chi-square distribution with 4BT degrees of freedom (accounting for two orthogonal polarizations and in-phase and quadrature components in both polarizations, according to our notation).

Therefore, any difference between the exact statistics and chi-square arises from the inclusion of eigenvalues in the "roll-off" region, which, in effect, describe the extent of noise correlations among adjacent bit-slots. The eigenvalues in the roll-off region become important for small BT products as a substantial difference

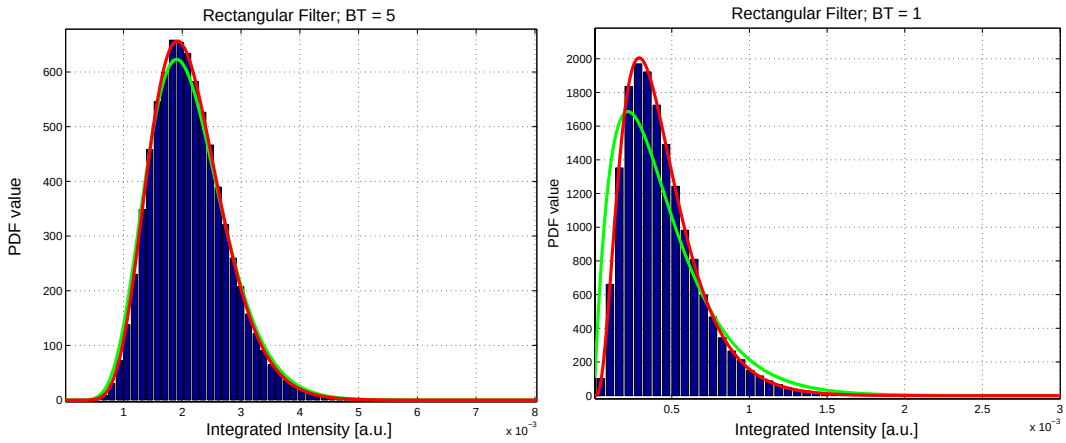

Fig. 4.3 Histograms of samples (bars) drawn from a complex Gaussian noise source (in two orthogonal polarizations) undergoing band-limiting, square-law operation and integration. Also shown are fits of the chi square distribution (green line) and the pdf obtained through Karhunen-Loeve expansion (red line) for time-bandwidth products of (a) 5, and (b) 1

between the non-central χ^2 and the exact distribution occurs (see Fig. 4.3). This is a consequence of the fact that for small BT products, the number of eigenvalues close to unity is commensurate with the number of eigenvalues in the roll-off region and the impact of the effect of the latter on the overall PDF becomes significant.

Fig. 4.3 shows histograms obtained simulating two different values of time-bandwidth products for NRZ modulation for 'all-zeros' (or a 'zero-rail') response where the dissimilarity between the to PDF's is the largest (see next Section). The chi-square function, with the number of degrees of freedom defined by the BT product of the system, under-estimates the histogram around the maximum value, whereas the exact statistical distribution follows the histogram much more closely, particularly for the low time-bandwidth product, BT = 1 shown in Fig. 4.3(b). As explained above, the discrepancy in the PDFs originates in neglecting noise correlations that result if the basis functions are not chosen to be the eigenfunctions of $R_n(\tau)$. The major assumption in the presented derivation is that the noise statistics before the square-law detector is a colored Gaussian process. The most obvious case when this assumption is satisfied is in a link, either with, or without all-optical dispersion compensation that contains a single optical preamplifier, such that nonlinear mixing of signal and noise occurs only due to the square-law detection and not during propagation. Alternatively, the signal statistics will obey those derived in this work, as long as the noise from the last amplifier in an amplifier chain dominates and signal-noise and noise-noise nonlinear mixings generated during propagation can be neglected.

4.3. MLSE in links containing a single optical pre-amplifier

The major impact of intersymbol interference (ISI) in communication systems is to increase the number of responses at the output with respect to the input [37]. Our previous derivation suggests that in an optically amplified system each of the responses at the output will have a different corresponding PDFs (i.e. likelihood functions). Fig. 4.4 shows an example of the PDFs, calculated using the method in the previous section, in both a linear and a logarithmic scale, for a total span of ISI of 3

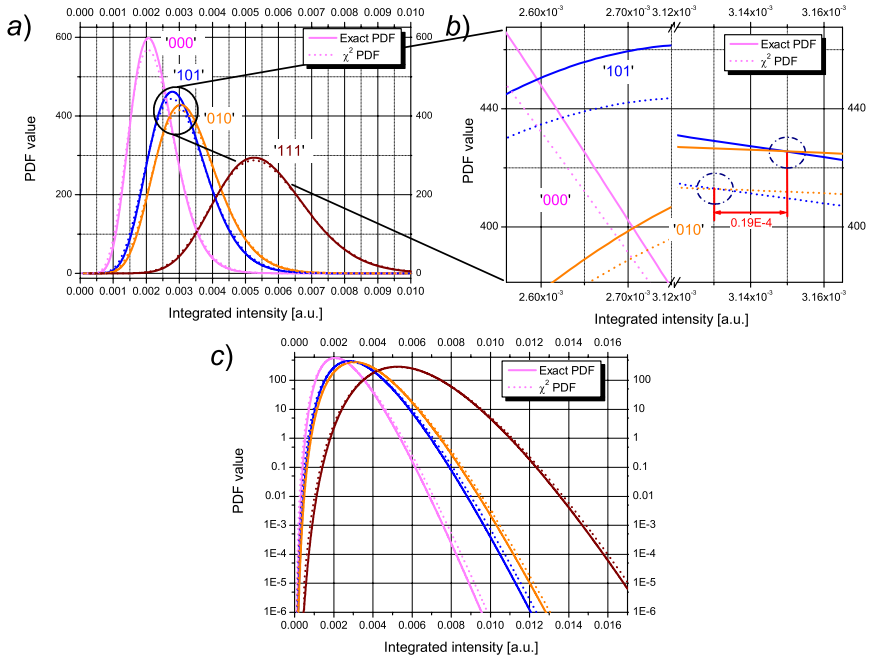

Fig. 4.4 (a) Comparison of the calculated PDF's (solid lines) with chi-square (dashed lines) for four channel responses at back-to-back for NRZ format at Eb/N0 = 10 dB for a rectangular filter for an '000', '111', '101' and '010' responses. (b) A zoomed in detail from the graph (a) that emphasizes how close the intersections of the likelihood functions are on the x-axis for the two forms of likelihood functions. (c) PDF's from part (a) in logarithmic scale

bits for a signal to noise ratio (SNR) of 10 dB. The span of ISI is defined as the total number of bits affected by the energy leakage to adjacent bit-slots, due to ISI. The calculated PDFs are shown for the following responses: *(i)* 'all-zeros' in magenta, *(ii)* 'all-marks' in dark red, *(iii)* 'isolated space' in blue, and *(iv)* 'isolated mark' in light orange. These responses are characteristic in the sense that in each one of them a mark (or a space) is surrounded by marks (or spaces) for the whole extent of ISI. In all three parts of the figure, superimposed are the non-central chi-square distributions (dashed lines) for the same time – bandwidth product BT. The relatively extent of the tails of the distributions is due to their $\sim exp(-x)$ dependence. For large SNR, the derived PDFs become more Gaussian-like with characteristic symmetry around the mean and $\sim exp(-x^2)$ behavior in the tails. Note additionally that PDFs corresponding to the responses with substantial deterministic field (such as marks, at back-to-back), the difference between the exact statistics and chi-square is significantly smaller than for responses with less optical power (e.g., spaces at back-to-back).

In order that MLSE based on the VA be applicable, the noise samples in different bit-slots need to be independent [8]. Note that the independence of noise samples, in a typical fiber-optic system shown in Fig. 4.1, cannot be achieved without a bank of optical filters that would achieve decorrelation physically. Thus, the practical receiver under consideration does not achieve optimal ML performance as there will always be some noise correlation between the adjacent bit-slots not taken into account in detection. However, the marginal densities derived in the previous

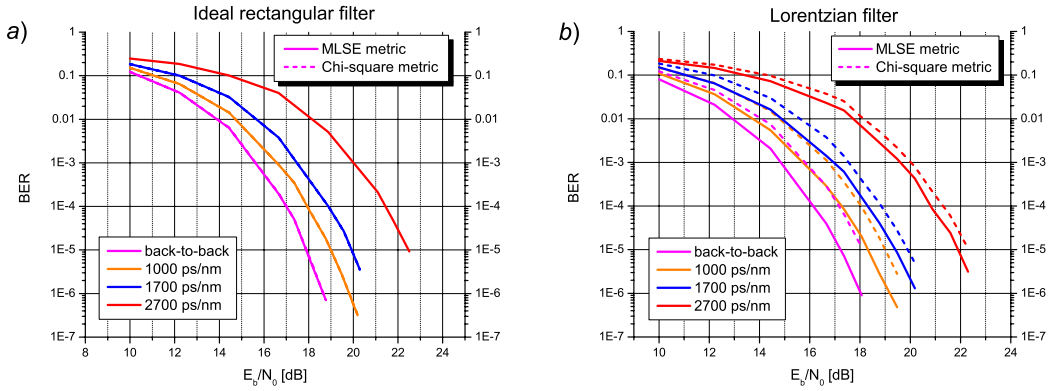

Fig. 4.5 Performance of the SE based on the exact statistic (solid lines) and the chi-square metric (dashed lines) with sequence estimation at four different amounts of accumulated dispersion. (a) Ideal rectangular filter used. Performance of the two approaches is virtually the same; (b) Lorentzian filter.

Section give a superior description of signal statistics than chi-square PDFs (see Fig. 4.3). Fig. 4.5 shows the performance of suboptimal, but practical sequence estimation (SE) in a fiber-optic communication system operating at 10 Gb/s using the exact statistics derived in the previous section at four different distances of propagation for two different filter shapes. All simulations were carried out for NRZ waveforms assuming a raised cosine shape with a roll-off parameter of 0.6 with the extinction of 13 dB. The performance curves are given with respect to the ratio of the average optical energy per bit E_b to the total noise power spectral density N_0. Note that, we assume that the four noise sources (the in-phase and in-quadrature components in two orthogonal polarizations) are independent, such that N_0 in this case equals four times the power spectral density per noise component $N_0'/2$. This quantity is, in our

opinion, the proper figure of merit that establishes a fair comparison between the signal and the noise.

As shown in Fig. 4.5, for an ideal rectangular filter, there is virtually no difference in SE performance for a time-bandwidth product BT = 5 (typical of the existing systems at 10 Gb/s with a 50 GHz band-pass filter), even though the resulting likelihood functions for the chi-squared distributions and the exact distributions are clearly different (See Fig. 4.4(a)). To clarify this surprising result, recall that the decision threshold is defined by the intersection of two likelihood functions. Note that the mean values, as well as the locations of maxima of both the chi-square distributions and the true PDFs virtually coincide Fig. 4.4(a)). If sequence estimation is performed assuming chi-square distributions for all responses, the abscissae of intersections of the different chi-square distributions are extremely close to the intersection abscissae of the true PDFs (see Fig. 4.4(b) that shows zoomed -in image of intersections of the exact statistical distributions in solid lines, and approximate chi-square curves from Fig. 4.4(a)). Different decisions on the incoming bits in using the two statistical distributions can occur only when a sample falls into the region between the intersections for the exact distribution and chi-square distribution. This event has a low probability of occurrence for the two families of PDFs considered. The resulting BER assuming non-central chi-square statistics is, thus, asymptotically the same as that of the true statistic which can be observed in Fig. 4.5(a). The performance difference is further reduced because the distinction between the true

statistics and chi-square becomes smaller for large values of SNR. Note that according to Eq. (B4) the increase of SNR reduces the effect of the eigenvalues in the roll-off region. This case is very much similar to the Gaussian approximation of a Poisson distribution where the overestimate of Gaussian relative to Poisson on the lower end is balanced with the underestimate on the higher end of the distribution. In a Gaussian approximation to a Poisson distribution, these effects cancel providing a good estimate for total BER, even though the PDF approximation is not nearly as satisfactory. To summarize, the performance estimates of fiber optic links containing optical pre-amplifiers (with or without ISI), based on the non-central chi-square distribution yield asymptotically correct result assuming rectangular band-pass filters, even though the decisions are based on an incorrect statistics.

The results in the Fig. 4.5(b), on the other hand, show chi-square statistics to be inadequate for filter shapes significantly different from an ideal rectangular filter with an equal filter bandwidth. For this general case, statistics derived from a KL expansion must be used. The performance difference for the exact statistics and chi square distribution for non-rectangular filters is reduced at longer propagation lengths (see Fig. 4.5(b)). As discussed in the previous section, when the responses with substantial amount of the deterministic field (in which the difference between the true statistics and chi-square is diminished) considerably outnumber channel responses with smaller deterministic energy content, which occurs with the increase of the ISI span at longer propagation distances, the average performance based on

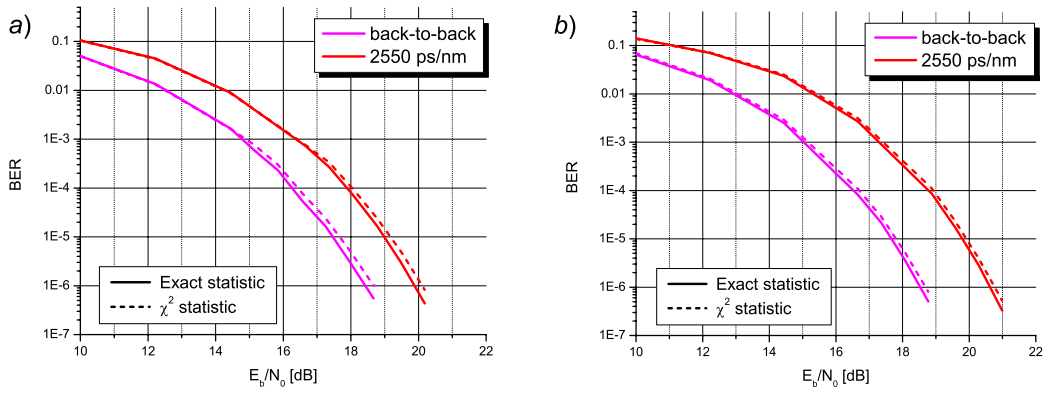

Fig. 4.6 Performance of sequence estimation for the exact and the chi-square distributions for BT = 1 at back to back and 150 km. (a) Rectangular filter; (b) Lorentzian shaped filter

chi-square distributions becomes closer to the decision making based on the exact statistics.

As the BT product is reduced, the eigenvalues uniformly decrease regardless of the filter used [76] (see Fig. 4.2 for BT = 1) and are close for different filter shapes. The statistics become substantially different from chi-square for systems with a BT product on the order of 1 (see Fig. 4.3(b)), and the distribution obtained through KL expansion is required.

Fig. 4.6 shows the performance of the system narrowly filtered with a 10 GHz optical filter, in a 10 Gb/s link, at back-to-back and 150 km for a rectangular, and a Lorentzian shaped optical filter.

The system with BT = 1 in Fig. 4.6 has the total span of ISI equal to 5 bits at back-to-back (2 bits on each side of an isolated mark, plus the mark itself), and, as such, cannot be used in conjunction with standard bit-by-bit decision. SE is capable of

retrieving the information for such a system at back-to-back (see Fig. 4.6(a)). Additionally, SE can extract the information at the distance of 150 km (see Fig. 4.6(a)) with a power penalty of 1.5 dB, which is in clear contrast with a 4.5 dB penalty in a common system with BT = 5 (see Fig. 4.5). Fig. 4.6(b) shows the performance of the system with BT = 1 at back-to-back and 150 km filtered by a Lorentzian type filter. The performance is close to that of a rectangular filter. Although the probability distributions are clearly different for BT = 1, the power penalty for using an incorrect, chi-square likelihood function is only 0.3 dB. This remarkable behavior is again attributed to the proximity of the likelihood intersections of the chi-square distributions relative to those using the exact channel statistics.

Narrowly filtered OOK systems (NF-OOK) systems can only be implemented jointly with electronic dispersion compensation. Note that tight filtering is necessary both at a transmitter, before launching (or multiplexing) to a transport fiber, and at a receiver in order to *(i)* limit the amplifier noise, as well as *(ii)* the crosstalk from the neighboring channels. Possible benefits from these systems are two-fold. They provide a very simple realization of high spectral efficiency, operating using standard on-off keying (OOK) modulation. In addition, the reduced spectral content of these systems makes them substantially more resilient to chromatic dispersion, yielding longer dispersion limited reach, even with respect to systems employing phase modulation such as duobinary [84], or DQPSK [85-86]. These systems allow a limited penalty in performance at back-to-back, whereas they could potentially give large

dividends in extending the dispersion limited reach. This is because the span of ISI of such systems, which determines circuit complexity for EDC, grows at a very slow rate due to their forced small spectral content. The main scope of this Chapter is signal statistics, however, and investigation of performance of NF-OOK with regards to the reach will be presented in the next Chapter.

4.4. Conclusion

In this Chapter, we have analyzed the statistics associated with detection in fiber optic communication systems optical amplifiers. In addition, we have examined the effect of these statistics on detection incorporating (ML)SE with ISI introduced by the accumulated dispersion in propagation and/or filtering performed at the transmitting and the receiving end of the link. The main difference with respect to un-amplifed systems examined in the previous chapters is signal-dependent correlated noise statistics. These statistics are a result of the amplified spontaneous emission noise from the optical amplifier undergoing band-limiting (due to an optical filter), interacting with the deterministic signal through square-law detection. The presence of signal-dependent correlated noise has two important consequences on detection: (i) In a general case, all of the attainable channel responses have different underlying statistics, (ii) Maximum likelihood detection is impeded by the noise correlation of the responses in different bit slots. In this Chapter, the proper signal statistics in these links were derived. The analysis by means of a Karhunen-Loeve

expansion clearly indicates that the signal statistics are profoundly dependent on the shape of the optical filter used and can be substantially different from the commonly assumed non-central chi-square distribution for the time-bandwidth products in existing systems. However, while inadequate for describing the signal statistics, we have found chi-square statistics to be surprisingly good for BER assessment. In fact, the BER estimation based on the approximate statistics is substantially superior to the resemblance of the actual approximate chi-square and the exact statistics PDFs. As demonstrated, the origin of this relatively small penalty for using improper statistics in detection lies in the close separation of likelihood intersections (for the exact signal statistics and the approximate – chi-square statistics). Consequently, this effect can be elucidated by partial cancellation of leading and trailing tails' contributions of the approximated and the exact PDFs in their effect on BER.

Lastly, we have for the first time introduced Narrowly filtered OOK systems that have a potential of substantially increasing spectral efficiency and/or dispersion limited reach of the existing WDM systems, when used in conjunction with electronic dispersion compensation. The analysis of such systems, as well as the signal processing based on the MLSE favor strict calculation of signal statistics.

4.5. Acknowledgement

The text in the Chapter 4, in part, is a reprint of the material as it appears in Optics Express, Alic, Nikola; Papen, George C.; Saperstein, Robert E.; Milstein

Laurence B.; Fainman Yeshaiahu. “Signal Statistics and Maximum Likelihood Sequence Estimation in Intensity Modulated Fiber Optic Links Containing a Single Optical Pre-amplifier,” Optics Express, Vol 13, 2005. The dissertation author was the primary researcher and/or author and the co-authors listed in this publication directed and supervised the research which forms the basis for this Chapter.

Chapter 5

Transmission Experiments with Sequence Estimation

5.1. Introduction

In this Chapter we will present experimental demonstrations of high-speed equalization performed by means of Viterbi Algrithm (VA)-based sequence estimation. These results are in a separate chapter because the complete preceding treatment of equalization in high-speed fiber optic links was exposed from the theoretical point of view. Theoretical receivers are often too complex for practical purposes at transmission speeds under consideration. The complexity reduction of practically realizable receivers comes at a cost of inferior performance. All of the experiments presented in this Chapter were designed to match the current technological capabilities. This practical impediment bounds the attainable performance and reach. Consequently, the results presented in this Chapter depart from the theoretical optimal predictions treated in the previous part Chapters. Unlike

"proof-of-concept" experimental validations presented in Chapters 2 and 3, in this Chapter, complete bit-error rate measurements will be presented.

The experiments incorporate a sampling oscilloscope to provide access to channel statistics and waveform responses, and remove the requirement for fast electronics. However, strictly speaking, they cannot be considered as full-scale transmission experiments as they do not contain clock recovery from the received data. In fact, the sampling scope in all of the experiments is synchronized by the pattern generator trigger (i.e. the transmitter) emitted synchronously with the data-frame repetition rate. While the frame synchronization in the experiments is perfect, the data collected from the sampling scope exhibit the same amount of timing jitter as the data in real time, and thus, the bit-wise synchronization is not perfect. For a small number of samples per bit period in a sampling scope capture, the observed jitter can be substantially worse than the real time jitter, owing to the coarse quantization of the oscilloscope time base, causing up to 0.5 dB power penalty.

In the rest of the Chapter, two sets of experiments will be discussed: *(i)* Equalization of standard Non-return to zero (NRZ) format in Metropolitan Area – type propagation distances (up to 250 km); and *(ii)* Long-haul propagation relying on a Narrowly Filtered OOK format that was introduced in the previous Chapter. The latter experimental demonstration presents both the first experimental demonstration of the novel modulation format, as well as, to date, the longest propagation distance

reached (600 km) without any use of optical dispersion compensation, pre-compensation and/or pre-chirping at the transmitter in 10 Gb/s links.

5.2. Equalization of the NRZ format and receiver structure trade-offs

As stated in Chapters 2 and 4, Maximum likelihood (ML) detection in the presence of ISI requires complete knowledge of the signal statistics. These statistics depend on the total number of bit slots affected by the spreading of the information bearing waveforms that we define as the span of ISI. If the Viterbi algorithm (VA) is used for the search for the most likely sequence, then in order to achieve ML performance: *(i)* the signal statistics must be independent on a bit-by-bit basis, and *(ii)* the equalizer must have information available about the channel responses for the complete span of ISI [33,8]. The first requirement is never true in optical links because the noise statistics are non-Gaussian and correlated [66-73], such that VA is not an optimal algorithm. The second requirement results in complex equalizer structures because the VA complexity increases exponentially with channel memory [33,8]. However, the trade-off between the algorithm efficiency and complexity still favors the application of sequence estimation (SE) based on VA with approximate channel statistics gathered through training for a fixed VA complexity. This suboptimal, low-complexity configuration has been demonstrated to achieve satisfactory performance and is becoming a method of choice in equalized high-speed fiber optic links [60]. In

Sections 5.2.1-5.2.2 we examine the performance of SE based on a low-complexity VA for several receiver structures.

5.2.1 **Experimental setup**

The experimental setup is shown in Fig. 5.1. A zero-chirp modulator was used to produce an OC-192 with EFEC (10.7 Gb/s) data stream. In-line optical amplification was performed after each of the 4 conventional single mode fiber (SMF) spans with average dispersion per unit length of 17ps/km-nm. The channel launch power into each span was maintained at -3 dBm using variable optical attenuators (VOA, not shown in the diagram). Preceding the pre-amplifier stage, the output from the span was combined with an Amplified Spontaneous Emission (ASE) noise source whose power was monitored and controlled by VOA1 for flexible adjustment of the Optical Signal to Noise Ratio (OSNR) at the receiver. An amplified PIN receiver was used for detection. VOA2 guaranteed a constant received power of -6 dBm throughout the experiment. The resulting in variable OSNR that was monitored on an optical spectrum analyzer in real time. Training and data sequences were loaded into a 10 Gb/s pattern generator serving as the primary data source. Traces from a fast sampling oscilloscope, triggered by the data pattern, were acquired and returned to the computer to perform data processing. Throughout the experiment, a 4-state VA with 3-bit A/D converter was assumed. The architecture fully emulates a dedicated receiver structure, as well as the bit-error ratio (BER) evaluation sub-module [88].

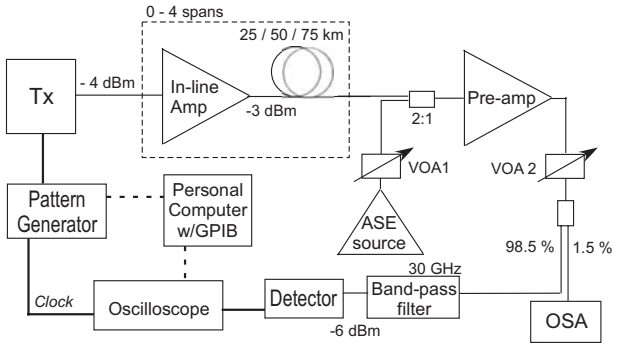

Fig. 5.1 Experimental setup

A short pseudorandom bit sequence (PRBS) was used for training, whereas BER measurements were performed using a long PRBS sequence that was run until at least 100 errors are detected. The appropriate PRBS sequences in both stages (training and BER measurement) of the experiment were divided into partially overlapping 230-bit parts allowing for performance degradation due to patterning effects. BER measurements were performed until the level of 10^{-3} is reached, ensuring operation below the practical 7% overhead FEC threshold of $2x10^{-3}$ [47].

5.2.2 **Experimental Results and Discussion**

An additional advantage of the experimental setup in Fig. 5.1 is that it facilitates the quantification of performance under different receivers supplying the information to the VA. In particular, we concentrate on the following cases: 1 sample per bit (spb), 2spb, 1- and 2-spb with the sampling is performed with a non-ideal sampler that spans a short time window instead of an (ideal) delta

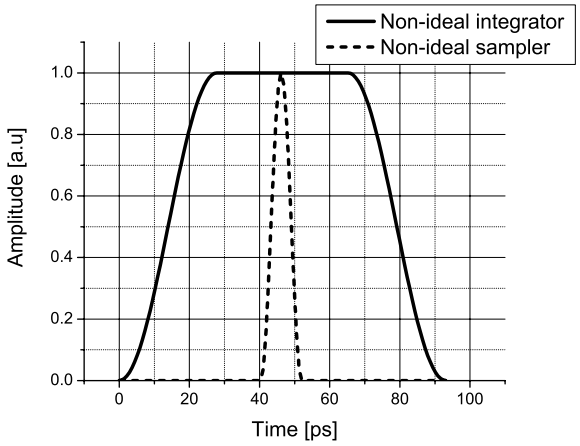

Fig. 5.2 Non-ideal integrator (0.6 roll-off raised cosine shape) and non-ideal ~12ps sampler impulse response shapes

function. For the best performance, 2spb waveforms were sampled at ¼ and ¾ of the bit interval [60], whereas 1spb was taken at the center of the bit-interval. Finally, to examine the effect of energy detection, samples gathered from the sampling oscilloscope were combined to produce the response of a non-ideal integrate-and-dump filter having a raised cosine shape with 0.6 roll-off parameter defined earlier. The sampling circuit convolves the input waveforms (consisting of signal and noise) with its own impulse response. We note that sampling can never be performed instantaneously and always spans a finite time duration. Here we examine the effect of an extended sampling time in conjunction with SE. The functional shapes of the non-ideal integrator and the non-ideal sampler are shown in Fig. 5.2. The measured required optical signal to noise ratio (OSNR) to achieve 10^{-3} BER for various detection strategies up to 225 km in increments of 25 km is shown in Fig. 5.3. The difference of

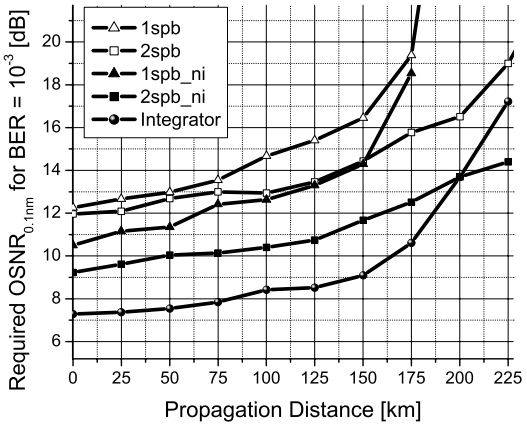

Fig. 5.3 Required OSNR for 10^{-3} BER for different receiver structures in sequence estimation (4-state VA with 3-bit A/D).

5 dB in required OSNR between different receiver configurations is noticeable. This difference reflects a tradeoff between the amount of the captured energy by various receiver structures and their ability to distinguish the waveforms for different channel responses. An additional benefit of the integrate-and-dump receiver and the "dirty" sampler is noise averaging that aids in detection.

Extending on the conclusions from Chapter 2, the detection of a binary sequence consisting of N bits in signal independent noise is equivalent to finding the closest (noiseless) signal point to the received sample, among the possible 2^N points in an N-dimensional signal space [8, 39-40]. Thus, the ability to capture more energy in detection is equivalent to a more dilated signal space (facilitating the detection). Alternatively, utilizing several samples per bit provides better performance through an increase of the space dimensionality which avails better distinction among the channel responses. In signal dependent noise, decision regions are defined by

intersections of the likelihood functions. Consequently, more advanced analysis methods for their investigation are required [89-90]. Nevertheless, the interpretation in terms of signal independent noise, outlined above, normally provides good qualitative guidelines on the overall performance.

Our experimental findings corroborate that energy detection outperforms few-samples-per-bit sampling as long as the complexity of the VA matches the accumulated span of ISI. The most important feature in Fig. 5.3 is the sharp performance deterioration for the integrate and dump receiver after 120 km. Note that a 4-state VA no longer has a complete knowledge about the channel responses after approximately 100 km, as the waveforms spread beyond 3 bits. Thus, even if the noise statistics were independent on a bit-by-bit basis, the requirement *(ii)* from Section 5.2. would not be satisfied, and the sequence estimation is not "Maximum Likelihood". For the given 4-state VA, the performance advantage of the non-ideal integrate-and-dump receiver diminishes after approximately 125 km. Finally, after 200 km, multiple-samples-per-bit receiver outperforms the integrator. To summarize, adopting several samples per bit detection strategy yields longer reach (up to 50 km for NRZ format) at a cost of inferior performance (up to 5 dB) at shorter propagation distances. This inferior performance of multiple samples per bit at shorter distances can be mitigated by the application of "dirty" sampling (displayed in Fig. 5.3 by the suffix _d). Employing "dirty" multiple-samples-per-bit detection combines partial noise averaging with better estimation of the response waveforms that correspond to

the increase of the dimensionality of the detection. In order to closely examine the performance for different receivers, Fig. 5.4 shows performance comparison at 75 km and 200 km. Results clearly indicate that the integrator provides superior performance to that provided by few-samples-per-bit, as long as the complexity of the VA matches the ISI. Note that at 200 km (see Fig. 5.4) after the initial better performance of the integrator for low OSNR's, the multiplicity of closely spaced error events in the signal space causes the error floor formation at approximately $5x10^{-4}$. However, as the span-contributed ISI overwhelms the available VA complexity, detection based on multiple-samples-per-bit is capable of better distinction between the channel responses, resulting in a longer. In Fig. 5.4 included are experimentally measured 16-spb performance curves at 75 km and 200 km demonstrating exceptional performance that results at the cost of substantial complexity of such

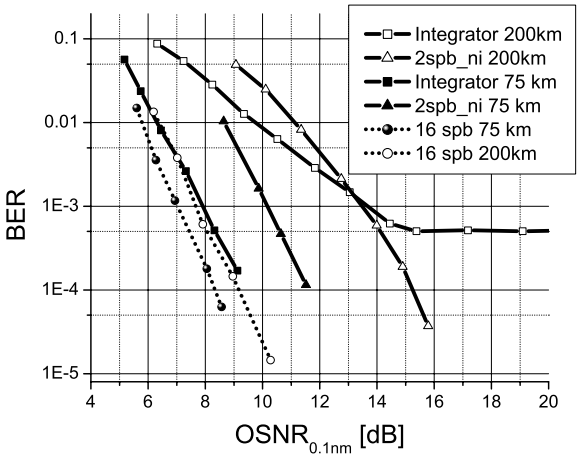

Fig. 5.4 Performance of different receiver structures in sequence estimation (4-state VA with 3-bit A/D) at 75km and 200km.

receivers. Note that detection based on 16-spb is still not optimal. Optimal detection in correlated noise must incorporate a bank of filters matched to the appropriate Karhunen-Loéve basis functions that are the eigenfunctions of the noise autocorrelation function. However, this optimal detection strategy, is impractical for current lightwave systems and was not attempted experimentally.

5.3. Extended dispersion limited reach and spectral efficiency through narrow filtering and equalization.

The experiments in the previous Section were focused on the equalization in metropolitan network distances, as well as receiver designs trade offs on performance. The reach of an equalized link is ultimately defined by the equalizer complexity (unless the signal space minimum distance is equal to zero).

With the application of EDC, the dispersion-limited reach is no longer directly related to the eye opening penalty, because detection is not performed on bit-by-bit basis (see Chapter 2). More important to determining the practically attainable reach is the complexity of the underlying algorithm, which dictates the complexity of the integrated circuit. Regardless of the equalization technique used, the complexity is related to the span of intersymbol interference (ISI). Unlike the analog equalizers such as traditional Feed-forward (FFE) and Decision-feedback equalizers (DFE), an additional performance penalty for digital equalizers is imposed by the analog-to-digital (A/D) conversion. Narrowly filtered On-Off-Keying (NF-OOK) modulation

format was proposed in the previous Chapter and in [91] in order to extend the reach of conventional equalized links. The rational behind this approach is to intentionally introduce ISI at the transmitter which reduces the subsequent span-contributed ISI yielding a longer reach for the equalized link. This, to our knowledge, is the first experimental demonstration of the new technique in extended dispersion-limited reach of NF-OOK, used in conjunction with sequence estimation (SE) at the receiver. The experiments have validated OC-192 transmission over 600km SMF link, and the results are in complete agreement with theoretical results.

5.3.1 **Experimental Setup**

The experimental setup is shown in Fig. 5.5. A zero-chirp modulator was used to produce an OC-192 data stream. In-line optical amplification was performed after each of the nine conventional single mode fiber (SMF) spans with average dispersion

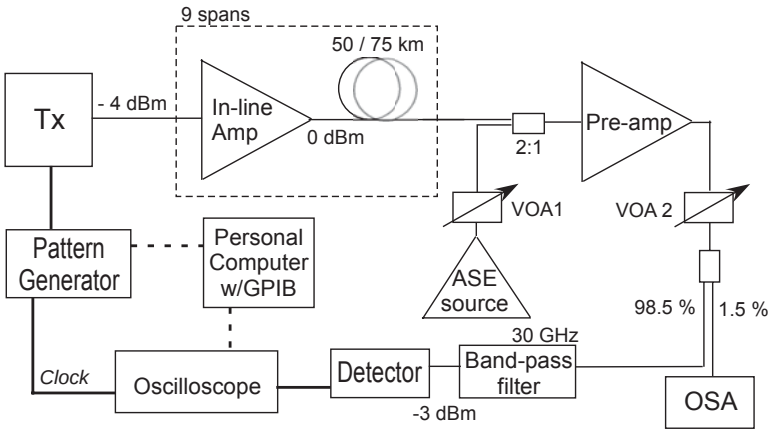

Fig. 5.5 Experimental setup block diagram for the 600 km NF-OOK reach

maintained at 0 dBm using variable optical attenuators (VOA, not shown in the diagram). Preceding the pre-amplifier stage, the output from the 600km span was combined with an ASE source whose power was monitored and controlled by VOA1 for flexible adjustment of the OSNR at the receiver. As before, an amplified receiver was used for detection. VOA2 guaranteed a constant received power of -6 dBm throughout the experiment, resulting in variable OSNR that was monitored on an optical spectrum analyzer in real time. Training and data sequences were loaded into a 10Gb/s pattern generator serving as the primary data source. Traces from a fast sampling oscilloscope, triggered by the data pattern, were acquired and returned to the computer to perform data processing. The architecture fully emulates a dedicated receiver structure, as well as the BER evaluation sub-module [88]. A short pseudorandom bit sequence (PRBS) was used for training, whereas BER measurements were performed using a long PRBS sequence that was run until at least 100 errors were detected. Processing and training were performed in blocks of 230 bits, where the appropriate PRBS sequences in both stages of the experiment were divided into partially overlapping 230-bit parts allowing for performance degradation due to patterning effects. BER measurements were performed until the level of 10^{-3} is reached, ensuring operation below the practical 7% overhead FEC threshold of $2x10^{-3}$ [47].

5.3.2 **Results and Discussion**

In order to exceed the dispersion limited reach of 500 km, standard NRZ was filtered to approximately 3.8 GHz FWHM bandwidth. Fig. 5.6 shows both the launched and standard NRZ spectrum measured using a 10-MHz resolution optical spectrum analyzer, as well as a back-to-back eye diagram for the launched NF-OOK. The ISI-span of NF-OOK at back-to-back, for the filter used, was measured and simulated at 3 bit slots, with completely closed eye, as illustrated in Fig. 5.6b. A conventional (unprocessed) bit-by-bit detection BER equals 0.17 for this heavily distorted launch state. The response of narrowly filtered waveforms does not change appreciably during the first 120 km, whereas the ISI-span gradually increases in subsequent spans, in approximate steps of 120km. This slower rate of information-bearing pulse spreading is primarily responsible for the extended reach of NF-OOK, and is a fundamental advantage used in our reduced-complexity detection scheme.

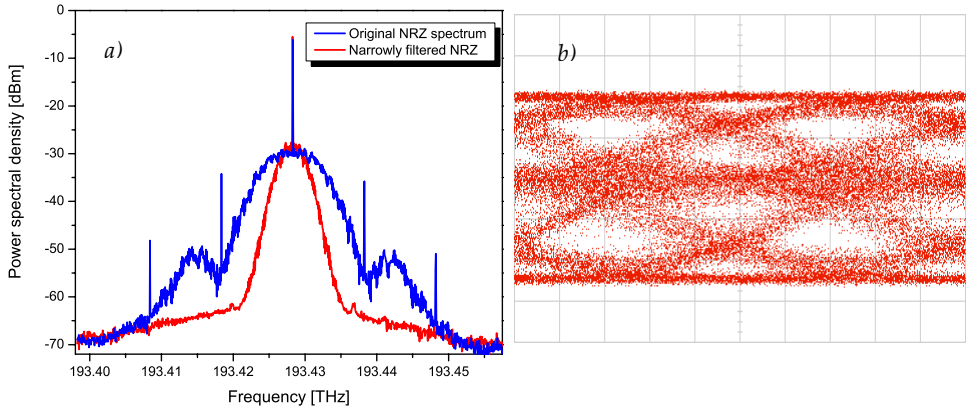

Fig. 5.6 (a) Comparison of narrowly filtered OOK (in red) and the conventional NRZ (in blue) spectra;
(b) Eye-diagram at back-to-back

The experimental setup including the sampling oscilloscope allowed BER measurement for several receiver structures preceding the Viterbi algorithm (VA): *(i)* ideal integrate-and-dump, *(ii)* a non-ideal integrator with a shape approximated by a 0.6 roll-off raised cosine; *(iii)* 1-sample per bit (spb), and *(iv)* 2 spb. A 64-state VA was used throughout the experiment, whereas the quantization depth was varied from 4 to 7 bits to investigate the impact of A/D conversion on the performance. Results for various combinations of receiver structures and the number of quantization bits, as well as the eye-diagram at 600 km are shown in Fig. 5.7. Note that 64-state VA with 4-bit A/D, presently a realistic architecture at 10 Gb/s is capable of driving BER well below the FEC threshold for all receiver structures under the consideration. More importantly, the low-pass filtered shape of the waveforms allows for negligible difference in performance between 1-spb and 2-spb receiver structures. BER curves

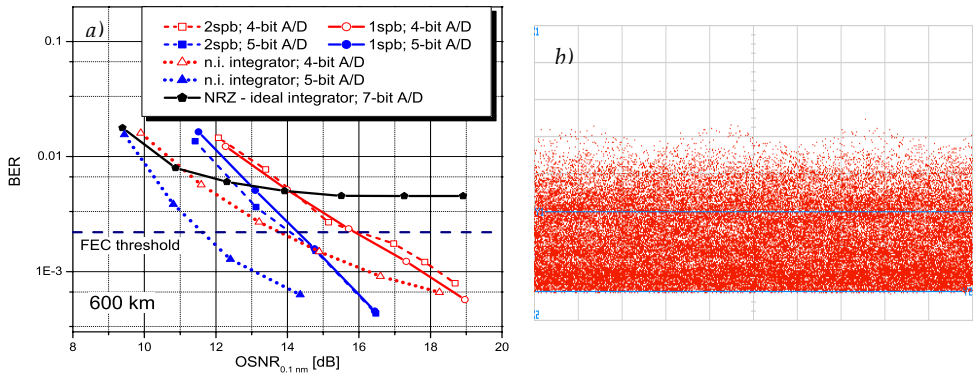

Fig. 5.7: (a) Viterbi equalizer performance for various receiver structure realizations; (b) Eye diagram at 600 km

for 5-bit A/D were also plotted to illustrate that the quantization process, rather than the VA complexity dominates the performance of sequence estimation at a given amount of accumulated dispersion. We note that the performance under a (non-ideal) integrate-and-dump receiver structure, capturing more energy of the information-bearing waveforms, shows superior performance to sparse sampling of the amplitude. However, the onset of the error-floor formation implies that the multiplicity of minimum-distance error events for the integrator is noticeably larger than that of multiple samples per bit detection.

Finally, Fig. 5.7 also illustrates the performance of NRZ format for the same complexity VA. An error floor above the FEC threshold is evident in the performance curve. Thus, even under advanced detection conditions for the NRZ receiver, i.e., an integrate-and-dump receiving filter and 7-bit A/D quantization, NF-OOK demonstrates a superior performance with respect to NRZ, at a given propagation distance and with the same complexity equalization scheme.

5.4. Chapter Summary

In this Chapter, experiments with sequence estimation were presented. In addition to performance evaluation, the investigation was also focused on receiver structure trade-offs. Results of two sets of experiments were presented: For the first part, equalization of the common NRZ format in metropolitan-type distances was demonstrated, whereas in the second part of the Chapter experimental demonstration

of the extended reach of the NF-OOK was presented, opening the possibility for equalization techniques to long-haul networks.

In particular, we have compared the performance of different receiver structures used in combination with the Viterbi-algorithm-based sequence estimation for the equalization of GVD-induced intersymbol interference in fiber optic links. Our experimental results demonstrate that energy detection, by means of a non-ideal integrate and dump filter, provides superior performance to intensity waveform sampling by few samples per bit detection, as long as the ISI does not overwhelm the available equalizer complexity. On the other hand, multiple samples per bit provide a longer reach at a cost of a more complex receiver structure that involves oversampling (at tens of giga-samples per second), and up to 5 dB power penalty for the case of 2 samples per bit. Our results suggest that detection based on multiple samples per bit can be substantially improved by employing "dirty" sampling by combining energy detection and waveform sampling, reducing the (required OSNR for 10^{-3} BER) power penalty to within 2 dB for 2 spb based on a 12 ps "sampling" window.

By reducing the bandwidth of the transmitter, we have demonstrated an extended reach of equalized links beyond 500 km, and a reach of 600 km at OC-192 speed was demonstrated (over cumulative dispersion of 10200 ps/nm). The technique, introduced in Chapter 4, employs narrow filtering of a conventional NRZ transmitter, enabling a substantial extension in the dispersion-limited-reach, if used

in conjunction with VA-based processing. As already pointed out in Chapter 4, the slow rate of increase of the ISI-span allows the use of low-complexity equalizers for the same amount of accumulated dispersion.

Chapter 6

Phase Coding for Suppression of Nonlinear Ghost Pulses in Long-Haul Fiber Optic Links

6.1. Introduction

In all of the previous chapters, mitigation of linear effects in fiber optic links was investigated. In particular, various aspects of electronic equalization for mitigation of chromatic and modal dispersion have been studied. In this Chapter mitigation of nonlinear effects will be examined. Specifically, mitigation of ghost pulses that arise in long-haul dispersion-managed links with lumped optical amplification will be investigated. The "ghost" pulses appear in return to zero (RZ) time slots carrying 0-bits in the transmitted data stream. They are generated by repeated nonlinear four-wave mixing (4WM) of the dispersion-broadened, partially overlapping data pulses carrying 1-bits.

In general, ultra-long haul links span several thousands of kilometers. Optical amplification in these links is performed in periods of 50 km (in submarine systems) to 100 km (in terrestrial links) [1]. The amplifier separation is determined by the tradeoff between the desired-end-of-link Optical Signal to Noise Ratio (OSNR), and the cost, as decreasing the EDFA separation leads to a slower accumulation of the amplified spontaneous emission (ASE) noise, whereas reducing the number of amplifiers (i.e. extending the separation between the amplification hubs) reduces the link cost.

As stressed at several occasions already, information bearing pulses spread in propagation. To counter this effect, all-optical compensation is used in long-haul links. Dispersion compensation is commonly performed periodically such that the compensation sites, that inherently add substantial losses, coincide with amplification hubs. Thus, in long-haul links, dispersion compensation is performed periodically with periods ranging from 50 km to 100 km. Although the nonlinear effects in optical fibers are relatively weak, the extremely long interaction lengths over trans-oceanic distances allow considerable buildup of (small) nonlinear contributions in propagation. Consequently, considerable signal degradations due to the nonlinearities incur in long-haul links. In fact, the non-linear effects present a major obstacle for reliable communication in these links. In this Chapter of the dissertation one specific example of nonlinear interaction will be studied. In 1999, formation of "Ghost pulses" in ultra-long haul systems was reported [91-93]. The term "ghost

pulses" was attributed to the apparition of pulses inside 0-bit slots that lead to decision errors in detection (see Fig. 6.1). It was soon concluded that the ghost pulses are a consequence of periodic nonlinear interaction in long-haul links are going to present an ultimate limit for optical links (both single, and multi-channel) operating at 40 Gb/s and higher. Therefore, mitigation techniques for this nonlinear impairment at high communication rates are necessary. Although several different approaches have been proposed for ghost pulse mitigation, the utilization of modulation codes will be investigated in this Chapter. Specifically, as will be demonstrated in Sec. 6.2. ghost formation can be mollified by encoding the phase of the information bearing

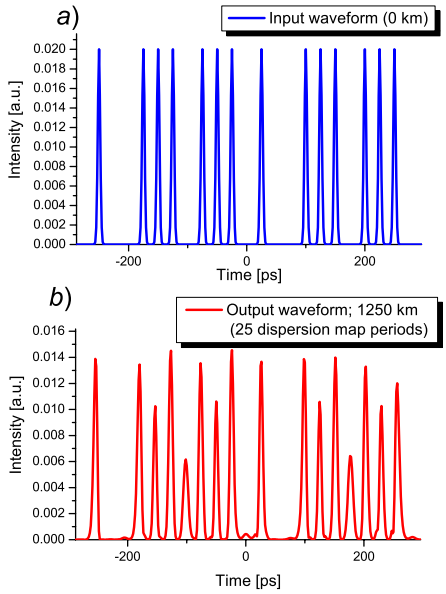

Fig. 6.1 Ghost pulse formation. (a) 21-bit stream at the input. (b) Same bit stream after 1250 km of propagation with periodic dispersion compensation and amplification performed every 50 km

pulses. Even though the modulation format is still OOK (i.e. intensity modulation), the proposed method relies on using the extra degree of freedom of optical phase by assigning specific phase patterns to the amplitude modulated information. Note that the optical phase is inconsequential in direct detection, however the phase encoding can impede formation of ghost pulses in such a way that it will enable reliable detection.

The rest of this Chapter is organized as follows: The physics of the ghost-pulse formation will be reviewed in Section 6.2. as well as the effect of the phase on the ghost pulse formation. Simple data-independent phase codes as a method for ghost pulse mitigation will be examined in Section 6.3. In section 6.4. , a better approach relaying on *data-dependent* phase encoding for ghost pulse mitigation will be introduced. It will be shown that data-dependent encoding strategies substantially improve performance in these links. Finally, a Chapter summary is presented in Section 6.5.

6.2. Physics of ghost pulses and intrachannel four-wave mixing

In order to determine mitigation techniques for ghost pulses, let us first examine physical effects leading to their formation. As stated in Chapter 1, pulse propagation in optical fibers is modeled by the Nonlinear Schrödinger (NLS)

Equation. Note, however that in long-haul links the NLS parameters become (quasi) periodic [94]:

$$i\frac{\partial u}{\partial z}=\frac{1}{2}d(z)\frac{\partial^2 u}{\partial t^2}+G(z)\,|u|^2\,u\,, \tag{6.1}$$

where $u(z,t)$ is the pulse complex amplitude of the optical field, z is the spatial coordinate in the direction of propagation, t is the time in the reference frame moving with the pulse center, and $d(z)$ and $G(z)$ are periodic functions that include the effects of dispersion management (DM), fiber nonlinearity, loss and gain. In our study we consider a return-to-zero (RZ) bit stream consisting of N pulses with a pulse shape $p(t)$ in a bit duration T. The total field of the bit stream $u(t)$ is described by $u(t)=\sum_{k=-N/2}^{N/2-1}a(k)\,p(t-kT)$, where $a(k)$ is either 1, or 0, when the corresponding information bit at the position k equals to "one", or "zero". Ablowitz and Hirooka [94] and Inoue and Maruta [95] modeled the formation of ghost pulses q_j in "space" slots of the bit stream using a linear equation with a periodic forcing term (under the small ghost magnitude assumption $|q_j|<<|u_k|$, where q_j is the complex amplitude of the ghost pulse in the j-th position):

$$i\frac{\partial q_j}{\partial z}+\frac{d(z)}{2}\frac{\partial^2 q_j}{\partial t^2}=-g(z)u_l^{*}u_m u_n \tag{6.2},$$

and $u_k\equiv p(t-kT)$ represents the pulse at the bit position $t=T_k$, and the location T_j of the ghost pulse is determined by phase matching condition in time:

$$j=n+m-l\,, \tag{6.3}$$

such that the pulses u_m, u_n and u_{m+n-j} interact through the four wave mixing (4WM) process affecting the information carrying bit in the position T_j, be it a one, or a zero. Note the similarity between the intrachannel 4WM in time positions in Eq. (6.3), and the phase-matching condition in Eq. (1.3) in frequency.

Next, we analyze a simple example of a bit stream consisting of a 3 bit sequence, 1 0 1, with the respective time positions T_k corresponding to indexes k = –1, 0, 1. Two pulses cannot form a ghost pulse between them (time position T_j corresponding to j = 0), because the phase matching condition cannot be fulfilled at this position. However, new pulses are formed in the time positions k = –3 and 3. Fig.,

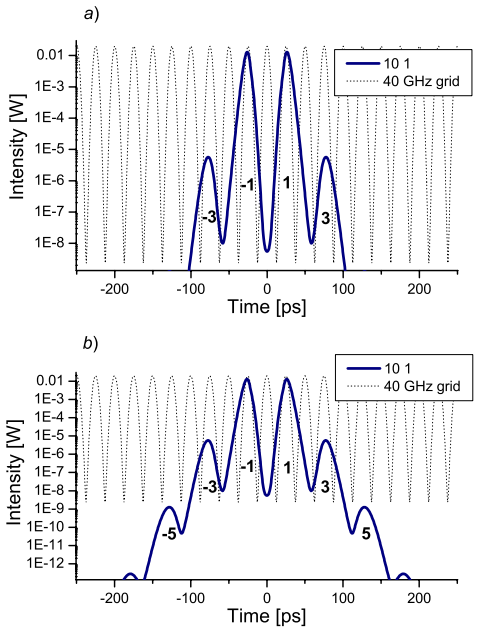

Fig. 6.2 Ghost pulse formation. (a) Echo pulses form in positions -3 and 3 as mirror images of genuine pulses in positions -1 and 1. (b) Higher order ghost pulse formation off first order ghost from part (a)

6.2a shows the result of a split step simulation applied to a 40 GHz pulse train with 5 ps pulse full width half maximum (FWHM) and average power of 6 dBm in a dispersion map consisting of 24 spans of 40 km of standard single-mode fiber (SSMF) and 10 km of dispersion compensating fiber (DCF) with amplification after each span. The results of Fig. 6.2(*a)* demonstrate that the intrachannel 4WM has the effect of forming "mirror image" pulses, or the pulse echoes, as they were fist termed by Mecozzi, Shtaif et al. [96-98] (i.e., mirror images around k = 1 and –1). Once the primary echoes are formed, their energy is readily used for alimenting the secondary and all subsequent echoes. The continuing echo formation is illustrated on a logarithmic plot in Fig. 6.2*b,* where additional higher order ghost pulses appear when the plot scale is extended to show the lower values.

One additional effect in Eq. (6.1) is of importance, namely the effect of the dispersion map on intrachannel 4WM. As stated above, the dispersion in Eq. (6.1)

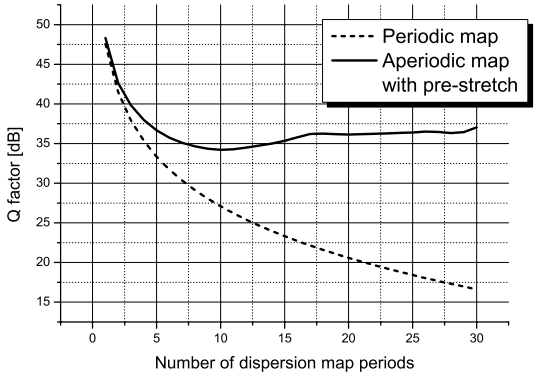

Fig. 6.3 Effect of dispersion map on Q factor evolution. Periodic map with fast Q drop in dashed line and aperiodic map much more resilient to intrachannel 4WM in solid line

enters through the periodic parameter *d(z)*. Judicious choice of dispersion maps were a focus of research attention in the early 2000's [99-100]. The effect of dispersion map configuration is illustrated in Fig. 6.3 that shows an evolution of the Q factor with propagation for a simple periodic map with complete compensation (dashed line in Fig. 6.3) and a more advanced map that includes both pre-stretching (pre-compensation) and incomplete compensation per span (solid line in Fig. 6.3). The chosen figure of merit (the Q factor) is the argument of the Q function from Eq. (2.1), stressing the average effect of eye-diagram degradation. This quantity has stuck with the field of optical communications despite the obvious confusing relation to the cumulative function of the Gaussian distribution, it originates from.

A counter-intuitive effect evident in Fig. 6.3 is that Q factor can ascend after an initial decrease. Such "magicdispersion maps " (as named by Turitsyn et al.) [100] need to be designed for each link separately, including all the parameters of propagation (e.g. number of channels, launch power per channel, amplification site separation, total propagation length, etc.). With these properties available to a designer, as demonstrated by Turitsyn and Essiambre [99-100] such effects of Q increase can be taken advantage of to substantially improve performance and increase the reach of long-haul links. However, although the dispersion mapping is a powerful technique, it cannot prevent ghost pulse formation altogether.

To summarize the effects of intrachannel mixing introduced in this section, Fig. 6.4 shows a simulation of an eye-diagram after 1250 km of propagation. For

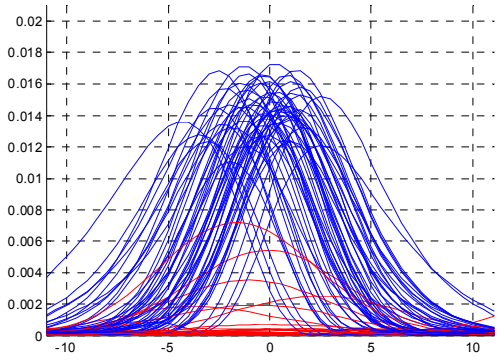

Fig. 6.4 Eye diagram after 2000 km propagation in a periodic map shown in Fig. 6.3

better illustration the total effect of intrachannel interactions, mark-positions are plotted in blue, whereas the 0-bit positions in the eye diagram are plotted in red. By close examination of Fig. 6.4, we conclude that there are three effects resulting from the intrachannel 4WM: *(i)* Ghost pulse formation, or the formation of pulses in the 0-bit positions; *(ii)* Amplitude jitter of the marks, that is a consequence of the energy redistribution through 4WM defined by Eq. (6.3); and *(iii)* large timing jitter that is a consequence of XPM-like intrachannel interactions in Eq. (6.3) when $j = n$ and $m = l$ [94]. Having briefly introduced physical effects leading to the formation of ghost pulses, we shall proceed to mitigation of this deleterious effect.

6.3. The pulse phase transfer in ghost pulse formation and simple data-independent encoding schemes

To approach phase encoding for mitigation of ghost-pulse formation, let us start out by inspecting the phase of the echo pulses. Several authors investigated this issue, [93-98] for pulse sequences with constant phase, concluding that the phase

difference of the echo pulses is retained during the propagation. Mathematically, the phase transfer can easily be established from the Eq. (6.2). Fig. 6.5 shows an interaction resulting from a 101 pattern, examined in the previous Section. Here, however, the initial pulses have an initial phase difference of 0 and π (emphasized by the 101 and 10-1 label in the plot, respectively). The phases of the first-order ghost pulses are shown in the lower part of Fig. 6.5. As demonstrated in the previous section, ghost pulses (as a consequence of 4WM) are formed as mirror images of the genuine 1-bits in the bit-stream. Concentrating on the phase of the formed mirror-image pulses Fig. 6.5 shows the result of the split-step simulation that demonstrates that the echo pulses retain the phase, or more precisely the phase difference, of their parent pulses. For example, the pulse in the position -3 that is the mirror image of the

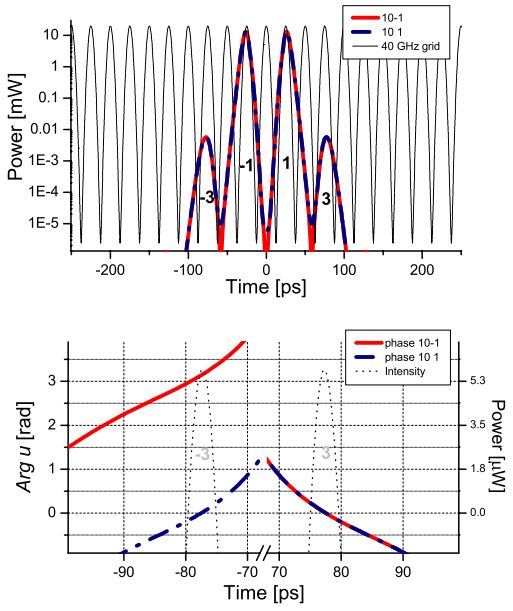

Fig. 6.5 Phase transfer in ghost pulses formation. Formed ghost pulses bear the same phase difference as their parent pulses either 0 (101 case in solid line), or π (10-1 case in dashed line).

pulse in the position 1 has a π phase shift, just as the its parent pulse (in position 1). Same conclusion is reached for the ghost pulse in position 3 and its parent in position -1. Consequently, the phase encoding can be used to our advantage to mitigate the ghost pulse formation. As stressed in the previous section, strong ghost pulses are formed in zero-positions surrounded by multiple marks on both sides.

Both Eq. (6.3) and the reasoning from the previous paragraph suggest that the 1-bit phases can be tailored such to achieve destructive interference of the ghost pulses, pictorially illustrated in Fig. 6.6(*a*). In addition, care must be taken not to inflict destructive interference in the positions where genuine marks reside. The latter effect is illustrated in Fig. 6.6*b* that shows a result of propagation of 5 consecutive marks (after 1250 km of propagation) encoded as -1111-1. Under these circumstances the two outer marks with the phase of π will be imaged onto the middle mark having the zero initial phase, and as a result of this unfair two-against-one interaction, the

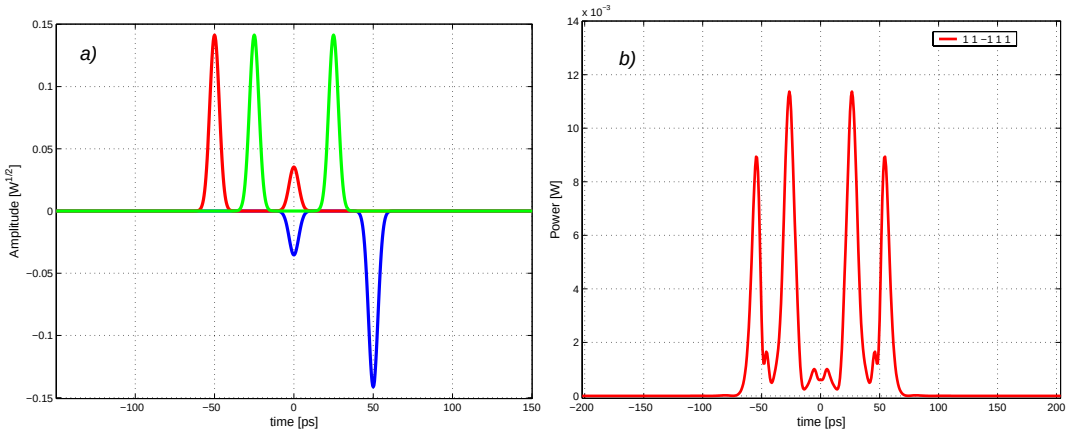

Fig. 6.6 (a) Destructive interference of ghost pulses from parent pulses having phase 0 and π. (b) Pitfall of phase encoding. Destructive interference of 2 outer pulses in the position where a genuine mark resides, but has an opposite phase from the outer pulses

middle mark is reduced, leading to an error at the receiver. Extending this reasoning, there are 3 possible simple encoding strategies capable of suppressing the strong ghost formation in a zero-slot surrounded by multiple marks on both sides (while ensuring that no genuine marks are affected by the encoding): *(i)* Single bit inversion, where one of the intermediate marks is encoded by a π phase shift; *(ii)* Duobinary encoding (DB) where a whole group of marks on one side of the zero-bit exhibits the phase-change and *(iii)* Alternate Mark Inversion (AMI), in which phase is changed by π for every other mark in the bit-stream. The three simple encoding approaches are illustrated in Fig. 6.7. We refer to these approaches as "simple" in that they are aimed

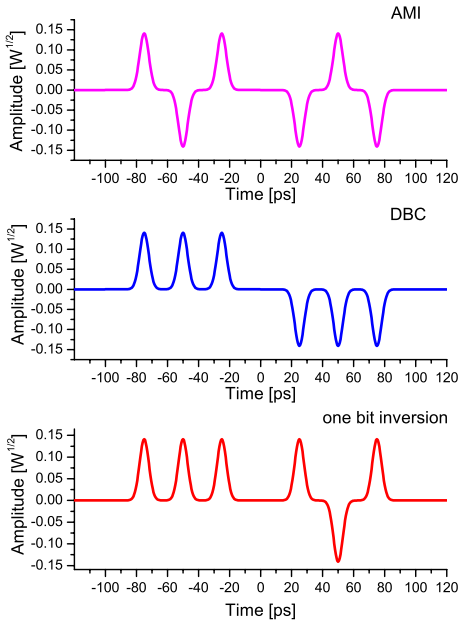

Fig. 6.7 Data independent phase encodings: Alternate mark inversion (AMI); Duobinary encoding (DBC); Single-bit inversion;

only at mitigation of the strong ghost, such that they can be thought of as short-span phase encodings (in terms of the length of the overall sequence). Fig. 6.8 shows the simulation result of the three encoding approaches. We can see that the AMI approach has slightly better overall performance than the other two approaches. The total average performance in terms of the Q improvement for AMI amounts to approximately 1.4 dB improvement in a long pseudo-random stream of pulses. Quantitatively speaking, the stated improvement of 1.4 dB is relatively modest. This small performance improvement is commensurate with the simplicity of the underlying coding schemes that are designed to counter only strong interaction encompassing up to five pulses. As demonstrated in the following Section, to achieve superior improvement and the overall system performance, more complex, data-dependent approach is necessary that takes into account the long channel memory illustrated in Fig. 6.2(b).

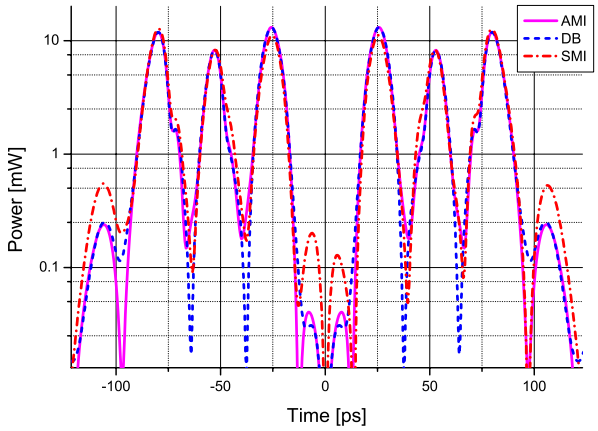

Fig. 6.8 Effect of three different data-independent (simple) phase encodings

Note that in difference to the equalization techniques examined in the previous chapters of the thesis, the phase encoding is performed at the transmitting end of the link. The virtue of the phase codes is that they do not introduce any increase in the line rate (or, equivalently do not reduce the information content transmitted), as no additional bits need be transmitted. The introduced redundancy is in the phase of the signal that otherwise does not affect the square-law detection. Phase codes, on the other hand require an additional phase modulator at the transmitter in addition to an encoder to accomplish phase encoding of the transmitted bits. For the phase encoding approach to be effective in mitigation of intrachannel 4WM, the pulse phases need to be conserved over long distances of propagation. More precisely, the destructive interference upon which the phase interactions are based necessitates only that the relative phase between the pulses entering the interaction be retained. The nonlinear interaction encompasses between 20 to 100 pulses in a 40 Gb/s stream. This is relatively tiny interval compared to the microsecond coherence time of modern telecommunication lasers. As the last and the strongest argument, the phase encoding has been demonstrated using differential phase shift keying (DPSK) modulation [86]. Indeed propagation beyond 5000 km at 40 Gb/s with DPSK have been demonstrated, corroborating the pulse phase difference in a data-stream is indeed sustained over long propagation distances. Consequently, our proposed method of using phase to suppress the ghost pulses can be used in the same way it enables DPSK.

6.4. Data-dependent encoding

As has been pointed out in the preceding sections of this Chapter, the greatest risk for bit errors from intrachannel 4WM comes from the ghosts arising in a single 0-bit slot surrounded by symmetric patterns of ones (e.g. 11011, 1110111 etc.) [97-98]. As an approach for reducing the strong ghost pulse formation, use of phase coding (e.g., duobinary coding (DB), modified duobinary (MDBC) and alternate mark inversion (AMI)] has been proposed in the previous section and demonstrated in [101-102]). The proposed phase coding schemes rely on the fact that the phase of a ghost pulse has a fixed relationship to the phases of the genuine "ones" in the bit-stream that enter the 4WM process. Thus, the strongest ghosts can be eliminated by tailoring the phase of the surrounding 1-bit slots to cause destructive interference between the various contributions to a ghost. However, while the above-mentioned coding techniques are highly efficient in eradicating strong ghosts, they do not mitigate weaker "side ghosts" that materialize in the time slots of multiple consecutive 0-bits. With the intention of suppressing these side ghosts as well, efforts should aim at energy redistribution among the 1-bits in a block of marks, instead of manipulating the phases of marks to achieve only destructive interference of the echo pulses [96], since, in according to Eq. (6.3), no code can achieve destructive interference in several consecutive time slots. Consequently, in this section we shall examine the use of data-dependent encoding that provides a 3 to 10 times the reduction in energy leakage from 1-bit slots to 0-bit slots as compared to the coding

schemes investigated in Sec. 6.3. , [101-102], and thus, significantly improves the performance. To the best of our knowledge this is the first accomplishment of efficient data-dependent coding for alleviation of nonlinear effects in fiber-optic transmission systems.

In order to provide an illustration and a mathematical framework for the data-dependent codes, we again first examine a 3-pulse interaction. Assuming a transmission system with small nonlinear effects, the nonlinearity can be treated as a perturbation to the solution of the linear part of the NLS , [103, 13]. The solution of the linear propagation equation for a Gaussian input pulse, $q_k(0,t)$, normalized such that $\max\left(|q_k(0,t)/A_k|\right)=1$, is given by [103,13]:

$q_k = A_k\sqrt{r(z)}\exp\left[-(p^2 - iC/2)(t-T_k)^2 + i\theta_k\right]$, where $p^2(z) = T_0^2/(T_0^4 + D^2(z))$; and $D(z) = \int_0^z \beta_2(s)ds$;

$C(z) = -D(z)/(T_0^4 + D^2(z))$, $r(z) = T_0^2/(T_0^2 - iD(z))$, such that A_k is the pulse amplitude (k=1,2,3), θ_k is the initial phase of the pulse, (T_{FWHM} is the input pulse full width at half maximum), T_k is the time slot corresponding to the k-th pulse and β_2 is the fiber group velocity dispersion parameter. The amplitudes, A_k, can be calculated from the pulse energy transfer equations. For instance [103-104]:

$$A_2(z) = \frac{E_0}{1 + 2\exp\left[-2E_0F(z)\right]} \tag{6.4}$$

where,

$$F(z) = -\int_0^z \gamma(s)D^2(s)p(s)T_0\sin(C\Delta T^2 - \Delta\theta)\exp(-2p^2\Delta T^2)ds \tag{6.5}$$

with energy conservation:

$$A_2^2(z) + 2A_1^2(z) = A_2^2(0) + 2A_1^2(0) \equiv E_0 \tag{6.6}$$

and, $a^2(z) = \exp\left(-\int_0^z \alpha(s)ds\right)$. In the previous equations α and $\gamma(z)$ are the fiber attenuation and nonlinear parameters, respectively. $\Delta T = T_{k+1} - T_k$ is the temporal pulse separation in the bit-stream. For our three-pulse example, the phase difference is defined as $\Delta\theta = 2\theta_2 - \theta_1 - \theta_3$ being the fiber attenuation and nonlinear parameters, respectively. For values $\theta_2 = \theta_1 = \theta_3 = 0$, Eq. (6.4) implies that energy will leak from the central pulse into the side pulses, however, by choosing $\theta_2 = \theta_1 = 0$ and $\theta_3 = \pi$, this process will be reversed and the two side pulses will pump the energy into the

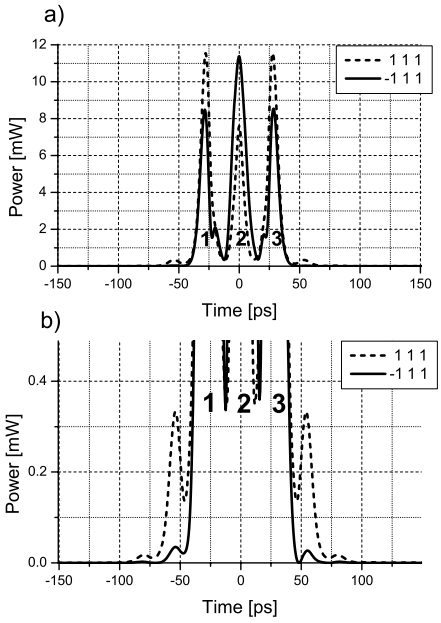

Fig. 6.9 (a)Pulse triple interaction depending on the phase of one of the one side pulses. (b) zoom into the lower power values from part (a) concentrating on the energy leakage in position 4 and -4.

central pulse. This process is illustrated in Fig. 6.9, showing the split-step simulation result of the output power distribution obtained from the 3-pulse interaction in a dispersion managed 1200 km fiber link. The features of interest, which are highlighted in Fig. 6.9b, are the side ghost pulses. It can be noted that, if the appropriate phase coding is applied (i.e. $\theta_2 = \theta_1 = 0$ and $\theta_3 = \pi$,) the side pulses will aliment the central pulse, and less energy will leak into the side ghosts.

Table 2. Binary phase encoding patterns yielding the strongest ghost suppression

Bit pattern	Phase Encoding
1101	1-101 or 110-1
11001	1100-1 or 1-1001
110001	1-10001
110011	11001-1 or 1100-11
1100011	11000-11
11101	11-10-1 or –11101
111011	11-101-1
111001	11-100-1 or –111001
1110011	11-10011
11100111	11-1001-1-1
1110001	11-10001
11100011	11-10011
111000111	11-1000-111
1111001	1-11-100-1

The existence of more than 3 pulses leads to more complex interactions that are difficult to analyze in a closed form. Consequently, by means of simulation, we have determined data dependent phase encoding patterns that yield the best ghost suppression. Our observations can be summarized as follows: (i) code has to be skew-symmetric about an isolated 0-bit surrounded by 2 blocks of marks to prevent strong

ghost formation [101]; (ii) alternate mark-doublet inversion (AMDI) of blocks of marks (dividing a block of marks into doublets and changing the phase by π of every other doublet) should be used to impede energy leakage into multiple successive 0-bit slots; and (iii) interaction between antipodal doublets within blocks of more than 3 consecutive marks, coded by AMDI, leads to an undesirable variance in the power of 1-bits after 10 dispersion map periods, implying that for these long blocks of marks, the alternate mark inversion is preferable. Table 1 summarizes empirically determined codes that achieve the best suppression of ghost pulses in the most frequent short bit patterns. Our investigations have been performed in dispersion

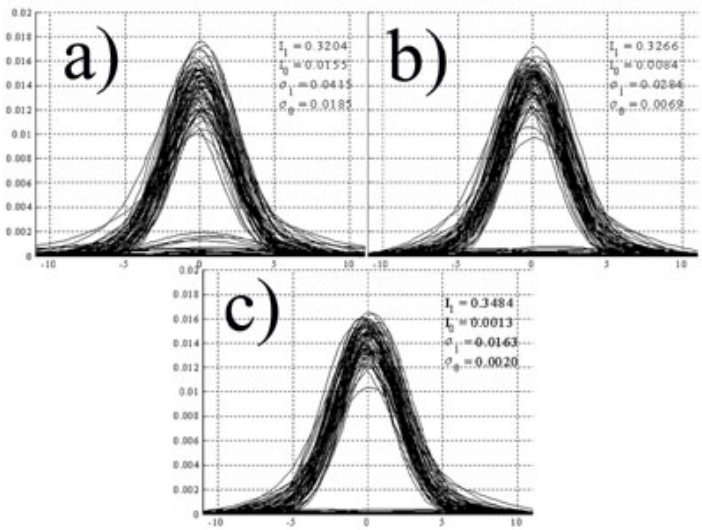

Fig. 6.10 Eye diagrams after 3000 km for average launch powers of 0 dBm. Means and deviations cited in arbitrary units. (a) Uncoded stream; (b) Stream coded by AMI, and (c) Data dependent phase encoding method. Simulated link consists of 30 spans of 100 km (approximately 95 km NZDSF fiber (D = -7.06 ps/nm-km) and 5 km DCF) with residual 20 ps/nm span and pre-compensation of –450 ps/nm.

maps with a fixed amount of pre-compensation in settings with complete, as well as residual, dispersion per-span. We found that, for complete compensation per span, both AMI [101] and our data-dependent phase codes, defined in Table I, increase the Q by approximately 2.8 dB and 6 dB, respectively. The number of overlapping pulses used in our simulations was varied between 8 and 20 pulses.

We have applied phase coding methods described above to pseudo-random bit sequences (PRBS) of 128 bits to quantify the performance. Fig. 6.10 shows eye-diagrams obtained for a 40 Gb/s stream after 3000 km (TFWHM = 5 ps). The simulated dispersion map consisted of approximately 95 km of non-zero-dispersion-shifted fiber (NZDSF) with D = 7.06 ps/nm-km and 5 km of dispersion compensating fiber (DCF) with 20 ps/nm residual dispersion per span and with –450 ps/nm pre-compensation. Applying code patterns described in Table 1, resulted in reduced values of mean and variance in the signal power of spaces (see Fig. 6.10). The high launch power in Fig. 6.10 was chosen to create a clearer illustration of the effect of coding. The dependence of performance improvement on the launch power, based on 20 random sequences, is summarized in Table 2. The unusually large values of Q are attributed to the fact that the amplifier noise was excluded from calculations, primarily to show the deterioration in performance due to ghost pulses. Compared to AMI, which suppresses only the strong ghosts appearing in symmetric patterns, our data- dependent coding technique reduces the average power-leakage into multiple 0-bit slots and, in so doing, further decreases probability of bit errors. Notice that

Table 3. Values of the Q factor and corresponding performance improvements for 3 different launch powers.

	Q [linear]		
	Encoding method		
Launch Power	no coding	AMI	Data-dependent
-4 dBm	81.0	95.0	127.4
0 dBm	30.2	36.5	57.3
6 dBm	7.1	9.5	12.8
	Q Improvement ($20\log(Q_{coded}/Q_{nc})$)[dB]		
	Encoding method		
Launch Power	no coding	AMI	Data-dependent
-4 dBm		1.4	4.0
0 dBm		1.6	5.8
6 dBm		2.6	5.2

symmetric patterns occur with low probability, making the data independent AMI less effective. In contrast, our novel data dependent coding approach increases the Q factor by 4 dB showing an additional improvement of about 2.6 dB at realistic input power levels (-4 dBm).

Strictly speaking, it is not valid to refer to the modulation technique introduced as a code since the encoding process for arbitrary length information sequences has not been defined. The importance of the work is in the fact that it represents the first instance of applying data-dependent patterns to mitigate the nonlinear effects in fiber optic communications.

It is important to stress the fact that the phase coding approaches cannot substantially increase the error-free distance of an ultra-long haul link, however, they do ensure an improved performance at any given point in the link, which was

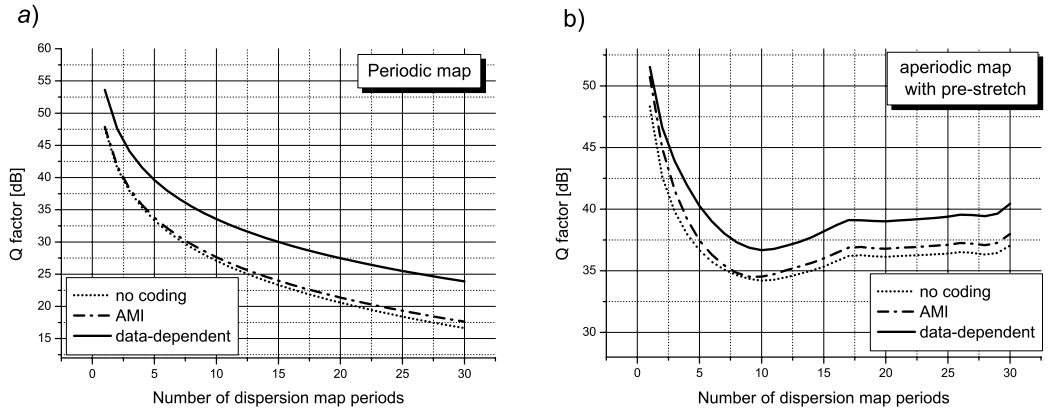

Fig. 6.11 Q factor evolution for different encoding approaches in (a) periodic and (b) aperiodic dispersion maps shown in Fig. 6.3

demonstrated quite recently in [105]. The extension of the error-free distance is determined by the gain in performance and amounts to approximately 10 dispersion map periods for our data-dependent phase encoding scheme.

In conclusion to this section we provide the evolution of the Q factor with propagation distance for different encoding methods under the same conditions presented in Fig. 6.3. Results clearly demonstrate superiority of data dependent encoding approach irrespective of the dispersion map used.

6.5. Chapter Summary

In this Chapter, mitigation of intrachannel four-wave mixing effects by means of phase encoding was investigated. This mitigation approach is effective independently of the dispersion map configuration, although the actual map does play a role in the amount of performance improvement. Phase encoding has the

benefit that all processing is lumped at the transmitting end of the link. Two general phase approaches have been investigated: (i) data-independent approaches (single-bit inversion, duobinary and alternate mark inversion) and (ii) data-dependent phase encoding. Data-independent approaches adopt simple phase encodings irrespective of the information content transmitted. They are aimed at diminution of strong ghost pulses formation that materialize in isolated 0-bit slots surrounded by multiple 1-bits on each side. The approach of choice among these simple coding schemes is the alternate phase inversion approach that introduces a phase-change by π at every 1-bit in the data stream. On average this coding approach provides only about 1.4 dB performance improvement that is a consequence of the fact that it redistributes the energy from strong ghost pulses into surrounding 0-bit slots. In addition, data-independent phase encoding approaches have been shown to introduce excess amplitude jitter of 1-bits, reducing the overall usefulness of the method. This outcome clearly led to the introduction of data-dependent phase encodings. The introduced data-dependent approach involves the use of a data-dependent phase patterns to suppress small ghost pulses that are resistant to previously proposed coding methods (e.g., DBC, MDBC, and AMI [101-102]). Our method is useful for practical low-power RZ systems, providing approximately 4 dB improvement of the Q factor. It shows about 2.6 dB additional improvement over that provided by data-independent phase coding methods on a typical terrestrial 100 km dispersion map period. The coding scheme provides comparable improvements for a broad interval of average launch

powers, both in dispersion maps with residual dispersion per span, as well as in those with complete compensation.

6.6. Acknowledgment

The text in the Chapter 6, in part, is a reprint of the material as it appears in IEEE Photonics Technology Letters, Alic, Nikola; Fainman Yeshaiahu. "Data-dependent phase coding for suppression of ghost pulses in optical fibers," IEEE Photonics Technology Letters, vol.16, 2004. The dissertation author was the primary researcher and/or author and the co-author listed in this publication directed and supervised the research which forms the basis for this Chapter.

Chapter 7

Summary and Future Directions

7.1. Thesis Summary

In this dissertation several approaches to mitigation of major impairments in fiber optic digital communications systems have been presented. The main interest was in the investigation of the applicability of equalization and, to a lesser extent, modulation and coding techniques. This is in difference to the more common (and currently universally employed) all-optical mitigation approaches in fiber optic systems. Our intention was to develop a firm theoretical foundation for the performance evaluation in fiber optic systems, as well as to quantify the performance of equalization under the constraint of the current state of processing technology. On the practical side, the aim of the investigation was to develop methods for mitigation of impairments in high-speed optical communication systems, which require little modification of the existing infrastructure. Consequently, for all of the presented approaches the complete processing is performed either at the transmitting, or the

receiving end of the link (or at both ends), thus not requiring any additional changes of the transport plant of the existing systems.

In the first five chapters of the dissertation, an extensive treatment of the maximum likelihood sequence estimation was developed in different channel regimes. In Chapters 2 and 3 MLSE in short-haul links containing no optical amplifiers was treated. The performance in these systems is dominated by the thermal noise component originating in the detector. A full scale theoretical apparatus was presented that enables rigorous performance evaluation. Extending on the previous work in linear coherent communication systems, the performance bounds for MLSE in optical links were derived. An excellent match between the theory and experimental result was established. In addition, the developed methodology enabled evaluation of MLSE performance for various modulation formats. It was shown that better performance under bit-by-bit decision translates into superior performance under MLSE. However, with the application of MLSE the difference in performance between different modulation formats considered diminishes.

Special attention was devoted to the interpretation of the results. The superior performance of MLSE in channels with ISI was related to the decision making based on groups of bits at a time. The size of this group of bits has to correspond to the extent of the ISI in the channel, in order to achieve optimal performance. A geometrical analogy of detection in channels with ISI to the decision making in a

multi-dimensional space was established. In addition, it was shown that the traditional bit-by-bit detection corresponds to decision making in a single dimensional space (which is a subspace of the MLSE signal space). Consequently, it was concluded that MLSE can never under-perform bit-by-bit decision.

An important observation from the results is that the power penalties incurred by employing equalization based on the non-coherent square-law detection are substantial and can exceed 6 dB. However, the real advantage of the approach is its low cost and flexibility in a network environment, or in adaptability to the ambient induced perturbations.

The focus of the investigation in Chapter 3 was the application of MLSE in directly modulated multimode fiber links. The experimental equalization results including MLSE in multimode fiber based links with directly modulated VCSELs were presented. In particular, the experimental BER was measured below 10^{-6}, after 400 m of propagation (for a completely closed eye) in a spool of legacy multimode fiber in which transmitting information over 100 m is seldom achieved. It was shown that in order to enable signal processing, the use of modulation codes that force data DC-balancing is required. The utilization of modulation codes enables the transmission of information on an otherwise dysfunctional link without any additional optical components.

Chapter 4 focused on the application of MLSE in longer reach links that incorporate optical amplification. The inclusion of optical amplifiers results in signal

dependent noise statistics. The exact statistics were derived by means of Karhunen-Loeve expansions. It was shown that the exact signal statistics not only substantially deviate from the thermal noise dominated regime (prevalent in the communications literature), but they also differ from the commonly cited chi-square statistics. The exact signal statistics depend heavily on the exact shape of the optical filter in the link. Due to the colored nature of the noise that is a consequence of optical filtering at the receiver, maximum likelihood detection becomes prohibitively complex. Nevertheless, suboptimal detection relying on a simple integrate-and-dump filter showed satisfactory performance. On the other hand, the performance improvement based on utilizing the exact statistics is relatively small and amounts to up to 1 dB in most cases. This surprising result was elucidated through the process of decision making in sequence estimation and the closeness of likelihood functions intersections' based on the exact and the approximate chi-square statistics. In addition, a novel modulation format was introduced in this Chapter – Narrowly Filtered OOK that incorporates very narrow filtering of the conventional NRZ format, at the transmitter. This narrow filtering is utilized as a means of taming the rate of increase of the span-contributed ISI, which, in turn, allows longer reach with the same complexity equalizers. In addition, the NF-OOK provides a simple way of increasing the spectral efficiency of the existing WDM systems by 2-5 times due to the confined spectral content achieved through narrow filtering at the transmitter.

Chapter 5 was devoted to experimental results of equalization by means of sequence estimation in metropolitan and long haul networks. Special attention was devoted to the performance of different receiver structures preceding the Viterbi equalizer. The experiments performed were based on the practical constraint of low complexity equalizers with low resolution A/D conversion. This technologically enforced complexity reduction necessarily entails deterioration of performance with respect to theoretical receivers. It was demonstrated that the integrator outperforms few samples per bit receivers by as much as 5 dB as long as the information bearing waveforms do not spread beyond the coverage of the employed Viterbi equalizer. As soon as this happens, the performance of the sequence estimation based on an integrator deteriorates rapidly and integrator receiver is outperformed by the multiple samples per bit that enable a longer reach for the same complexity of the underlying equalizer. The advantage of employing "dirty" samplers whose "sampling" window extends over an extended period of time was discussed. Through this extended sampling, more energy is captured and the noise is averaged, bringing the performance closer to that of the integrator. Experimentally, a power penalty reduction from 5 dB to 2 dB was demonstrated for a 12 ps dirty sampler that retained an extended reach of 50 km over the integrate-and-dump receiver for the same complexity equalizer. The first experimental demonstration of the NF-OOK format was also presented in this Chapter. A current record reach of 600 km was achieved utilizing a zero-chirp modulator at the transmitter in a link containing no

optical dispersion compensation. This result clearly indicates the validity of the theoretical predictions regarding the reduced ISI spreading that is a consequence of the forced reduced spectral content of the modulation format.

All of the impairments treated in this dissertation present various realizations of intersymbol interference (ISI). Whereas the first five chapters focused on a more common chromatic dispersion caused ISI mitigation, Chapter 6 was devoted to mitigation of ISI mediated by the fiber nonlinearity. The "ghost" pulses materialize in 0-bit slots in ultra-long haul optical links causing errors in detection. The formation of the ghost pulses is a consequence of periodic nonlinear interactions and energy transfer between the dispersion broadened 1-bit pulses in propagation. An approach of applying phase codes was proposed and investigated for mitigation of this severe effect that is predicted to be the main impairment in the next generation 40 Gb/s long haul links. The method relies on assigning specific phase patterns onto the information-bearing pulses' envelope (in the intensity modulated data stream) that prohibits and/or mitigates the formation of ghost pulses in these links. The main conclusion of the investigation is that data-dependent phase encoding approaches yield a substantially superior performance to the data-independent codes (e.g. alternate mark inversion, or duobinary). The superiority of data dependent codes was demonstrated for various launch powers, as well as dispersion map configurations. Although the developed code patterns were 'ad-hoc' and lack rigor, their significance is in that they represent the first instance of the successful coding application in

mitigation of nonlinear effects in optical fiber communications. In fact, since the first publication of the work presented in this dissertation, several research groups pursued the outlined approach, defining more powerful codes, as well as developing information-theoretic bounds on the achievable performance of the method.

7.2. Future Directions

Although the dissertation covered in depth both theoretical and practical aspects of equalization in high-speed optical links, many problems remain unanswered and require further investigation. In particular, in order to place the results obtained in a firm information theoretic framework, the capacity of the fiber optic channel needs to be addressed. This is especially true with respect to the application of the introduced narrowly filtered modulation formats. Closely related to the investigation of the capacity of the fiber optic systems is the use of advanced error correction coding approaches. The technological advancements are close to availing fully integrated iterative detection techniques at 10 Gb/s transmission speeds. Consequently, advanced detection techniques relying on turbo equalization and/or incorporating Low Density Parity Check codes are expected to become commercialized within years. Although sporadic attempts to evaluate performance of these advanced coding approaches in fiber optic channel have been undertaken, no systematic investigation has been conducted. In particular, as has been proven in the

past, the experimental demonstration of these techniques is going to be both exciting and challenging.

Within the last year, the interest in coherent optical communication has been revived. With respect to this latest development, it is important to stress that the methods presented in this dissertation, with appropriate modifications, can be used both for practical equalization, and theoretical evaluation of equalization performance in coherent optical links.

In the present work, only single channel systems and/or impairments in single channel systems were examined, both theoretically and in the experiments. Further research should certainly incorporate evaluation of equalization in a more realistic WDM environment. The detection in fiber optic links is based on single user detection where each user (or alternatively few time-division multiplexed users) has a pre-assigned single frequency band (i.e. a WDM channel). Many of the impairments in the fiber optic channel discussed in this dissertation naturally open a possibility for multi-user detection as well as cross channel coding in which no single user has a dedicated communication band (or equivalently – a channel), where the information is transmitted and detected in parallel for all the interfering channels. Such approaches do not fit the current infrastructure of the fiber optic systems, but nevertheless present an interesting alternative, as well as almost completely unexplored research area. This research direction offers a possibility for both

scientific exploration, as well as communication beyond the limits imposed by the existing system architecture.

Appendix A

This appendix contains the detailed derivation of the performance bounds from Chapter 2 that is an adaptation of the theory presented in [3,24]. Throughout the derivation, it is invariably assumed that error events can be shorter than the whole transmitted sequence (sometimes referred to as elementary error events), which has the virtue of neglecting the leading and the trailing zeros of the error vector.

An upper bound to P_e

The probability of error for the error event $\{\underline{s}_1 \to \underline{s}_2\}$ is:

$$P(\underline{e}) \le P\left\{\phi_{\underline{a}_1+\underline{e}} > \phi_{\underline{a}_1} \mid A(\underline{e})\right\} \cdot P\left\{A(\underline{e})\right\}, \tag{A1}$$

where $P\{A(\underline{e})\}$ is the probability that the particular elementary error event, starting at the given position in the sequence, occurs. Since the event that $P\{A(\underline{e})\}$ starts at the given position is already included in the event $P\left\{\phi_{\underline{a}_1+\underline{e}} > \phi_{\underline{a}_1}\right\}$, the probability of error can be only upper bounded in Eq. (A1), and hence the inequality sign. The only thing left is to calculate $P\{A(\underline{e})\}$. For a sequence of independent data, the probability of an error pattern $\underline{e}$ of length R can be expressed as:

$$P\{A(\underline{e})\} = \prod_{k=1}^{R}\left(1 - \frac{\underline{e}(k)}{2}\right), \tag{A2}$$

on the premise that all errors are equally likely.

Let the union of all possible error events $\underline{e}$ be a set E. The bit-error probability Pe can be calculated as the sum of all possible error-patterns weighted by the number of errors in each one of them:

$$P_e = \sum_{\underline{e}\in E} w(\underline{e}) \cdot P(\underline{e}) \le \sum_{\underline{e}\in E} w(\underline{e}) \cdot Q\left(\frac{d\left(\underline{s}_1, \underline{s}_2\right)}{\sqrt{2N_0T}}\right) \cdot P\{A(\underline{e})\}. \tag{A3}$$

Owing to the sharp descent of the error-function-complement, in the moderate to high signal-to-noise ratio (SNR) operation regime, the expression for Pe will be dominated by the sequences that are the hardest to distinguish, i.e. minimum distance error events, separated by the distance d_{min}

$$d_{\min} \triangleq \min_{\underline{e}\in E}\{d(\underline{e})\}. \tag{A4}$$

Consequently, we finally reach the expression for the upper bound of the probability of error:

$$P_e \le \psi'(d_{\min}) \cdot Q\left(\frac{d_{\min}}{\sqrt{2N_0T}}\right), \tag{A5}$$

where

$$\psi'(d_{\min}) = \sum_{\underline{e}\in E(d_{\min})} w(\underline{e}) P\{A(\underline{e})\}, \tag{A6}$$

and $E(d_{min})$ is the subset of E including the error events with the distance d_{min}.

A lower bound to P_e

In order to estimate a lower bound to the bit-error probability, we consider an idealized situation in which the detection process is aided by a genie that supplies additional information on the transmitted sequence to the receiver. In such a case, it should be obvious that this idealized receiver will outperform any receiver working without this sort of genie assisted detection. Specifically, let us assume the genie operates as follows: when a sequence $a = (a_0, ..., a_{M-1})$ is transmitted, the genie at random chooses another sequence $\underline{a}' = \underline{a} + \underline{e}$, which has at least an error on the k-th transmitted symbol a_k. Next, upon detection, it is assumed that the genie tells the receiver that either $\underline{a}$, or $\underline{a}'$ was transmitted. Therefore, the receiver is supposed to make a decision between only two sequences. This can be achieved optimally with a probability of error:

$$P_G(\underline{e}) = Q\left(\frac{d(\underline{e})}{\sqrt{2N_0T}}\right). \tag{A7}$$

Thus, the probability that the genie-aided receiver makes an incorrect decision on a_k is:

$$P_G = \sum_{\underline{e} \in E} w(\underline{e}) \cdot Q\left(\frac{d(\underline{e})}{\sqrt{2N_0T}}\right) \cdot P\{A(\underline{e})\}, \tag{A8}$$

where, similarly to the previous case, $P\{A(\underline{e})\}$ is now the probability of occurrence of the particular error pattern $\underline{e}$ offered by the genie. Neglecting the less probable error

events from the summation in Eq. (A8) and, as before, keeping only the dominant term corresponding to d_{min}, we arrive at:

$$P_e \geq \psi''(d_{\min}) \cdot Q\left(\frac{d_{\min}}{\sqrt{2N_0T}}\right), \tag{A9}$$

where, now

$$\psi''(d_{\min}) = \sum_{\underline{e} \in E(d_{\min})} P\{A(\underline{e})\} \tag{A10}$$

is the probability that a data sequence chosen at random is such that $d(\underline{e}) = d_{\min}$. From the Eq. (A9) and Eq. (A5), it becomes obvious that the minimum distance is the most important parameter that defines the system performance. Although the multiplicities ψ' and ψ'' of the error events separated by d_{min} affect the bounds (A5) and (A9), their contribution can be significant only at low signal-to-noise ratios due to the sharp descent of the *erfc* function [3].

Appendix B

Appendix B contains several important relationships of Karhunen-Loéve expansion used for computation of eigen-quantities required for the signal probability density function calculation in optical links containing optical amplifiers from Chapter 4.

The relationship between ASE with noise power spectral density $N_0'/2$ and variance ν_0^2 per quadrature, per polarization, and the noise autocorrelation function (of a wide-sense stationary AWGN process) after filtering with a filter, $H(f)$, (in the optical domain) is established by the following Fourier transform relationship:

$$R_n(t-t') = 2 \cdot \widetilde{R}_n(\tau) = \mathbb{F}^{-1}\left\{2 \cdot \nu_0^{\,2} \mid H(f) \mid^2\right\} \tag{B1}$$

where $\widetilde{R}_n(\tau)$ is the autocorrelation function of the noise process in one quadrature (the noise processes in the two quadratures are independent), and $\mathbb{F}^{-1}\{\cdot\}$ represents the inverse Fourier transform.

As required by the derivation, in order to de-correlate variables n_k, the expansion needs to be done in terms of eigenfunctions of the filtered noise autocorrelation function $R_n(t - t')$ [63] that is, according to Eq. (B1), closely related to $\widetilde{R}_n(\tau)$:

$$\int_0^T \widetilde{R}_n(t-t')\cdot\phi_k(t')\,dt' = \nu_0^2\cdot\int_0^T\left\{h(t-t')*h^*(t'-t)\right\}\phi_k(t')\,dt' = \sigma_k^2\phi_k(t)\,. \tag{B2}$$

In Eq. (B2) * stands for the convolution operator and h^* is the conjugate of the optical filter impulse response. Eq. (B.2), can be expressed in the normalized form:

$$\int_0^T\left\{h(t-t')*h^*(t'-t)\right\}\phi_k(t')\,dt' = \widetilde{\lambda_k}\,\phi_k(t) \tag{B3}$$

where

$$\widetilde{\lambda}_k = \sigma_k^2/\nu_0^2 \tag{B4}$$

It is obvious that eigen-quantities need to be calculated only once for a given system configuration. Specifically, while the eigenfunctions are uniquely defined, the eigenvalues need only be scaled by the value of the noise variance for the particular conditions to be able to generate the PDF for a given signal to noise ratio. Note that the eigenvalue equation in Eq. (B.2) is expressed in terms of a single quadrature component of the field (either the real or the imaginary part). Assuming that real and imaginary parts of the noise process are independent, Eq. (B.2) can be rewritten for each polarization by multiplying it by a factor of 2. In this case, however, the eigenvalues obtained from (B.2), and used as noise variances for KL terms in Eq. (4.2)-(4.4) need to be divided by 2.

For an arbitrary filter shape, the eigen-quantities need to be calculated numerically. The simplest, although sometimes not sufficiently accurate approach to find the eigen-quantities consists of forming a square autocorrelation matrix of the filtered noise process Γ (same as autocorrelation function of the optical filter for

AWGN input) of order equal to (or greater than) the number of samples per bit period in the simulation. The middle row of this symmetric Toeplitz matrix should be the central portion of the autocorrelation function – symmetric around zero. The eigen-value decomposition of this matrix provides approximate eigenvalues and sampled versions of the eigenfunction for the given filtered white noise process. However, standard routines in double precision can be imprecise for this particular problem when several eigenvalues are closely spaced as in the case of a flat-top filter. In this case special numerical approaches have to be adopted [80, 83]. Note that if the continuous autocorrelation function $R_n(\tau)$ is being sampled and represented by an $N \times N$ matrix Γ, although the elements of Γ can be made arbitrarily close to the autocorrelation function $R_n(\tau)$, this does not necessarily imply that the eigenvalues of the matrix will converge to the eigenvalues of the (continuous) autocorrelation function for any common matrix norm [87]. However, the imprecision in the PDF calculation will marginally influence the BER, in a way similar to the BER estimate based on the chi-square distribution treated in the main body of the Chapter 4.

References

[1] N. Bergano, "Undersea Communications," in *Fiber Optical Telecommunications IV-B*, (I. Kaminow and T. Li eds.) Academic Press (2002).

[2] J. Zyskind, R. Barry, G. Pendock, M. Cahill, J. Ranka, "High-Capacity, Ultra-Long-Haul Networks," in *Fiber Optical Telecommunications IV-B*, (I. Kaminow and T. Li eds.) Academic Press (2002).

[3] O. Ait Sab, "FEC Techniques in Submarine Transmission Systems," OFC 2001, paper TuF1.1, (2001).

[4] A. Mahapatra, E.J. Murphy, "Electrooptic Modulators," in *Fiber Optical Telecommunications IV-A*, (I. Kaminow and T. Li eds.) Academic Press (2002).

[5] G.P. Agrawal, *Fiber-Optic Communication Systems*, Second Edition, John Wiley and Sons, (1997).

[6] A. Yariv, *Optical Electronics in Modern Communications*, Fifth Edition, Oxford University Press, (1997).

[7] J.G. Proakis, *Digital Communication Systems*, Fourth Edition, McGraw Hill, (2001).

[8] S. Benedetto, E. Biglieri, *Principles of Digital Transmission*, Second Edition, Kluwer Academic Press, (1999).

[9] R.E. Ziemer, R.L. Peterson, *Introduction to Digital Communication*, Second Edition, Prantice Hall, (2001).

[10] E. Desurvire, J.R. Simpson, D. Lee, "High Gain Erbium Doped Traveling Wave Fiber Amplifier," Optics Letters, Vol. 12, pp. 888-890, (1987).

[11] R.J. Mears et al., "Low noise erbium-doped fiber amplifier operating at 1.54 μm," Electronics Letters, Vol. 23, pp. 1026-1028, (1987).

[12] C.R. Giles, E. Desurvire, "Modeling erbium-doped fiber amplifiers," J. Lightwave Technol., Vol. 9, pp. 271-183, (1991).

[13] G.P. Agrawal *Nonlinear Fiber Optics*, Second Edition, Academic Press, (1999).

[14] J.-C. Diels, W. Rudolph, *Ultrashort Laser Pulse Phenomena*, Academic Press, (1996).

[15] J. Goodman, *Introduction to Fourier Optics*, Second Edition, McGraw Hill, (1996).

[16] H. Kogelinik, R.M. Jopson, L.E. Nelson, "Polarization-Mode Dispersion" in *Fiber Optical Telecommunications IV-B*, (I. Kaminow and T. Li eds.) Academic Press (2002).

[17] R. Boyd, *Nonlinear Optics*, Academic Press (1992).

[18] A. R. Chraplyvy, "Limitations on lightwave communications imposed by optical-fiber nonlinearities," J. Lightwave Technol., Vol. 8, No. 10, pp. 1548-1557, (1990).

[19] A. Willner, B. Hoanca, "Fixed and Tunable Management of Fiber Chromatic Dispersion" in *Fiber Optical Telecommunications IV-B*, (I. Kaminow and T. Li eds.) Academic Press (2002).

[20] B.H. Marcus, R.M. Roth and P. H. Siegel, "Constrained systems and coding in recording channels,"in *Handbook of Coding Theory*, (V. Pless, W. C. Huffman and R. A. Brualdi Eds.), North Holland (1998).

[21] J.H. Winters and R.D. Gitlin, "Electrical signal processing techniques in long-haul fiber-optic systems," IEEE Trans. Commun., vol. 38, no. 9, pp. 1439-1453, September 1990.

[22] J.H. Winters and S. Kasturia, "Constrained maximum likelihood detection for high-speed fiber optic systems," in Proc. GLOBECOM '91, pp. 1574-1579. 1991.

[23] H.F. Haunstein et al., Design of near optimum electrical equalizers for optical transmission in the presence of PMD", in Proc. OFC, Anaheim, CA, 2001, Paper WAA4-1.

[24] A. J. Weiss, "On the Performance of Electrical Equalization in Optical Fiber Transmission Systems", IEEE Photon. Technol. Lett., Vol. 15, No. 9, 2003, pp. 1225-1227

[25] A.C. Houle et al., "Emerging Optical Technologies for Multi-Service Metro Networks", WP1, LEOS Annual Meeting, Tucson, AZ, USA, 26-29 October, 2003.

[26] S. D. Personick, "Receiver Design for digital fiber optic communication systems, I", Bell Syst. Tech. J, vol. 52, no. 6, pp. 843-874. 1973.

[27] K. Yonenaga, S. Kuwano, "Dispersion-Tolerant Optical Transmission System Using Duobinary Transmitter and Binary Receiver", Journal of Lightwave Technology, Vol. 15, No. 8, pp. 1530-1537, August 1997.

[28] M. Shtaif, and A.H. Gnauck, "The Relation Between Optical Duobinary Modulation and Spectral Efficiency in WDM Systems", IEEE Photonics Technology Letters, Vol. 11, No. 6, pp. 712-714, June 1999.

[29] D. Penninckx, M. Chbat, L. Pierre, J-P.Thiery, "The phase-shaped binary transmission (PSBT): a new technique to transmit far beyond the chromatic dispersion limit.", IEEE Photonics Technology Letters, vol.9, no.2, pp.259-61, Feb. 1997.

[30] N. Alić, G. C. Papen and Y. Fainman, "Performance of Maximum Likelihood Sequence Estimation with Different Modulation Formats," IEEE Workshop on Advanced Modulation Formats, paper FD2, July 2004.

[31] J. Conradi, "Bandwidth Efficient Modulation Formats", in *Fiber Optic Telecommunication IVB*, I. Kaminow and T. Li, editors, Academic Press, San Diego (2002).

[32] A.D. Whalen, *Detection of Signals in Noise*, Academic Press 1971.

[33] G.D. Forney Jr., "Maximum-Likelihood Sequence Estimation of Digital Sequences in the Presence of Intersymbol Interference", IEEE Trans. Inform. Theory, Vol. IT-18, No. 3, May 1972.

[34] L.R. Bahl, J. Cocke, F. Jelinek, J. Raviv, "Optimal Decoding of Linear Codes for Minimizing Symbol Error Rate," IEEE Trans. Inf. Theory, Vol. 20, No. 2, pp. 284-7, March 1974.

[35] A.J. Viterbi, J.K. Omura, Principles of digital communication and coding, McGraw-Hill, 1979.

[36] G.D. Forney Jr., "Viterbi Algorithm", Proceedings of the IEEE, vol.61, no.3, pp.268-78, March 1973.

[37] N. Alić, G. C. Papen, L. B. Milstein, P. H. Siegel and Y. Fainman, "Performance Bounds of MLSE in Intensity Modulated Fiber Optic Links," in *Optical Communication Theory and Techniques*, (Enrico Forrestireri, ed.), Springer 2005. (presented at 2004 Tyrrhenian International Workshop on Digital Communications, Pisa, Italy, paper 4.5, October 2004).

[38] N. Alić, G. C. Papen and Y. Fainman, "Theoretical Performance Analysis of Maximum Likelihood Sequence Estimation in Intensity Modulated Short-Haul Fiber Optic Links," Proc. IEEE LEOS Annual Meeting, Puerto Rico, paper ThB3, Nov. 2004.

[39] G.J. Foschini, "Performance Bound for Maximum-Likelihood Reception of Digital Data", IEEE Trans. Inform. Theory, Vol. IT-21, No. 1, Jan. 1975.

[40] Y.J. Liu, I. Oka and E. Biglieri, "Error probability for Digital Transmission Over Nonlinear Channels with Application to TCM", IEEE Trans. Inform. Theory, Vol. 36, No. 5, Sept. 1990.

[41] VPItransmissionMaker and VPIcomponentMaker are products for Photonic Design Automation licensed by VPIsystems, www.vpiphotonics.com

[42] M. Saxena, "Optimum Encoding in Finite State Coded Modulation", Report TR83-2, Dept. Electrical, Computer and Systems Engineering, Rensselear Polytechnic Institute, Troy, NY, 1983.

[43] M.G. Mullegan and S.G. Wilson, "An improved algorithm for ealuating trellis phase codes, " IEEE Transactions on Information Theory, Vol. 30, pp. 846-851, 1984.

[44] A.J. Viterbi, "Convolutional Codes and Their Performance in Communication Systems", IEEE Trans. Comm. Tech., Vol. Com-19, No. 5, pp. 751-772, October 1971.

[45] J.A. Heller, I.M. Jacobs, "Viterbi Decoding for Satellite and Space Communication", IEEE Trans. Commun. Tech., Vol. Com-19, No. 5, pp. 835-848, October 1971.

[46] R. E. Saperstein, D. Panasenko, Y. Fainman, "Demonstration of a microwave spectrum analyzer based on time-domain optical processing in fiber," Optics Letters, Vol. 29, Issue 5, pp. 501-503, OSA March 2004

[47] International Telecommunication Union Telecommunication Standardization Sector (ITU-T), Series G: Transmission Systems and Media, Digital Systems and Networks, G975.1, 2004.

[48] R.R. Patel, S.W. Bond, M.D. Pocha, M.C. Larson, H.E. Garrett, R.F. Drayton, H.E. Petersen, D.M. Krol, R.J. Deri, M.E. Lowry, "Multiwavelength parallel optical interconnects for massively parallel processing," IEEE J. Sel. Topics in Quantum Electronics, Vol. 9, No. 2, pp. 657 - 666 (2003).

[49] Rokitski R, Fainman, S. Propagation of ultrashort pulses in multimode fiber in space and time. Optics Express, vol. 11, no. 13, p 1497-150, (2003).

[50] K.M. Patel, S.E. Ralph, "Enhanced multimode fiber link performance using a spatially resolved receiver," IEEE Photonics Technology Letters, Vol. 14, No. 3, pp. 393 – 395 (2002).

[51] L. Raddatz, I.H. White, D.G. Cunningham, M.C. Nowell, "An experimental and theoretical study of the offset launch technique for the enhancement of the bandwidth of multimode fiber links," J. Lightwave Technol., Vol. **16**, No. 3, pp. 324 – 331, (1998) .

[52] S. Fan and J. M. Kahn, "Principal Modes in Multi-Mode Waveguides", Optics Letters, vol. 30, no. 2, pp. 135-137 (2005).

[53] Pepeljugoski, P.; Kuchta, D.; Kwark, Y.; Pleunis, P.; Kuyt, G. "15.6 Gb/s transmission over 1 km of next generation multimode fiber," in Proc. Optical Communication, 2001. ECOC '01. Pp. 440 - 4412001

[54] G.J. Foschini and M.J. Gans, "On Limits of Wireless Communications in a Fading Environment when Using Multiple Antennas," Wireless Personal Communications 6, 311, (1998)

[55] S.Al-Sowayan and K.L.Lear, "Data Pattern Dependence of VCSEL Far-Field Distributions", IEEE Photon. Technol. Lett., Vol. 15, No. 9, 2003, pp. 2215-2217.

[56] Alic et al. in Proc. CLEO 2005, Baltimor, MD paper no. CWG7, 2005.

[57] R. Walker and R. Dugan. Low overhead coding proposal 10 GbE serial links. Presented at IEEE802.3 Higher Speeed Study Group Plenary Week Meeting. Available online at: http://group.ieee.org/groups/802/3/10G_study/public/nov99/index.html

[58] 6. H. Bulow, G. Thielecke, "Electronic PMD mitigation-from linear equalization to maximum-likelihood detection" in Proc. OFC 2001, 2001, Paper WAA3-1.

[59] H. F. Haunstein, W. Sauer-Greff, A. Dittrich, K. Sticht, and R. Urbansky, "Principles for Electronic Equalization of Polarization-Mode Dispersion" Journal Of Lightwave Technology 22 1169-82 (2004).

[60] A. Faerbert, S. Langenbach, N. Stojanovic, C. Dorschky, T. Kupfer, C. Schulien, J.-P. Elbers, H. Wernz, H. Griesser, C. Glingener, "Performance of a 10.7 Gb/s Receiver with Digital Equaliser using Maximum Likelihood Sequence Estimation," Proc. of ECOC'O4, Th.4.1.5, (2004).

[61] J.-P. Elbers, H. Wernz, H. Griesser, C. Glingener, A. Faerbert, S . Langenbach, N. Stojanovic, C. Dorschky, T. Kupfer, C. Schulien, "Measurement of the Dispersion Tolerance of Optical Duobinary with an MLSE-Receiver at 10.7 Gb/s," Proc. of OFC'O5,OthJ4, (2005).

[62] P.A. Humblet and M. Azizoglu, "On the Bit Error Rate in Lightwave Systems with Optical Amplifiers," J. Lightwave Tech. 9, 1576-82 (1991).

[63] R.N McDonough and A.D. Whalen, Detection of Signals in Noise, Second Edition (San Diego, Academic Press 1995).

[64] J. M. Wozencraft and I. M. Jacobs, Principles of Communication Engineering (Waveland Press, reprint 1990).

[65] E. Arthurs and H. Dym, "On the Optimum Detection of Digital Signals in the Presence of White Gaussian Noise – A Geometric Interpretation and a Study of

Three Basic Data Transmission Systems", IRE Trans. on Communication Systems 10, 336-372 (1962).

[66] J. Lee et al., "Bit-error-rate analysis of optically preamplified receivers using an eigenfunction expansion method in optical frequency domain", J. Lightwave Technol. 12, 1224-1229 (1994).

[67] I. T. Monroy, G. Einarsson, "On Analytical Expressions for the Distribution of the filtered Output of Square Envelope Receivers with Signal and Colored Gaussian Noise Input," IEEE Transactions on Communications 49, 19-23 (2001).

[68] G. Jacobsen, K. Berlitzon, Z. Xiapin, "WDM Transmission System Performance: Influence of non-Gaussian Detected ASE Noise and Periodic DEMUX Characteristic," Journal of Lightwave Technology, 16, 1804-1812 (1998).

[69] I. T. Monroy, G. Einarsson, "Bit Error Evaluation of Optically Preamplified Direct Detection Receivers with Fabry-Perot Optical Filters," Journal of Lightwave Technology, 15, 1546-1553 (1997).

[70] G. Bosco, A. Carena, V. Curri, R. Gaudino, P. Poggiolini, and S. Benedetto, "A Novel Analytical Method for the BER Evaluation in Optical Systems Affected by Parametric Gain," IEEE Photonics Technology Letters, 12, 152-4, (2000).

[71] G. Bosco, A. Carena, V. Curri, R. Gaudino, P. Poggiolini, and S. Benedetto, "A Novel Analytical Approach to the Evaluation of the Impact of Fiber Parametric Gain on the Bit Error Rate" IEEE Transactions On Communications, 49, 2154-63 (2001).

[72] I. B. Djordjevic, B. Vasic, "Receiver Modeling for Optically Amplified Communication Systems," International Journal of Electronics and Communications, 57, 381-390 (2003).

[73] F. Buchali and H. Bulow, "Correlation sensitive Viterbi equalization of 10 Gb/s signals in bandwidth limited receivers," in Proc. OFC 2005, Paper F020.

[74] R. Loudon, T.J. Shepherd, "Properties of the Optical Quantum Amplifier," Optica Acta, 31, 1243-1269 (1984).

[75] C. Dorrer, C.R. Doerr, I. Kang, R. Ryf, J. Leuthold and P.J. Winzer, "Measurement of eye diagrams and constellation diagrams of optical sources using linear optics and waveguide technology", J. Lightwave Technol. 23, 178-186 (2005).

[76] B. Saleh, *Photoelectron Statistics, With Applications to Spectroscopy and Optical Communication*, (Springer-Verlag, 1978).

[77] C. Flammer, Spheroidal Wave Functions (Stanford Univ. Press, 1957).

[78] D. Slepian and E. Sonnenblick, “Eigenvalues Associated with Prolate Spheroidal Wave Functions of Zero Order,” Bell Sys. Tech. Journal, 45, 1745-59 (1965).

[79] D. Slepian, “Fluctuations of Random Noise Power,” Bell Sys. Tech. Journal, 37, 163 (1958)

[80] D. Slepian, “A Numerical Method Of Determining EigenValues And EigenFunction Of Analytic Kernels” SIAM Journal of Numerical Analysis, 5, 586-600 (1968).

[81] D. Slepian, “On Bandwidth,” Proc. Of IEEE, 64, 292-300 (1976).

[82] I. C. Moore and M. Cada, “Prolate spheroidal wave functions, an introduction to the Slepian series and its properties” Appl. Comput. Harmon. Anal. 16, 208–230 (2004).

[83] D.B. Percival, and A.T. Walden Spectral Analysis for Physical Applications: Multitaper and Conventional Univariate Techniques (Cambridge, Cambridge University Press, 1993).

[84] K. Yonenaga, S. Kuwano, “Dispersion-Tolerant Optical Transmission System Using Duobinary Transmitter and Binary Receiver”, Journal of Lightwave Technology, 15, 1530-1537 (1997).

[85] R. A. Griffin and A. C. Carter, “Optical differential quadrature phaseshift keying (oDQPSK) for high capacity optical transmission,” in Proc. OFC, 2002, Paper WX6C.

[86] A.H. Gnauck, P.J.Winzer, “Optical phase-shift-keyed transmission,” J. Lihthwave Technol, 23 , 115 - 130 (2005).

[87] P. Stoica and R. Moses, Introduction to Spectral Analysis (Prentice Hall, 1997).

[88] C.R.S. Fludger, J.E.A. Whiteaway, P.J. Anslow, in Proc. OFC 2004, Paper WM7. (2004).

[89] A. Kavcic and J.M.F. Moura, "The Viterbi Algorithm and Markovian Noise Memory." IEEE Transactions on Information Theory. Volume: 46 (1), pp. 291 – 301, (2000).

[90] N. Alić, G. C. Papen, R. E. Saperstein, L. B. Milstein, and Y. Fainman, "Signal Statistics and Maximum Likelihood Sequence Estimation in Intensity Modulated Fiber Optic Links Containing a Single Optical Pre-amplifier," Opt. Express 13, 4568-4579 (2005).

[91] I. Shake, H. Takara, K. Mori, S. Kawanishi and Y. Yamabayashi, Electron. Lett. 34, 1600 (1998);

[92] R. J. Essiambre, B. Mikkelsen, and G. Raybon, Electron. Lett, 35, 1576 (1999);

[93] P. V. Mamyshev and N. A. Mamysheva, Opt. Lett. 24, 1454 (1999);

[94] M. J. Ablowitz and T. Hirooka Optics Letters, Vol 25, No. 24, (p. 1750-2)

[95] T. Inoue and A. Maruta:, J. Opt. Soc. Am. B, Vol. 19, No. 3 (p. 440-7).

[96] A. Mecozzi, C. B. Clausen and M. Shtaif, IEEE Photon. Technol. Lett., Vol. 12, No. 4, (p. 392-4)

[97] A. Mecozzi, C. B. Clausen and M. Shtaif, IEEE Photon. Tech. Lett., Vol. 12, No. 12 (p. 1633-5)

[98] A. Mecozzi, C. B. Clausen M. Shtaif, S.-G. Park, and A. H. Gnauck IEEE Photon. Tech. Lett., Vol. 13, No. 5, p. 445-7.

[99] J.-R. Essiambre "Pseudo-Linear Transmission of High-Speed TDM Signals: 40 and 160 Gb/s" in *Fiber Optical Telecommunications IV-B*, (I. Kaminow and T. Li eds.) Academic Press (2002).

[100] S. K. Turitsyn, M. P. Fedoruk, T. S. Yang and W. L. Kath, "Magic dispersion maps for multi-channel soliton transmission," IEEE J. Quantum Electron. **36,** Vol. 3, pp. 290-299 (2000)

[101] K.S. Cheng, J. Conradi "Reduction of pulse-to-pulse interaction using alternative RZ formats in 40-Gb/s systems", IEEE Photon. Technol. Lett., vol.14, no.1, pp.98-100 (2000).

[102] X. Liu, X. Wei, A. H. Gnauck, C. Xu, L. K. Wickham, Opt. Lett. 27, 1177 (2002).

[103] S. Kumar, "Intrachannel Four-Wave Mixing in Dispersion Managed RZ Systems", IEEE Photon. Technol. Lett., 13 800 (2001)

[104] M.J Ablowitz, T. Hirooka, "Intrachannel pulse interactions in dispersion-managed transmission systems: energy transfer", Opt. Lett. 27, 203 (2002)

[105] P.J. Winzer, A.H. Gnauck, G. Raybon, S. Chandrasekhar; Y. Su, J. Leuthold, "40-Gb/s return-to-zero alternate-mark-inversion (RZ-AMI) transmission over 2000 km", IEEE Photon. Technol. Lett . 15. 766 (2003)

[106] N. Alic and Y. Fainman, "Data-dependent phase coding for suppression of ghost pulses in optical fibers." IEEE Photonics Technology Letters, vol.16, no.4, pp.1212-14 (2004).